

MINERAL SEQUESTRATION OF CO₂
BY REACTION WITH ALKALINE RESIDUES

Dissertation zur Erlangung des Grades

Doktor der Naturwissenschaften

(Dr. rer. nat.)

An der Fakultät Biologie/Chemie/Geowissenschaften

vorgelegt von

Martin Back

geb. am 25.02.1977 in Ludwigshafen

Die Arbeiten zur vorliegenden Dissertation wurden im Zeitraum von März 2005 bis Februar 2008 am Lehrstuhl für Hydrologie der Universität Bayreuth unter Betreuung von Herrn Prof. Dr. Stefan Peiffer durchgeführt.

Vollständiger Abdruck der von der Fakultät für Biologie, Chemie und Geowissenschaften der Universität Bayreuth genehmigten Dissertation zur Erlangung des akademischen Grades eines Doktors der Naturwissenschaften (Dr. rer. nat.).

Dissertation eingereicht am: 10.10.2011

Zulassung durch die Prüfungskommission: 19.10.2011

Wissenschaftliches Kolloquium: 31.05.2012

Amtierender Dekan:

Prof. Dr. Beate Lohnert

Prüfungsausschuss:

Prof. Dr. Stefan Peiffer (Erstgutachter)

Prof. Dr. Christoph Clauser (Zweitgutachter)

Prof. Dr. Klaus Bitzer (Vorsitz)

Prof. Dr. Britta Planer-Friedrich

Prof. Dr. Egbert Matzner

TABLE OF CONTENTS

TABLE OF CONTENTS	I
LIST OF FIGURES	IV
LIST OF TABLES	IX
SUMMARY	X
ZUSAMMENFASSUNG.....	XIII
INTRODUCTION AND OUTLINE OF THESIS	1
CLIMATE CHANGE AND ATMOSPHERIC INCREASE OF ANTHROPOGENIC CO ₂	1
THE ROLE OF CARBON CAPTURE AND STORAGE (CCS).....	1
MINERAL CARBONATION.....	3
USING OF ALKALINE RESIDUES FOR CO ₂ SEQUESTRATION.....	5
OBJECTIVE OF THE DISSERTATION	6
CONTRIBUTIONS TO DIFFERENT STUDIES	9
1 REACTIVITY OF ALKALINE LIGNITE FLY ASHES TOWARDS CO ₂ IN WATER	13
1.1 INTRODUCTION	14
1.2 EXPERIMENTAL SECTION.....	15
<i>Sample characterisation</i>	15
<i>Experiments</i>	15
1.3 RESULTS AND DISCUSSION	17
<i>Composition of fly ashes</i>	17
<i>Reaction between fly ash and water</i>	18
<i>Reaction between CO₂ and fly ash</i>	19
<i>Effect of process variables on CO₂ uptake</i>	22
1.4 IMPLICATIONS FOR A TECHNICAL REALIZATION	26
<i>Acknowledgement</i>	27
1.5 SUPPORTING INFORMATIONS.....	28
<i>Section A: Experimental setup</i>	28
<i>Section B: Accuracy of the methods used for determination of the total uptake of CO₂, TDIC and carbonate precipitation</i>	28
<i>Section C: SEM-pictures of lignite fly ash</i>	31
<i>Section D: Grain size analysis</i>	32

Table of Contents

<i>Section E: Mineralogical composition (XRD, Rietveld analysis)</i>	32
2 SEQUESTRATION OF CO ₂ AFTER REACTION WITH ALKALINE EARTH METAL OXIDES CAO AND MGO.....	35
2.1 INTRODUCTION	36
2.2 MATERIALS AND METHODS	38
<i>Experimental setup</i>	38
<i>Measurements and calculations</i>	39
<i>Sets of experiments</i>	41
2.3 RESULTS AND DISCUSSION.....	43
<i>Reaction of CaO/Ca(OH)₂ suspensions with CO₂</i>	43
<i>Reaction of MgO suspensions with CO₂</i>	45
<i>Controls on CO₂ transfer to the water phase</i>	53
2.4 CONCLUSIONS	58
<i>Acknowledgements</i>	60
3 APPLICATION OF A PHREEQC BASED KINETIC MODEL TO SIMULATE PROCESS AND DYNAMICS OF THE CARBONATION OF ALKALINE MATERIALS BY GAS PHASE DERIVED CO ₂ IN AQUEOUS SYSTEMS	63
ABSTRACT	63
3.1 INTRODUCTION	65
3.2 MATERIALS AND METHODS	68
<i>Experimental section</i>	68
<i>CO₂ uptake (carbonation) experiments by alkaline materials</i>	70
<i>Modelling section</i>	70
3.3 RESULTS AND DISCUSSION.....	72
<i>Determination of rate constants and model setup</i>	72
SIMULATION OF THE CARBONATION IN SYSTEMS WITH MULTIPLE MINERAL PHASES	80
<i>Simulation of lignite fly ash carbonation</i>	87
3.4 CONCLUSIONS	91
<i>Acknowledgements</i>	92
SUPPORTING INFORMATIONS.....	92
4 MINERAL TRAPPING OF CO ₂ IN OPERATED HYDROGEO THERMAL RESERVOIRS....	96
4.1 INTRODUCTION	97

Table of Contents

4.2	SUITABLE GEOTHERMAL RESERVOIRS	98
4.3	TRANSFORMATION OF ANHYDRITE INTO CALCITE	100
4.4	CORE FLOODING EXPERIMENT	102
4.5	SUITABLE SOURCES OF ALKALINITY	104
	<i>In-situ alkalinity source</i>	<i>104</i>
	<i>Alkalinity provided from fly ash</i>	<i>107</i>
4.6	SUMMARY AND CONCLUSIONS	107
	<i>Acknowledgement</i>	<i>108</i>
EPILOGUE		109
	CONCLUSIONS INDIVIDUAL CHAPTERS	109
DISCUSSION AND OUTLOOK		111
NOTATIONS.....		116
REFERENCES.....		117
DANKSAGUNG		128
ERKLÄRUNG		130

LIST OF FIGURES

Figure 0.1: Proposed treatment scheme using reacting lignite fly ashes: Direct Carbonation (I) of Ca/Mg-minerals as a sink of CO₂. The residual ACS (II) can be used for injection into aquifers for mineral trapping7

Figure 1.1: Batch experiments with deionized water and fly ash at a s/l-ratio of 12.5 g L⁻¹ and a temperature of 25 °C under nitrogen atmosphere. -A: Release of Ca and Mg (meq g⁻¹) during pH-stat-experiments. -B: Release of main elements (meq g⁻¹). The pH was always > 12..... 18

Figure 1.2: Reaction progress in fly ash experiment with water and CO₂ (s/l-ratio = 75g L⁻¹; initial pCO₂ = 0.02 MPa; stirring rate = 300 rpm). -A: pH, pCO₂ and EC.-B: total uptake of CO₂, precipitated amount of carbonate, TDIC and dissolved contents of Ca and Mg per gram fly ash.21

Figure 1.3: CO₂-transfer (millimoles per gram fly ash) into carbonate and TDIC as a function of pCO₂ (s/l = 75 g L⁻¹; T = 25 °C; stirring rate = 450 rpm; gas flux = 1 L min⁻¹). Experimental accuracy was calculated based on replication of experiments at least twice.23

Figure 1.4: Dependence of CO₂ transfer at 25 °C and pCO₂ = 0.01 MPa on –Top: s/l-ratio (stirring rate 600 rpm) and –Bottom: stirring rate (s/l-ratio 75 g L⁻¹).24

Figure 1.5: Dependence of CO₂ transfer on temperature (pCO₂ = 0.02 MPa, stirring rate 600 rpm, s/l-ratio 75 g L⁻¹). -Top: time course of pH, -bottom: CO₂ transfer. Note that the total uptake of CO₂ at 75 °C is identical to the amount of carbonate precipitated.26

Figure 1.6: Experimental setup: Reactor system with CO₂ flow-through.....28

Figure 1.7: Plot of calculated CO₂ uptake derived from IR sensor measurements versus TDIC concentrations derived from headspace measurements. Process parameters were varied between pH 7-10, stirring rates of 300-700 rpm at a constant temperature of 25 °C and a initial pCO₂ of 0.01 MPa.....29

Figure 1.8: Comparison of the amounts of precipitated carbonate calculated as the difference between IR-sensor-derived CO₂ uptake and TDIC, with analytical results obtained after acidification of samples (Eq. 1-S) for two fly ash experiments.30

List of Figures

Figure 1.9: SEM pictures of fresh ash (A), eluated fly ash after 120 minutes (B) and carbonated ash after 120 minutes of reaction (C).....	31
Figure 1.10: Grain size distribution of the fresh lignite fly ashes measured with laser diffraction.....	32
Figure 1.11: X-ray diffractogramm of the investigated brown coal fly ash (black) and calculated diffractogramm (grey) based on Rietveld analysis	32
Figure 2.1: Aqueous batch reactor with stirrer, heating mantle, continuous CO ₂ flow, sensors.....	39
Figure 2.2: Set A: Reaction progress of CaO/Ca(OH) ₂ with CO ₂ in aqueous solution (25 °C, pCO ₂ = 0.01 MPa, stirring rate = 600 rpm): a) pH, c(TDIC), c(Ca), cumulative CO ₂ uptake, solid phase calcite content (all mmol L ⁻¹); b) uptake rate of CO ₂ (mmol L ⁻¹ s ⁻¹) and solution EC (mS cm ⁻¹); c) solution speciation modelled with PHREEQC based on the measurement of pH, TDIC and Ca concentration.....	46
Figure 2.3: Set A: Reaction progress of MgO/Mg(OH) ₂ with CO ₂ in aqueous solution (25 °C, pCO ₂ = 0.01 MPa, stirring rate = 600 rpm): a) pH, c(TDIC), c(Mg) and cumulative CO ₂ uptake (all mmol L ⁻¹); b) uptake rate of CO ₂ (mmol L ⁻¹ s ⁻¹) and solution EC (mS cm ⁻¹); c) solution speciation modelled with PHREEQC based on the measurement of pH, TDIC and Mg concentration	48
Figure 2.4: Set C: Effect of pH and NaHCO ₃ concentration (0 – 50 mmol L ⁻¹) on the dissolution rate of MgO in water. The pH was stabilized by automatic titration with 0.1 N HCl: c(MgO) = 0.025 mol L ⁻¹ , T = 25 °C, stirring rate = 600 rpm.....	48
Figure 2.5: Set B: Effect of an increase in (I) MgO input concentrations from 0.05 to 0.125 mol L ⁻¹ and (II) temperature from 25 to 75 °C on precipitation of magnesium carbonates: pCO ₂ = 0.01 MPa, stirring rate = 600 rpm; a) pH, c(TDIC), c(Ca) or c(Mg), cumulative CO ₂ uptake, solid phase carbonate content (all mmol L ⁻¹); b) MgCO ₃ concentration and saturation indices as calculated by PHREEQC	51
Figure 2.6: Set B: SEM images of the precipitated magnesium carbonates –left: nesquehonite at 25° C and –right: hydromagnesite after 120 minutes of reaction at a temperature of 75 °C	52

List of Figures

- Figure 2.7: Set B: Effect of stirring rate (300 – 600 rpm) on CO₂ uptake rates in CaO (a) or MgO (b) suspension: T = 25 °C, pCO₂ = 0.01 MPa54
- Figure 2.8: Set D: CO₂ dissolution rate in de-ionized water at different stirring rate (300 – 600 rpm) and pH (7 – 12). The pH was stabilized by automatic titration with 0.1 N HCl: T = 25 °C, pCO₂ = 0.01 MPa55
- Figure 2.9: Set B: Effect of different CaO or MgO input concentrations (0.0125 to 0.125 mol L⁻¹) on the CO₂ uptake rates and maximum pH values of carbonation experiments: T = 25 °C, pCO₂ = 0.01 MPa, stirring rate = 600 rpm.....56
- Figure 2.10: Set B: Effect of different temperature (25 °C to 75 °C) on the CO₂ uptake rates and maximum pH values of CaO or MgO carbonation experiments: c(CaO) = 0.05 mol L⁻¹ or c(MgO) = 0.025 mol L⁻¹, pCO₂ = 0.01 MPa, stirring rate = 450 rpm....57
- Figure 3.1: The dissolution kinetic of CO₂ in water valid for our experimental setup as a function of stirring rate and pH at close to equilibrium conditions of CO₂. The standard derivation was calculated by comparison of the measured CO₂-uptake (sensor technique, see method section) and increase of TDIC in solution (headspace method) versus time73
- Figure 3.2: CaO dissolution experiment at 25 °C at nitrogen atmosphere for a suspended amount of 0.05 mol L⁻¹ CaO at constant stirring of 600 rpm.74
- Figure 3.3: Rate model for the dissolution of CaO (0.05 mol L⁻¹) at 25° C under nitrogen atmosphere and constant stirring of 600 rpm.75
- Figure 3.4: Comparison of results from laboratory experiments with simulation results performed with PHREEQC (x=3, n=3.4, k=0.94 mmol m⁻²s⁻¹) for the reaction between CO₂ (pCO₂: 0.01 MPa) and CaO (0.05 mol L⁻¹) suspended in water at a temperature of 25 °C and constant stirring of 600 rpm.77
- Figure 3.5: MgO dissolution experiment at 25 °C at nitrogen atmosphere for a suspended amount of 0.05 mol L⁻¹ MgO at constant stirring of 600 rpm.....78
- Figure 3.6: Rate model for the dissolution of MgO (0.05 mol L⁻¹) at 25° C under nitrogen atmosphere and constant stirring of 600 rpm.78

List of Figures

- Figure 3.7: Comparison of results from laboratory experiments with simulation results performed with PHREEQC for the reaction between CO_2 and a suspensions of MgO of 0.05 mol L^{-1} 79
- Figure 3.8: Comparison of results from laboratory experiments with simulation results performed with PHREEQC for the reaction between CO_2 and a suspensions of CaO and MgO both of 0.05 mol L^{-1} 81
- Figure 3.9: Simulation with PHREEQC for the reaction between CO_2 and a suspensions of CaO and MgO both of 0.05 mol L^{-1} . -A: Comparison of calculated SI values of CaO , MgO and calcite. -B: Dissolution kinetics of CaO , MgO and CO_2 compared to rate of calcite precipitation.82
- Figure 3.10: 0.05 mol L^{-1} MgO are suspended in a solution containing 0.136 mol L^{-1} CaCl_2 at a pCO_2 of 0.01 MPa , $25 \text{ }^\circ\text{C}$ and constant stirring of 600 rpm83
- Figure 3.11: Comparison of the PHREEQC simulation (A) and laboratory experiment (B), the reaction of 0.05 mol L^{-1} MgO at $25 \text{ }^\circ\text{C}$, at a pCO_2 of 0.01 MPa and agitation rate of 600 rpm . After 120 minutes of reaction 0.05 mol anhydrite have been added (I: pH, pCO_2 , EC; II: total concentration of dissolved TDIC, Ca, Mg, sulphate and amount of precipitated calcite; III: activities of certain dissolved species).86
- Figure 3.12: Comparison of the calculated activities of dissolved species (HCO_3^- , MgSO_4 , MgHCO_3^-) and total concentrations of TDIC, pCO_2 -out, calcite and anhydrite from PHREEQC simulation after the addition of 0.05 mol L^{-1} anhydrite to the solution containing 0.05 mol L^{-1} MgO at $25 \text{ }^\circ\text{C}$, at a pCO_2 of 0.01 MPa and agitation rate of 600 rpm87
- Figure 3.13: Simulation of lignite fly ash experiments (50g L^{-1}) with PHREEQC (A) and comparison with the laboratory experiment (B)90
- Figure 3.14: Solution concentration in Ca^{2+} and Mg^{2+} vs. measured EC and theoretical EC92
- Figure 4.1: Geothermal heating plant with a common bore hole doublet arrangement.....98
- Figure 4.2: (left) Calcite formed and CO_2 bound versus initial pH of solution as modelled with PHREEQC; boundary conditions: mass of solution = 1 kg , 0.16 M NaHCO_3

solution, infinite amount of anhydrite, $T = 30\text{ }^{\circ}\text{C}$, $p\text{CO}_2 = 1\text{ MPa}$. (right) Evolution of calcite in suspension during a transformation experiment. 101

Figure 4.3: Core flooding of a sandstone sample (length 5.8 cm, diameter 3 cm) cemented with anhydrite and flooded with $1\text{ mol L}^{-1}\text{ Na}_2\text{CO}_3$ solution at a constant flow rate of 2 mL per hour. Anhydrite is dissolved and detected by the sulphate concentration at the core outlet. The average permeability across the core length increases with time. ... 103

Figure 4.4: Thermodynamic batch reaction calculation at $25\text{ }^{\circ}\text{C}$ for the Stralsund site. Initial chemical composition of the formation water and the reservoir rock are taken from Bartels and Iffland (

2000). The pH decreases with increasing amount of added CO_2 . Weathering of plagioclase (dissolution indicated by negative values) and precipitation of secondary kaolinite (indicated by positive values) are prerequisites for calcite precipitation. Anhydrite is not a chemical driver of the reaction. 105

Figure 4.5: Kinetic batch reaction calculation for the Stralsund site. Initial chemical composition of the formation water and the reservoir rock are taken from Bartels and Iffland (2000). The reaction rate of anhydrite is given in equation (5) and the one for calcite is defined following Plummer et al. (1978). All others are taken from Palandri and Kharaka (2004). After 80 days, at a pH of 5.4 calcite precipitation kicks in. 106

LIST OF TABLES

Table 0.1: Estimated storage capacity of discussed CCS-options.....	3
Table 1.1: Relative mineralogical composition of the lignite fly ash before and after 10 minutes of CO ₂ treatment (s/l-ratio: 75g L ⁻¹ , pCO ₂ : 0.02 MPa, stirring rate: 450 rpm, T: 25 °C).	18
Table 2.1: Table 1: Effect of an increase in MgO input or T (Set B experiments) on precipitation of magnesium carbonates. Mineral compounds in wt % of the total analyzed solid phase as determined by XRD analysis after MgO carbonation at pCO ₂ = 0.01 MPa, stirring rate = 600 rpm; “High MgO”: 25 °C, 0.125 mol L ⁻¹ MgO, 180 min; “High T”: 0.05 mol L ⁻¹ MgO, 75 °C, 120 min	50
Table 2.2: Minor and trace elements of the used powders of CaO and MgO determined by ICP-MS after digestion with hydrofluoric acid	60
Table 3.1: List of experiments.....	72
Table 3.2: Relative mineralogical composition of the lignite fly ash before and after 10 minutes of CO ₂ treatment (s/l-ratio:75g L ⁻¹ , pCO ₂ : 0.02 MPa, stirring rate: 450 rpm, T: 25 °C)	91
Table 4.1: Data for the geothermal site Stralsund.....	99
Table 4.2: Formation water composition and rock mineralogy of the Stralsund reservoir given for 58 °C reservoir temperature (Bartels and Iffland, 2000).....	104
Table 5.1: Cost ranges for the components of a CCS system as applied to a given type of power plant or industrial source. The costs of the separate components cannot simply be summed to calculate the costs of the whole CCS system in US\$ CO ₂ ⁻¹ avoided. All numbers are representative of the costs for large-scale, new installations, with natural gas prices assumed to be 2.8-4.4 US\$ GJ ⁻¹ and coal prices 1-1.5 US\$ (IPCC, 2005).....	124

SUMMARY

With the onset of industrialization within the last 150 years, a significant increase in the concentration of the greenhouse gas carbon dioxide (CO₂) is recorded in the atmosphere. According to current scientific understanding the rising atmospheric CO₂ levels can be linked with high probability to the observed phenomenon of global warming. Consequently, the reduction of anthropogenic greenhouse gas emissions has become a global challenge of environmental research and policy.

In this thesis, a novel approach to achieve a long-term mineral sequestration of CO₂ was studied, using alkaline residue materials. This study examined for the first time a process that allows for rapid removal of CO₂ from flue gas through reaction with lignite fly ashes in aqueous solution.

In this process the basicity of the residues is utilized for mineral trapping of CO₂ by precipitating stable calcite. Lignite fly ashes are a cheap, inexpensive, highly reactive byproduct of coal combustion. Due to the exposure to heat, these waste streams generally contain high amounts of reactive Ca/Mg (hydr)oxides and thus offer a high alkalinity. The alkaline residues were therefore not considered as an environmental problem, but rather as useful reactants for technical CO₂ neutralization in the context of combustion processes.

Carbonates are end-products of weathering processes at the earth surface and mineral carbonation is thus assessed to be a permanent and safe storage option of CO₂. Compared to alternative forms of carbon storage (e.g. the injection into gas reservoirs) cost-intensive monitoring programs for safety reasons can be omitted. Also, the carbonation generally leads to heavy metal fixation in the residues, allowing for an environmentally less problematic disposal of the products or even their industrial re-use (e.g. road construction, cement industry). Due to the common high reactivity of alkaline fly ashes no pre-treatment (e.g. grinding, using chemical additives) is needed compared to the use of natural silicate minerals as feedstock material. For these reasons mineral carbonation of alkaline residues can be considered as a process with low costs and low energy consumption, thus making it an interesting CO₂ reduction pathway from an economical point of view.

In **Chapter 1**, the mechanisms and rates of reactions between alkaline lignite fly ash and CO₂ in aqueous suspensions were evaluated. Aqueous laboratory experiments showed that CO₂ from flue gas can be bound directly as carbonate. Additionally, solutions with high dissolved inorganic carbon content are formed, which can be injected into aquifers for

mineral CO₂ sequestration. As the dissolution rates of the alkaline mineral phases are high, gas phase CO₂ transfer into the aqueous phase is mostly the limiting factor for the overall carbonation process. CO₂ dissolution is controlled by the solution pH, by the available surface area of the gas/water interface and by the gradient at that interface.

The maximum conversion of 5.2 moles of CO₂ per kg fly ash ($\approx 0.23 \text{ kg kg}^{-1}$) obtained at 75 °C demonstrates the high potential of alkaline fly ashes to sequester CO₂. This value accounts for a CO₂ sequestration capacity of nearly 3.5 million t of CO₂ in Germany alone based on the available lignite fly ash, which corresponds to 2 percents of the CO₂ emissions from lignite power combustion ($168 \text{ million t a}^{-1}$ in 2009).

In **Chapter 2**, laboratory carbonation experiments are described, which were carried out with the individual mineral phases CaO and MgO in aqueous solution. The process showed parallels with the reactions observed during carbonation of lignite fly ashes, suggesting that Ca and Mg (hydr)oxides can be used as proxies to estimate alkaline waste reaction with CO₂ in general.

The carbonation of CaO happens fast, occurs at high pH values > 12 and is controlled at the mineral surface by the dissolution of Ca(OH)₂. As long as Ca(OH)₂ is available CO₂ uptake by the system is high and leads to the simultaneous precipitation of calcite (CaCO₃). Under similar conditions MgO carbonation is a slower and much more complex process. In the presence of MgO an initial pH of ~ 10.8 , indicating solubility equilibrium, was reached. Subsequently, TDIC concentrations and EC increased almost linearly. The pool of MgO based alkalinity can be made available for mineral trapping if the kinetic restrictions for precipitation of Mg-carbonate can be overcome, e. g. by running the processes at higher temperature ($> 50 \text{ °C}$) and higher s/l-ratio. Corresponding to related work the precipitation of hydromagnesite ($\text{Mg}_5(\text{CO}_3)_4(\text{OH})_2 \cdot 4\text{H}_2\text{O}$) is found for temperatures above 50 °C already at a suspended amount of 4 g L^{-1} . Precipitation of nesquehonite ($\text{MgCO}_3 \cdot 3\text{H}_2\text{O}$) starts upon a suspended amount of MgO of more than 10 g L^{-1} at 25 °C .

In **Chapter 3** the setup and the results of a model are shown, which was used to simulate and evaluate the process of alkaline material carbonation over time. Experimentally derived specific dissolution rates for CaO/MgO and CO₂ are used for the development of a kinetic geochemical model based on the freely available PHREEQC algorithm. The software offers the access to databases, which containing thermodynamic constants of all common dissolved species in natural and industrial processes.

Experimental assays conducted in an aqueous carbonation reactor (see Chapter 1 and 2) were used as reference to test the model and evaluate its robustness and sensitivity.

The reaction course of the experiments based on the use of the pure phases (CaO and MgO) was successfully reproduced by our simulations. The developed model may thus be used as a valuable tool for the optimization of technical scenarios/facilities for CO₂ sequestration. In order to study different mineral sequestration scenarios for calcite precipitation, we used the simulation to test the variation of process parameters and the addition of chemical additives (CaCl₂, CaSO₄). Finally, the simulation of the carbonation of lignite fly ash was tested using our simplified model based on CaO, MgO, calcite, anhydrite as kinetic reactants. It was shown that advanced techniques to determine the exact mineralogy of combustion residues and the extension of the availability of thermodynamic data of specific mineral phases are necessary to improve geochemical modelling in future work.

In **Chapter 4**, the potential contribution of lignite fly ash to mineral CO₂ trapping in a high anhydrite (CaSO₄) containing aquifer were analyzed. The study examined the possibility of combining underground CO₂ storage and geothermal heat/energy production from an anhydrite rich aquifer. In such a scenario Ca²⁺ for the precipitation of calcite could be provided from the dissolution of the calcium sulfate. The dissolution of anhydrite concurrently releases acid, being counterproductive with respect to the formation of carbonates. The possibility of pH buffering by the addition of alkaline lignite fly ash is therefore appraised to optimize the conditions of carbonate precipitation.

The performed laboratory experiments, as basis for thermodynamic simulations with PHREEC, confirmed that the buffering capacity derived from the fly ashes is essential for calcite precipitation in such a system. Already with an addition of 0.1 weight percent of fly ash per volume of the injection solution the amount of precipitated calcite was maximized. The dissolution of anhydrite is associated with a concurrent increase in pore space and can balance the porespace reduction by precipitation of carbonates and secondary silicates in the geothermal reservoir.

ZUSAMMENFASSUNG

Mit Beginn der Industrialisierung seit Ende des letzten Jahrhunderts ist bis heute ein signifikanter, anthropogen verursachter Anstieg des Treibhausgases CO_2 in der Atmosphäre zu verzeichnen. Mit hoher Wahrscheinlichkeit steht nach gegenwärtigem wissenschaftlichem Verständnis damit der in den letzten Jahrzehnten beobachtete Anstieg der globalen Durchschnittstemperatur in Zusammenhang. Die Folgen und das Entgegenwirken der global beobachteten Klimaerwärmung stellen langfristig eine der größten Herausforderungen der Menschheit da.

Im Rahmen dieser Dissertation wurde ein Ansatz zur langfristigen, mineralischen Bindung von CO_2 unter Verwendung von Reststoffen untersucht. Im Fokus der Untersuchung stand erstmalig die Reaktion von Flugaschen aus der Braunkohle-Verbrennung mit CO_2 in wässriger Lösung. Bei alkalischen Flugaschen handelt es sich um ein kostengünstiges, hochreaktives Nebenprodukt der Kohleverbrennung. Die hohe Säure-Neutralisationskapazität (SNK) und Reaktivität der alkalischen Flugaschen eignet sich für die CO_2 -Bindung in technischen Prozessen. Sie gründet auf dem hohen Gehalt der alkalischen Elemente Kalzium (Ca) und Magnesium (Mg), welche durch den Feuerungsprozess vorwiegend in oxidischer Form (CaO , MgO) vorliegen. Die alkalischen Reststoffe werden damit nicht als ein Umweltproblem, sondern als nützliche Reaktanden für technische Prozesse zur CO_2 -Neutralisation bei Verbrennungsprozessen betrachtet.

Karbonate bilden aufgrund ihrer Stabilität im globalen Kohlenstoffkreislauf eine entscheidende CO_2 -Senke. Im Vergleich zu alternativen Speicherformen (z.B. Injektion in Gaslagerstätten) kann CO_2 auch über geologisch lange Zeiträume sicher gebunden und dem Kreislauf der Atmosphäre entzogen werden. Eine kostspielige Überwachung der Ablagerungsräume entfällt aufgrund der chemischen Stabilität der mineralischen Bindung. Die Karbonatisierung führt zusätzlich zu einer Schwermetall-Fixierung in den Reststoffen, wodurch eine umweltverträglichere Endlagerung bzw. die industrielle Weiterverwendung (z.B. im Straßenbau, Zementindustrie) möglich wird. Aufgrund der hohen Reaktivität der Verbrennungaschen ist im Gegensatz zu natürlichen Silikatmineralien keine Vorbehandlung (z.B. Aufmahlen, chemische Additive) notwendig. Daher fällt die Nettobilanz für die speicherbare CO_2 -Menge in Bezug zur eingesetzten Stoffmenge des Reaktionsmaterials für alkalische Reststoffe sehr hoch aus.

In **Kapitel 1** wird Geschwindigkeit und Mechanismus der Reaktionen zwischen alkalischen Braunkohle-Flugaschen und CO_2 in wässrigen Suspensionen beschrieben. Die

Karbonatisierungs-Experimente zeigen, dass CO_2 aus Rauchgas entweder direkt als Karbonat gebunden werden kann oder alternativ als alkaline Lösung für die spätere Injektion in einem Aquifer zur mineralischen Bindung von CO_2 bereitgestellt werden kann. Durch die schnelle Lösungskinetik der in den Flugaschen enthaltenen alkalischen Oxide (CaO und MgO) ist der CO_2 -Transfer in den Batch-Experimenten durch die Lösungskinetik von CO_2 limitiert. Die Löslichkeit der Oxide bestimmt dabei maßgeblich den pH-Wert der Prozesslösung und damit die CO_2 -Lösungs-Kinetik im System. Diese hängt vom pH-Wert aber auch von der verfügbaren Gas/Wasser-Grenzfläche und den Gas-/Wasser- CO_2 -Gradienten ab.

Bei einer Prozesstemperatur von 75 °C wurde die Bindung von 5.2 Mol CO_2 pro kg Flugasche ($\approx 0.23\text{ kg kg}^{-1}$) überwiegend in Form von Kalzit erreicht. Bezogen auf die verfügbare Menge an Braunkohleflugaschen in Deutschland entspricht das einer Neutralisationskapazität von 3.5 Millionen Tonnen CO_2 pro Jahr, was eine mögliche Reduktion 2 Prozent der CO_2 -Emissionen von Braunkohlekraftwerken bedeutet (168 Millionen t a^{-1} im Jahr 2009).

In **Kapitel 2** werden die Prozessabläufe der Reaktion der Einzelphasen CaO und MgO mit CO_2 in wässriger Lösung untersucht, da diese den CO_2 -Transfer in Reaktion mit den Braunkohle-Flugaschen maßgeblich bestimmen.

Die Auflösung von CaO verläuft schnell und führt dabei zur Freisetzung von Alkalität (pH-Werte > 12). Im Bereich des Lösungsgleichgewichtes von CaO ist die CO_2 -Aufnahme durch die hohen pH-Werte begünstigt und führt zur gleichzeitigen Ausfällung von Kalzit (CaCO_3). Bei der im Vergleich zu CaO langsameren Lösung von MgO stellen sich folglich kleinere pH-Werte (Lösungsgleichgewicht: $\sim 10,8$) ein. Bei gleichen Prozessbedingungen wird entgegen einer Karbonat-Ausfällung im MgO -System ein kontinuierlicher Anstieg von gelösten Mg-CO_2 -Spezies im Wasser beobachtet. Übereinstimmend mit verwandten Arbeiten kann gezeigt werden, dass die Fällung von Magnesium-Karbonaten aufgrund kinetischer Limitierungen erst bei Temperaturen oberhalb von 50 °C durch die Fällung von Hydromagnesit ($\text{Mg}_5(\text{CO}_3)_4(\text{OH})_2 \cdot 4\text{H}_2\text{O}$) oder für eine suspendierte Menge von MgO von mehr als 10 g L^{-1} bei 25 °C durch die Fällung von Nesquehonit ($\text{MgCO}_3 \cdot 3\text{H}_2\text{O}$) einsetzt. Die Lösungsexperimente zeigen zudem, wie die Belegung der Oberflächen-Plätze durch CO_3^{-2} und Protonen die Auflösung von MgO beeinflusst.

Die bestimmten „in-Situ“ Lösungsraten der Mineralphase CaO/MgO und von CO_2 wurden für den Aufbau des in **Kapitel 3** beschriebenen kinetischen, geochemischen Modells auf Basis des frei verfügbaren PHREEQC-Algorithmus verwendet. Der Algorithmus ermöglicht

den Zugriff auf Datenbanken, welche eine Vielzahl von thermodynamischen Konstanten gelöster Spezies in natürlichen und industriellen Prozessen enthalten.

Die Labor-Ergebnisse aus den Karbonatisierungs-Versuchen mit reinem CaO/MgO oder Flugaschen (Mineral-Lösung, -Ausfällung, CO₂-Lösung) (Kapitel 1 und Kapitel 2) dienen dabei zur Evaluierung des Modells hinsichtlich seiner Robustheit und Sensitivität.

Der Reaktionsverlauf der Experimente auf Basis der Verwendung von mineralogischen Einzelphasen (CaO und MgO) konnte durch den Modellansatz mit hoher Übereinstimmung reproduziert werden. Damit ist ein wertvolles Werkzeug für die Konzeption einer technischen, oberirdischen CO₂-Sequestrierung bereitgestellt. Die Simulationsergebnisse dienen des Weiteren der Prüfung optimierter Sequestrierungsszenarien zur mineralischen Bindung von Kalzit. Im Zuge der Simulation der Karbonatisierung von Flugaschen in wässriger Lösung waren die Unterschiede im Reaktionsverlauf im Wesentlichen auf die heterogene Zusammensetzung des Materials zurückzuführen. Das größte Verbesserungspotential für das hier verwendete Modell liegt in den genutzten Eingangsdaten. Als Hauptansatzpunkte für eine verbesserte Bewertung der Neutralisationskapazität von alkalischen Reststoffen sind die Entwicklung von verbesserten Untersuchungsmethoden bei der quantitativen Mineralphasenanalyse und die Bereitstellung charakteristischer thermodynamischer Daten für zukünftige Untersuchungen ausschlaggebend.

In **Kapitel 4** wurde die Zugabe von Braunkohle-Flugasche im Rahmen eines Sequestrierungs-Szenario untersucht, indem CO₂ in einen durch Anhydrit (Ca-Sulfat) geprägten Aquifer zur Reaktion gebracht wird. Die steigende Ca-Konzentration aus der Lösung der Sulfate soll dabei die Bildung von Kalzit aktivieren. Es wurde dabei erstmalig untersucht, das Potential einer möglichen CO₂-Speicherung in Verbindung mit dem Betrieb einer Anlage zur geothermischen Energiegewinnung zu nutzen.

Bei der Lösungsreaktion von Anhydrit kommt es zur Säurefreisetzung, die der Ausfällung von Kalzit im Allgemeinen entgegenwirkt. Die Möglichkeit der pH-Pufferung durch Beimengung von alkalischen Braunkohleflugaschen wurde daher zur Optimierung der Bildungsbedingungen für die Karbonatausfällung untersucht. Auf Basis der durchgeführten Laborexperimente zeigten thermodynamische Simulationsrechnungen, dass bereits mit einer Zugabe von 0.1 Gewichtsprozent Flugasche bezogen auf das Volumen der Injektionslösung die Menge an ausgefällten Kalzit maximiert werden kann. Es konnte weiterhin aufgezeigt werden, dass die Auflösung von Anhydrit mit einer Vergrößerung des Porenvolumens einhergeht, die die Volumen-Inanspruchnahme der ausgefällten Karbonaten und

von sekundären Silikaten sogar übersteigt. Dadurch ist die Grundvoraussetzung des Erhaltes der hydraulischen Permeabilität des geothermischen Reservoirs gegeben.

INTRODUCTION AND OUTLINE OF THESIS

Climate change and atmospheric increase of anthropogenic CO₂

The greenhouse effect has its origin in the absorption and reflection of thermal radiation from the earth's surface by gases and aerosols in the atmosphere. One major task of climate science is the quantitative comparison of the strength of different human and natural agents in causing climate change (IPCC, 2007). This is for example done by the concept of radiative forcing, which describes the change in the net irradiance of the tropopause (Ramaswamy et al., 2001). Compared to other long-lived greenhouse gases (e.g. methane (CH₄), nitrous oxide (N₂O), halocarbons and sulphur hexafluoride (SF₆)), carbon dioxide (CO₂) has the highest impact on global warming. While the impact of global warming still is a controversial issue on a political and scientific level, a substantial increase of the atmospheric CO₂ concentration from ~ 280 ppm in the pre-industrial era to 379 ppm in the year of 2005 is recorded at the remote site Mauna Loa, Hawaii (Baldwin et al., 2005). However, the first increase by 50 ppm above the pre-industrial value was reached in the 1970s after more than 200 years, whereas the second 50 ppm step was achieved in about 30 years. The highest average growth rate (19 ppm per decade) since direct atmospheric CO₂ measurements began in the 1950s was measured between 1995 and 2005 (IPCC, 2007). Particularly by the increasing energy demand of the developing countries, the U.S. Energy Information Administration (EIA) predicts an increase of world-wide CO₂ emissions from 29.7 to 42.4 billion metric tons (~ 70 percents) within the time period of 2007 to 2035 (EIA, 2010).

Various feedback mechanisms like the sea level rise and the cumulation of world-wide extreme weather events are assigned as major effects of global warming. Hence, the reduction of anthropogenic greenhouse gas emissions has become a global challenge of environmental research and policy.

The role of carbon capture and storage (CCS)

Strategies for the reduction of CO₂ emissions into the atmosphere generally imply the improvement of energy efficiency, use of renewable energy sources and carbon sequestration. Carbon dioxide capturing and storage (CCS) is a process consisting of the separation of CO₂ from industrial and energy-related sources, transport to a storage location and long-term isolation from the atmosphere (IPCC, 2005). The aim of carbon sequestration is to store the carbon dioxide released by the use of fossil fuels in order to prevent its emis-

sion to the atmosphere. CCS has recently emerged as an important option for reducing greenhouse gas emissions. However, to significantly reduce global emissions to pre-industrial levels, huge volumes of CO₂ must be sequestered.

The existing CCS technologies can be generally subdivided into three storage mechanisms: I) physical, II) biological and III) chemical storage.

Physical storage includes a wide range of sequestration techniques. Most conventional it may use a dense layer of impermeable rock that overlies the CO₂ deposit, which is for instance the case for depleted oil and gas reservoirs (Bachu and Shaw, 2003; Bergmann et al., 1997) or deep saline formations (Kaszuba et al., 2003; Soong et al., 2003). Also still operational oil or gas reservoirs can be used, and in this case the injection of CO₂ allows for an enhanced oil recovery from the reservoir. After injecting supercritical CO₂ into an aquifer in > 800 m depth, it will dissolve in the water, forming a dense fluid that may sink to the bottom of the storage reservoir. The same effect is exploited by deep ocean storage (Adams and Caldeira, 2008). Either the formation of lakes as CO₂ hydrate in deep basins or the dissolution of CO₂ in the water is thereby considered (Aya et al., 2004; Brewer et al., 2000). Moreover, an often discussed physical storage option is the adsorption of CO₂ onto unminable coal seams or mining waste (Hamayun, 2000; Kempka, 2006). The term “enhanced coal bed methane recovery” is in this context often used and describes the process of stimulating the recovery of methane present in unminable coal beds by CO₂ injection.

Biological storage includes the emplacement of CO₂ into the terrestrial biosphere (e.g. for-estation) and also one of the latest discussed fixation techniques proposing marine micro-organisms (e.g. algae) as carbon sink (Bennemann, 2003).

The fixation of CO₂ as inorganic carbonate is the most eminent process in terms of *chemical storage* and is often termed as mineral carbonation. The process is based on the reaction with CO₂ with a divalent metal oxide (MeO) to form insoluble carbonates (Eq. 1). The reaction is one of the major processes in the long-term global carbon cycle and is thermo-dynamically favored.



A further aspect of *chemical storage* is the fixation of CO₂ in different industrial processes, as for instance by the formation of synthetic organic compounds (Koinuma, 2007), however, with minor relevance up to date.

Many studies investigated the technical feasibility, potential, economics and barriers of different options of CCS. However, safety aspects, implying the long-term storage of CO₂, are key factors for the public acceptance and for the sustainability of reducing CO₂ emissions into the atmosphere.

The world-wide amount of CO₂ fossil-fuels emissions was estimated to be about 8.3 Gt C per year in 2007 (Marland et al., 2007). For comparison, Table 0.1 illustrates the estimated storage capacities of the different introduced CCS-options. It should be noted however, that the sequestration estimates for saline aquifers and coal beds are highly uncertain, although in the past several years, there has been some progress in developing standard methods for capacity estimation and improving regional estimates (Bachu et al., 2007). The theoretical capacity estimation of ocean storage is based on the saturation capacity of the water body without considering any secondary reactions. Focusing primarily on the estimated storage capacities, ocean and geological storage appear to be one of the most promising technologies (Table 0.1). The risk of environmental impact and the release of CO₂ back to the atmosphere are the major disadvantages of these techniques. To minimize these risks geological storage will though require extensive and cost-intensive monitoring programs.

Table 0.1: Estimated storage capacity of discussed CCS-options

Option	Estimated global capacity in gigatons of carbon (GtC)	Source
Ocean storage	5.000 - 10.000	(Adams and Caldeira, 2008)
Geological storage		
Aquifers	1.000 – 10.000	(Benson and Cole, 2008)
Depleted oil and gas fields	675 – 900	(Benson and Cole, 2008)
Unminable coal seams	3 – 200	(IPCC, 2005)
Mineral carbonation	very large/ inexhaustible	(Lackner et al., 1995)

Mineral carbonation

The volume of carbonate rocks world-wide illustrates the potential of mineral carbonation of CO₂ as a carbon sink. About 40.000 times more carbon is present in carbonate rocks than in the atmosphere (Oelkers et al., 2008). The process of carbonation is omnipresent in nature and is thermodynamically favoured. Carbonates are end-products of geological processes and mineral carbonation is thus assessed to a permanent and safe storage option of CO₂. However, the efficiency and kinetic of the overall procedure is under debate.

The supply of divalent metals, like calcium (Ca), magnesium (Mg) and iron (Fe), is the pre-condition and rate limiting step for the carbonation reaction to occur. These elements are

available in huge amounts in the earth crust, originally bound in silicate minerals of variable chemical compositions. However, it is complex to evaluate the total amount of available metal oxides usable for mineral carbonation. With respect to the total amount of available carbon from fossil fuels, the theoretical availability can be considered as inexhaustible. For instance, the naturally occurring mineral peridotites and serpentinites alone exceed the total Mg requirement to neutralize the CO₂ from all worldwide coal resources estimated at 10,000 Gt (Lackner et al., 1995).

Silicate minerals are generally characterized by a high chemical stability and may be exposed to different weathering processes over thousands of years until the dissolution and release of the metal ions occurs. As the most considerable acid in the natural environment, dissolved CO₂ itself increases the weathering process of silicate minerals and thereby contributes to an enhanced neutralizing process.

Basic rock conditions are characterized by high elemental contents of Ca, Mg and Fe against a higher content of sodium (Na), potassium (K) and silicic acid (SiO₂) being significant in acid rock compositions (Wilson, 1993). According to the required metal cations for carbonation (see above) this explains why basic rock compositions are most suitable for CO₂ sequestration. Furthermore, the trend of decreasing chemical stability from acid to basic mineral compositions is advantageous for intended CO₂ sequestration.

With respect to the advantage of long-term and safe storage of CO₂ by mineral carbonation, main research has been done in the last 20 years in order to characterize the technical feasibility, potential, economics and barriers of mineral carbonation using natural basic silicates as feedstock materials (Huijgen and Comans, 2005; Huijgen et al., 2007b; Huijgen et al., 2006b; Lackner et al., 1995; Oelkers et al., 2008; Zevenhoven et al., 2006).

The studied process routes can be classified in:

Ex situ vs. in situ: Carbonation performed as part of an industrial process or through the injection of CO₂ into geological formations (Oelkers et al., 2008).

Direct vs. indirect route: The mineral is carbonated in a single process step or metal cations are first extracted from the mineral matrix and then precipitated into carbonates in a second process step (Huijgen and Comans, 2003).

Gas-solid vs. aqueous carbonation route: Reaction of gas phase CO₂ with the mineral components occurs either in a dry step or with the help of water as reaction mediator, in which the dissolution of CO₂ the release of metal ions and finally the precipitation of carbonates take place.

Due to the low solubility of silicate minerals, direct aqueous carbonation has been found as the most promising process route because the presence of water enhances the reaction rate of mineral dissolution and the rate of carbonate precipitation (Huijgen and Comans, 2003). On the basis of the slow dissolution rates of most silicate minerals, heat or chemicals are needed to accelerate the process in a technical system. Moreover, mining and transportation is necessary to provide the mineral material. For the pre-processing of natural silicate minerals *mechanical* (e.g. mining, crushing, grinding and separation) and *chemical* (e.g. using heat, salts and acids) conditioning as process accelerator are proposed.

Using of alkaline residues for CO₂ sequestration

As an alternative to natural minerals different alkaline waste materials, such as residues from coal combustion, municipal waste combustion, steel production, oil shale combustion, cement production or the paper industry also have a potential for CO₂ binding and offer a high reactivity under ambient conditions (Baciacchi et al., 2009; Baciacchi et al., 2010; Back et al., 2008; Bonenfant et al., 2008; Huijgen et al., 2005; Huntzinger et al., 2009; Perez-Lopez et al., 2008; Teir, 2006; Uibu et al., 2009).

As byproducts of combustion or energy intense manufacturing processes these materials have formed at high temperatures and are commonly produced at CO₂ point sources. Caused by the high temperatures during combustion, these waste streams generally contain reactive Ca/Mg (hydr) oxides and therefore offer a high alkalinity and basic metal content. Many alkaline residues contain considerable amounts of free lime as the most active component (Uibu et al., 2009). In order to achieve chemical stabilization and avoid heavy metal leaching, huge amounts of pH neutralizing agents such as limestones are commonly added during landfilling operations and represent a significant cost to electric utilities.

Furthermore, alkaline wastes often have a large specific surface area and small grain size and thus offer a high reactive surface area (Fernandez Bertos et al., 2004; Huijgen et al., 2005; Lekakh et al., 2008). The basic mineral phases are commonly highly reactive and unstable under pH neutral conditions. This leads to a fast dissolution in an aqueous environment releasing metal and hydroxide ions. The resulting high pH accelerates CO₂ dissolution in water and the dissociation of carbonic acid (Usdowski, 1982). Finally, the supersaturation of the solution leads to the precipitation mainly of Ca and Mg carbonates and carbon is permanently removed from the atmosphere.

Treatment of alkaline residues with CO₂, as neutralizing agent, can therefore lead to a sustainable waste management, since accelerated carbonation is achieved and the emission of CO₂ is diminished. The waste streams thus represent an opportunity to reclaim some of the carbon dioxide emitted during the manufacturing process. Furthermore also physical changes caused by the carbonation reaction might be beneficial for further use (Stolaroff et al., 2005). In order to make CO₂ binding by alkaline materials technically feasible, treatment pathways are required, in which the potential is utilized to a large extent within short periods of time.

Beside the carbonation above ground, a further aspect is to use alkaline residues as caustic material for mineral trapping in brine solutions, as already proposed by Soong et al. (2006).

Objective of the dissertation

Germany is one of the leading lignite coal producers with 155 Mt of lignite coal being used for power generation in 2009. This corresponds to 168 Mt/year of CO₂-emissions and to round about 15 Mt/year accumulating as fly ash during combustion process. The potential of the neutralizing reactions of these residues is therefore considered substantial in terms of emission trade. The largest amount of brown coal fly ash is still being deposited in landfills as residual waste material and is therefore available for CO₂ neutralisation.

The overall objective of this thesis is to propose a technical procedure that sufficiently fast removes CO₂ from flue gas by using alkaline residues. By the process of aqueous carbonation using alkaline residues, CO₂ can be sequestered either I) directly as carbonate or II) as an alkalinity-containing solution (ACS) that is ready for injection into a proper aquifer for mineral trapping. The carbonated alkaline residual material might be finally used as feedstock material for other industrial purposes or being deposited in landfills (Figure 0.1). Both, the neutralisation of carbonic acid and the carbonation process provide two effective mechanisms for CO₂ binding in a technical system.

In order to evaluate the potential of lignite fly ash carbonation for CO₂ sequestration laboratory experiments were carried out and a geochemical reaction model was set up. The experiments were designed in order to allow the direct treatment of the flue gas at ambient process conditions. This way the process can be evaluated independently from the specific CO₂ source.

To provide necessary geochemical and kinetic data, the dependence of the CO₂ uptake rate on the relevant process variables, e.g. partial pressure of CO₂ (pCO₂), solid/liquid(s/l)-ratios and purging rates were studied in batch reactor experiments.

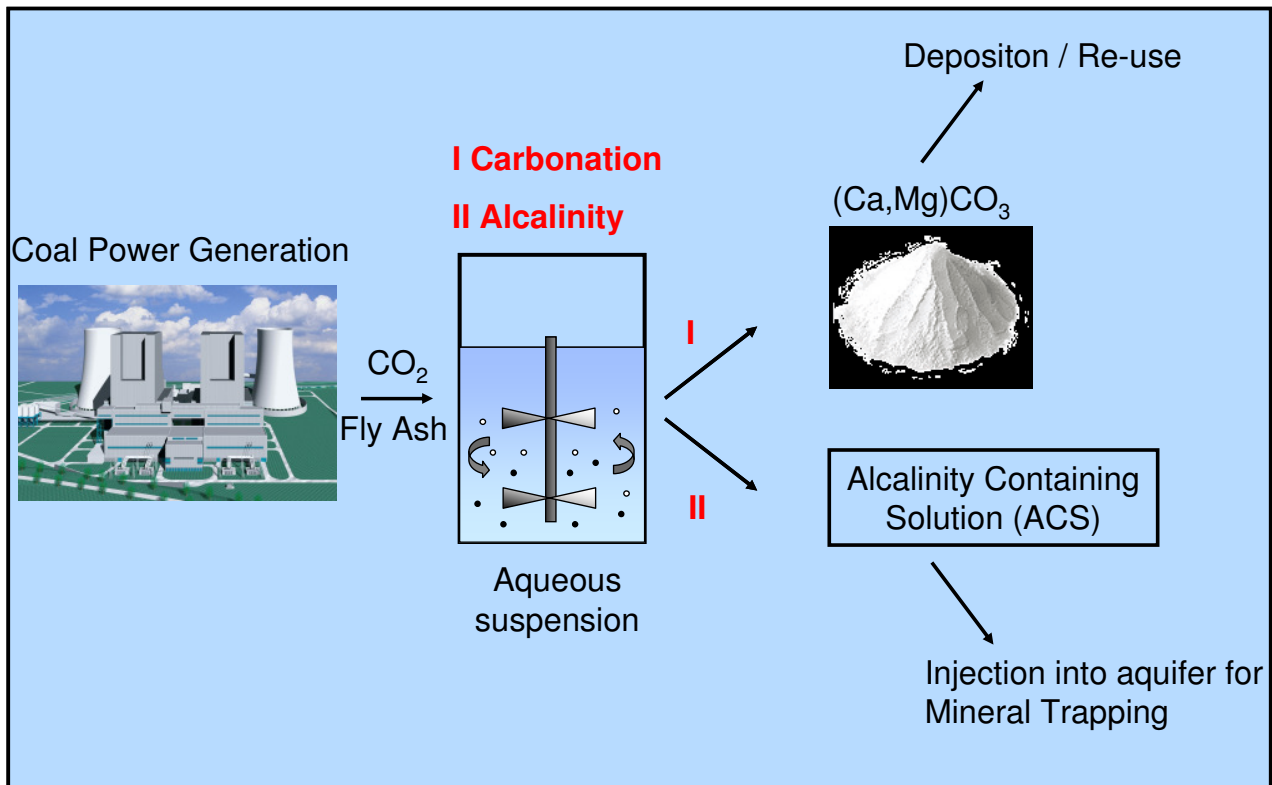


Figure 0.1: Proposed treatment scheme using reacting lignite fly ashes: Direct Carbonation (I) of Ca/Mg-minerals as a sink of CO₂. The residual ACS (II) can be used for injection into aquifers for mineral trapping

In the second step the experiments were designed to gain principal information about the reactivity and reaction mechanisms of CO₂ with pure alkaline CaO/Ca(OH)₂ and MgO/Mg(OH)₂ phases. The intention was to understand the overall limiting factors of CO₂ transfer into an alkaline aqueous solution in order to obtain maximum CO₂ binding and to elucidate the conditions at which Ca and Mg carbonate precipitation is preferential.

Moreover, the determined rate parameters for the dissolution of Ca and Mg oxides/hydroxide and CO₂ were intended to be used for the development of a geochemical model to simulate and optimize different sequestration scenarios using alkaline residues for mineral trapping more generally at the desired process conditions of low-temperatures (25 °C – 75 °C) and low partial CO₂ pressures (0.01 MPa – 0.03 MPa) of CO₂.

The **outline** of this thesis is as follows:

Chapter 1 focuses on the aqueous carbonation reaction using lignite fly ashes and flue gas in chemical reactors at the desired process conditions of low-temperatures (25 °C – 75 °C) and low partial CO₂ pressures (0.01 MPa – 0.03 MPa) of CO₂. In order to provide kinetic parameters to calculate scenarios for an optimum treatment strategy, the dependence of the CO₂ uptake rate on the relevant process variables, e.g. partial pressure of CO₂ (pCO₂), solid/liquid(s/l)-ratios and purging rates of CO₂ are performed in batch reactor experiments.

Chapter 2 presents the response of the (hydr)oxides of Ca and Mg in reaction with CO₂ in aqueous suspensions at low-temperatures (25–75 °C) and low partial pressures of CO₂ (0.01 MPa). Experiments are designed with pure mineral phases in order to evaluate the controls on the mechanisms of mineral dissolution and Mg carbonate precipitation.

For the development of a geochemical model based on the PHREEQC code, the experimentally determined dissolution rate constants of CaO/MgO and CO₂ are put together with published rate expressions for calcite and anhydrite dissolution/precipitation (**Chapter 3**). This is done to review our process understanding of aqueous carbonation using alkaline phases and to identify further lack of knowledge. After testing its sensitivity and robustness the evaluated model is then used to predict the carbonation reaction of selected sequestration scenarios like the addition of dissolved CaCl₂ or solid anhydrite into a solution based on MgO derived alkalinity. Finally, we test the feasibility of simulating the more complex chemical scenario of lignite fly ash carbonation by our simplified model approach.

In **Chapter 4** the evaluation of a novel approach of CO₂ sequestration that is based on the combination of CO₂ storage and geothermal energy production is presented. The feasibility of the injection of an ACS into a reservoir is simulated to initiate the precipitation of calcite in return of anhydrite dissolution. The proposed process of mineral trapping requires alkalinity which is tested to generate with lignite alkaline fly ashes or from plagioclase in the reservoir. The simulations are based on results from batch experiments to study mineral dissolution (e.g. anhydrite, lignite fly ash) and core flooding experiments at reservoir conditions.

In the **Epilogue**, the final conclusions and the feasibility of mineral carbonation using alkaline residues are drawn and recommendations for further research are given.

CONTRIBUTIONS TO DIFFERENT STUDIES

Chapter 1

Reactivity of alkaline lignite fly ashes towards CO₂ in water

M. Back:	70 %	Laboratory work: Batch reaction and chemical analysis; Data analysis; Discussion of results; Manuscript preparation
M. Kühn:	5 %	Discussion of results
H. Stanjek:	5 %	Analysis of mineralogical composition; Discussion of results
S. Peiffer:	20 %	Discussion of results; Manuscript preparation

Chapter 2

Sequestration of CO₂ after reaction with alkaline earth metal oxides CaO and MgO

M. Back:	70 %	Laboratory work: Batch reaction and chemical analysis; Data analysis; Discussion of results; Manuscript preparation
M. Bauer:	20 %	Discussion of results; Manuscript preparation; Text editing
S. Peiffer:	10 %	Discussion of results

Chapter 3

Application of a PHREEQC based kinetic model to simulate process and dynamics of the carbonation of alkaline materials by gas phase derived CO₂ in aqueous systems

M. Back:	70 %	Laboratory work: Batch reaction and chemical analysis; Data analysis; Simulation; Manuscript preparation
M. Bauer:	20 %	Discussion of results; Laboratory experiments using anhydrite; Text editing
S. Peiffer:	10 %	Discussion of results; Text editing

Chapter 4

Mineral Trapping of CO₂ in operated hydrogeothermal reservoirs

M. Back, S. Peiffer	15 %	Laboratory experiments; Discussion of results; Manuscript preparation
M. Kühn, C. Clauser:	60 %	Laboratory work: Batch reaction and chemical analysis; Data analysis; Discussion of results; Manuscript preparation
K. Vosbeck, H. Stanjek:	15 %	Laboratory experiments; Discussion of results
V. Meyn:	10 %	Analysis of mineralogical composition; Discussion of results

Chapter 1

REACTIVITY OF LIGNITE FLY ASHES TOWARDS CO₂ IN WATER

Published in similar form as:

M. Back, M. Kühn, H. Stanjek & S. Peiffer (2008) Reactivity of Alkaline Lignite Fly Ashes toward CO₂ in water, *Environmental Science and Technology* 42, 4520-4526.

1 REACTIVITY OF ALKALINE LIGNITE FLY ASHES TOWARDS CO₂ IN WATER

Martin Back¹, Michael Kühn², Helge Stanjek³, Stefan Peiffer¹

The reaction kinetics between alkaline lignite fly ashes and CO₂ (pCO₂ = 0.01 MPa - 0.03 MPa) were studied in a laboratory CO₂ flow-through reactor at 25 °C – 75 °C. The reaction is characterized by three phases that can be separated according to the predominating buffering systems and the rates of CO₂ uptake. Phase I (pH > 12, < 30 min) is characterised by the dissolution of lime, the onset of calcite precipitation and a maximum uptake, the rate of which seems to be limited by dissolution of CO₂. Phase II (pH < 10.5, 10 – 60 min) is dominated by the carbonation reaction. CO₂ uptake in phase III (pH < 8.3) is controlled by the dissolution of periclase (MgO) leading to the formation of dissolved magnesium-bicarbonate. Phase I could be significantly extended by increasing the solid-liquid ratios and temperature, respectively. At 75 °C the rate of calcite precipitation was doubled leading to the neutralization of approx. 0.23 kg CO₂ per kg fly ash within 4.5 hours, which corresponds to nearly 90 percent of the total acid neutralizing capacity.

¹ Department of Hydrology, University of Bayreuth, BayCEER, D-95440 Bayreuth, Germany

² Applied Geophysics, RWTH Aachen University, D-52065 Aachen, Germany

³ Clay and Interface Mineralogy, RWTH Aachen University, D-52065 Aachen, Germany

1.1 Introduction

Amongst the various CO₂ sequestration scenarios, mineral trapping is regarded to be the most promising technique with regard to a permanent and inherently safe storage of CO₂ (Lackner et al., 1995). Carbonation of Ca and Mg-rich minerals (e. g. wollastonite) is well known from natural weathering processes (Wolff-Boenisch et al., 2006) and may have the capacity to bind the global CO₂ emission from fossil fuel combustion (1). Since the carbonation process proceeds with slow reaction kinetics (Wolff-Boenisch et al., 2006), its acceleration by technical means has been widely studied (Huijgen et al., 2006a; Teir et al. 2005). However, the use of natural silicate minerals is generally associated with high energy and economic costs and it is therefore discussed critically (Huijgen et al., 2006c).

Alternatively, alkaline ashes from combustion processes are proposed as a feedstock material that is cheap, highly reactive and that is generated as a by-product of power generation (Huijgen et al., 2006a; Soong et al. 2006; Stolaroff et al., 2005). In this work, we present results from an experimental study on the reaction between fly ashes from lignite combustion and CO₂ in aqueous solution. Lignite fly ashes are available in large amounts in many coal combusting countries and commonly have a high acid neutralizing capacity (ANC) of up to 7 meq g⁻¹ (RWE, 1995). In Germany, about 15 million tons of lignite fly ashes accumulate per year that are being mainly deposited in landfills (RWE, 1995). Hitherto, studies on the reactivity of fly ashes had been performed mainly with respect to the long-term leaching behavior (Fernandez Bertos, 2004; Meima et al., 2002; Querol et al., 2001) classifying them as non-hazardous waste material (EPA, 2000). Our knowledge about the short term reactivity of fly ashes with CO₂ is, however, scarce.

In particular, we aim to establish a general model for the mechanisms controlling the CO₂ transfer to the ash minerals at a time scale relevant for a technical solution. We have therefore set up experiments to study CO₂ storage by lignite fly ashes in aqueous suspensions at low temperature (25 °C – 75 °C) and CO₂ partial pressures comparable to flue gas observed from lignite combustion (0.01 MPa - 0.03 MPa). These conditions allow to mimic CO₂ removal from flue gas at a distinctly lower energy demand compared to other CO₂ sequestration techniques (Huijgen et al., 2006c). The aqueous route was chosen because generally higher reaction rates are observed compared to the gas-solid route (Bertos et al., 2004). The effect of transport phenomena at the solid-liquid and gaseous-liquid interfaces on the rate of CO₂ transfer was tested by variation of the stirring rate in the suspensions. Similarly, the effect of solution chemistry on mineral dissolution and CO₂ transfer mechanisms was studied by variation of the solid-liquid (s/l) ratios.

1.2 Experimental section

Sample characterisation

Fly ashes from a lignite coal power plant (Neurath, Germany) were used in this study. The fly ashes were collected from the 1st filtering step of connected electrostatic precipitators and stored in containers sealed from ambient air. Residual coal particles > 250 µm were separated from the ashes by sieving.

The chemical composition of the fly ashes was determined using X-ray fluorescence analysis (XRF) after measuring and correcting for the loss of ignition (LOI) at 1150 °C. The mineralogical composition was studied by X-ray powder diffraction (XRD) with a *Huber 423* goniometer with scan runs from 2° to 110° (2 θ, Co K_α), increments of 0.018° and 10 seconds counting time per step. Quantitative phase analysis based on the Rietveld technique was performed with the program BGMN (Bergmann & Kleeberg, 1998). Due to the common problem of mineral phase quantification in materials containing amorphous phases we added an internal standard (ZnO) which enabled to re-calculate the proportion of unaccounted phases during the Rietveld procedure. The single-point BET surface area of the fresh fly ashes was determined by using a porosimetry system (*Micromeritics ASAP 2010*). Particle size distribution was measured by laser diffraction (*Malvern Mastersizer 2000*) after decomposition of organic matter with H₂O₂ (30 %) and dispersion of the suspension in an ultrasonic bath. SEM pictures were taken using a *LEO-1450VP* SEM equipped with an EDX system (*Inca, Oxford Instruments*).

Experiments

A 3.7 L batch reactor facility (*ALF, Bioengineering*) was used to perform experiments in the presence of CO₂ at different solid-liquid ratios, partial pressure of CO₂ (pCO₂), stirring rates, and temperatures. Control experiments in the absence of CO₂ were run in a nitrogen atmosphere. The experimental setup is shown under Supporting Information Section A.

The ashes were inserted through a port at the top of the reactor using a funnel. The electrical conductivity (EC), pH, pCO₂, and temperature were recorded continuously during each experimental run. The suspension was sampled periodically and filtrated (nylon filter: 0.45 µm) to analyze the composition of both the solid and the liquid phases. Solid samples were freeze-dried and homogenised to determine the mineralogical (XRD) and elemental composition (XRF). The content of organic carbon was determined as the difference between the total carbon content (as measured with an element analyzer) of unreacted samples and samples after dissolution in HCl. The filtrate was acidified with 1 vol.-% of HNO₃

(65 %). Main (Ca, Mg, Na, K, S) and trace elements (Al, Ba, B, Cd, Mn, Fe and Sr) were determined by ICP-OES.

The suspension was flushed with CO₂ at different partial pressures (10-30 % at atmospheric total gas pressure) that were obtained after mixing of N₂ and CO₂ at different proportions with two mass flow controllers (*MKS Instruments, Type 258C*) at a total gas flow of 1 L min⁻¹. The gas was bubbled into the solution through a gas frit.

The CO₂ uptake of the system (mmol g⁻¹) was determined by measurement of the CO₂ concentration of the exhaust gas using an optical IR-sensor (*Vaisala, GMP221*) and from known gas fluxes. The partial pressure of CO₂ was calculated from the CO₂ concentration measured at atmospheric gas pressures:

$$CO_2 \text{ uptake (mmol g}^{-1}\text{)} = \sum_i^n \frac{(pCO_{2in} - pCO_{2out})_i \cdot \Delta t \cdot Q}{R \cdot T \cdot M} \quad (\text{Eq. 1.1})$$

pCO_{2out}: mean value of pCO₂ in the outflow in a 10 sec time (Δt) interval (10⁻³ N m⁻²)

Q: flow rate (m³ s⁻¹)

R: gas constant (0.083144 J mol⁻¹ K⁻¹)

T: temperature (K)

M: mass of fly ash (g).

The IR sensor had a response time T₆₃ (cf. Supporting Information Section B) of 20s which implies a certain delay upon fast changes of the measured pCO₂. The water temperature was kept constant and equilibrated with a certain pCO₂ before the addition of the ashes into the reactor. The stirring rate was varied between 150-600 rounds per minute and the s/l-ratio between 25 g L⁻¹ -100 g L⁻¹.

Total dissolved inorganic carbon (TDIC) was determined as CO₂ in a gas sample taken from gas-tight vials after acidification of a sample taken from the reactor with a gas-tight syringe. After filtering the sample through a nylon filter (0.45 μm), 0.5 ml -1 ml of the solution was injected into N₂ purged vials containing 100 μL of HCl (c = 6 mol L⁻¹). CO₂ was measured by gas chromatography with a TCD/FID detector. The amount of TDIC was calculated applying Henry's law considering the known volumes of headspace and solution:

$$TDIC = \frac{ppm}{10^6} \left(K_H + \frac{V_G}{R \cdot T \cdot V_W} \right) \quad (\text{Eq. 1.2})$$

V_G: gas volume of headspace (L)

V_W: volume of solution (L)

K_H: henry constant (10^{-1.41} mol L⁻¹ atm⁻¹ at 25 °C)

The mass transfer of CO₂ into solid metal carbonate was calculated as the difference between the total uptake of CO₂ and TDIC. The accuracy of this method was tested as described under Supporting Information Section B. Ca conversion was calculated from the amount of precipitated calcite and the amount of Ca in solution normalized to the Ca content of the initial fly ash.

The reactor system was equipped with an automatic titration system, which allowed to perform pH-stat experiments in a N₂ atmosphere to determine the ANC of the fly ashes and the release of the main elements at pH = 7-10 ($c(\text{HCl}) = 1 \text{ mol L}^{-1}$). Additionally, pH-stat experiments were run with NaOH ($c = 1 \text{ mol L}^{-1}$) in deionized water to measure the specific dissolution rate of CO₂ at varying pH (7-10) and stirring rates (300 rpm - 700 rpm). The effect of the variable ionic strength was not considered in these experiments.

1.3 Results and discussion

Composition of fly ashes

Combined XRD/Rietveld analysis (Table 1.1) of the untreated ashes revealed the occurrence of brownmillerite ($\text{Ca}_2(\text{Fe}_{1.634}, \text{Al}_{0.366})_2\text{O}_5$), anhydrite (CaSO_4), periclase (MgO), lime (CaO), calcite (CaCO_3), sodium sulphate (Na_2SO_4), quartz (SiO_2) and traces of gehlenite ($\text{Ca}_2\text{Al}_2\text{SiO}_7$), magnetite (Fe_3O_4), portlandite $\text{Ca}(\text{OH})_2$ and microcline (KAlSi_3O_8), respectively. The content of non-crystalline phases was calculated to be 28.5 wt.-% which seem to be mainly molten glass as indicated by the SEM images (cf. Supporting Information Section-D). The main elements in terms of wt.-% of oxides were CaO (37.3 ± 3), MgO (15.4 ± 0.4), SO₃ (13.7 ± 0.7), Fe₂O₃ (10.1 ± 1), SiO₂ (8.7 ± 2.5), Na₂O (3.4 ± 0.4), Al₂O₃ (2.7 ± 0.9) K₂O (0.4 ± 0) and C_{tot} (6.5 ± 0.5), as determined by XRF and CNS. After separating residual coal particles the content of organic carbon decreased to 2.5 wt.-% \pm 0.5 wt.-%.

The untreated ash generally seems to be very fine-grained with more than 90 percent of the particles being smaller than 100 μm (cf. Supporting Information Section-D) containing a large surface area of 38 $\text{m}^2 \text{g}^{-1}$.

Table 1.1: Relative mineralogical composition of the lignite fly ash before and after 10 minutes of CO₂ treatment (s/l-ratio: 75g L⁻¹, pCO₂: 0.02 MPa, stirring rate: 450 rpm, T: 25 °C).

mineral phase (Rietveld analysis)	wt.-% unreacted	wt.-% CO ₂ -treated after 10 min
brownmillerite	20.5	20.5
anhydrite	13	7
lime	11.5	3
periclase	11.5	11.5
Na ₂ SO ₄	5	0
calcite	3.5	6
quartz	3	3
amorph. compounds	28.5	42.5
ettringite	0	3.5

Reaction between fly ash and water

The acid neutralizing capacity of the fly ashes seems to be controlled by the dissolution of lime as indicated by the release of Ca with values up to 6 meq (g ash)⁻¹ at pH 7 after only 60 minutes of reaction at a s/l-ratio of 12.5 g L⁻¹ (Figure 1.1-A). The initial release rate of Ca increases with decreasing pH, i.e. with increasing distance from the solubility equilibrium of lime. Mg release became relevant only at pH <8 with a maximal concentration of 0.4 meq g⁻¹ at pH 7. Contrary to lime, dissolution of periclase as the Mg bearing phase requires neutral to acidic conditions to allow detachment of surface bound Mg²⁺ (Vermilye, 1996).

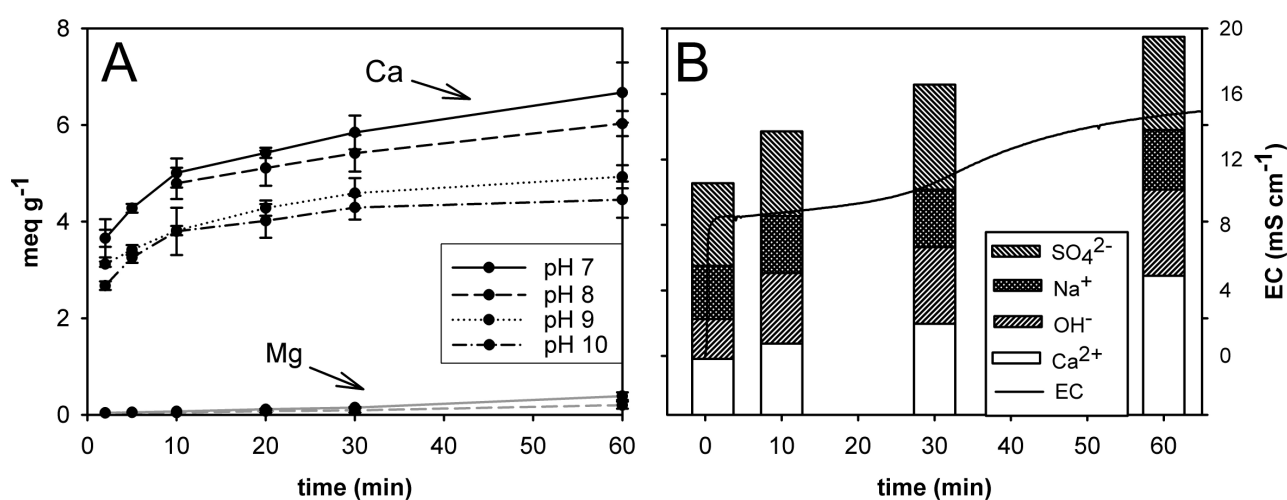


Figure 1.1: Batch experiments with deionized water and fly ash at a s/l-ratio of 12.5 g L⁻¹ and a temperature of 25 °C under nitrogen atmosphere. -A: Release of Ca and Mg (meq g⁻¹) during pH-stat-experiments. -B: Release of main elements (meq g⁻¹). The pH was always > 12.

The absence of Fe and Al in solution coincides with the observed precipitation of ettringite (Ca₆(Al(OH)₆)₂(SO₄)₃ · 26H₂O) of ~ 3 wt.-% (data not shown) and also reflects the low solubility of brownmillerite and gehlenite.

Once exposed to water, the fly ashes were highly soluble and showed a rapid release of the main constituents Ca, Na, SO₄²⁻ and OH⁻ into the solution (Figure 1.2-B), which was accompanied by a strong increase of pH (up to 12.8) and electric conductivity (EC) up to 11 mS cm⁻¹ only seconds after addition of the ashes.

Na concentrations released from fly ashes remained almost unchanged over the whole experimental run, suggesting that the dissolution of Na₂SO₄ was complete already after the first minutes (Eq. 1.3):



The amount of sulfate was nearly twice the value of Na indicating also the dissolution of anhydrite in the initial phase, the content of which decreased by 30 % within the experimental period. Ca together with OH⁻ concentrations further increased with time. Ca release appears to occur in two stages: an initial rapid release due to the dissolution of both, anhydrite, (Eq. 1.4)



and of lime (Eq. 1.5):



which explains also the rapid increase of the pH. Similar to the observations made at constant pH (Fig. 1-B), the dissolution rate of lime seems to decelerate upon increase of the pH which we attribute to both, the saturation with respect to lime and the exhaustion of the lime pool (11.5 to ~ 3 wt.-% after 10 minutes, Table 1.1).

Reaction between CO₂ and fly ash

Figure 1.2-A shows the temporal variation of pH, EC and pCO₂ during one experimental run. Three reaction phases can be identified that can be separated according to the two pH-inflection points *i*₁ at pH = 10.3 and *i*₂ at pH = 8.3.

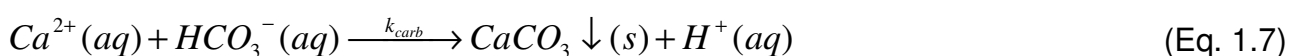
Phase I is characterised by high pH values accompanied by a strong increase of EC. The inflection point matches the equivalence point of the CO₃²⁻/OH⁻-system which, depending on the TDIC concentration, is located at pH ≈ 10.3 (Stumm & Morgan, 1996). Hence, the

high pH values measured in phase I reflect the caustic alkalinity generated by the dissolution of lime (Eq. 1.5). Dissolution of periclase



is negligible in this phase since its dissolution rate is low at high pH (16).

The occurrence of caustic alkalinity suggests that the dissolution of lime is significantly faster in this phase than the OH⁻-consuming carbonation reaction. This assumption is supported by the build-up of high Ca concentrations after only seconds of reaction. The following drop of EC, accompanied by a decrease of Ca in solution, denotes the onset of the carbonation reaction (Eq. 1.7) after 5 minutes,



which is accompanied by a maximum CO₂ uptake of 0.7 mmol g⁻¹ after 10 minutes (the 2-3 minutes delay of the pCO₂ minimum relative to the EC maximum is caused by the inertia of the CO₂-sensor). Rapid calcite precipitation in phase I could be confirmed by XRD measurements. Calcite seems to be the only carbonate mineral since magnesium carbonates were not detectable in the CO₂-treated fly ash samples at any time. The continuous drop in pH therefore seems to be related to the direct transfer of Ca from the lime pool into calcite. Exhaustion of this pool decreases the dissolution rate of lime to values significantly lower than the carbonation rate which then leads to a significant shift of the pH regime into the carbonate buffer system.

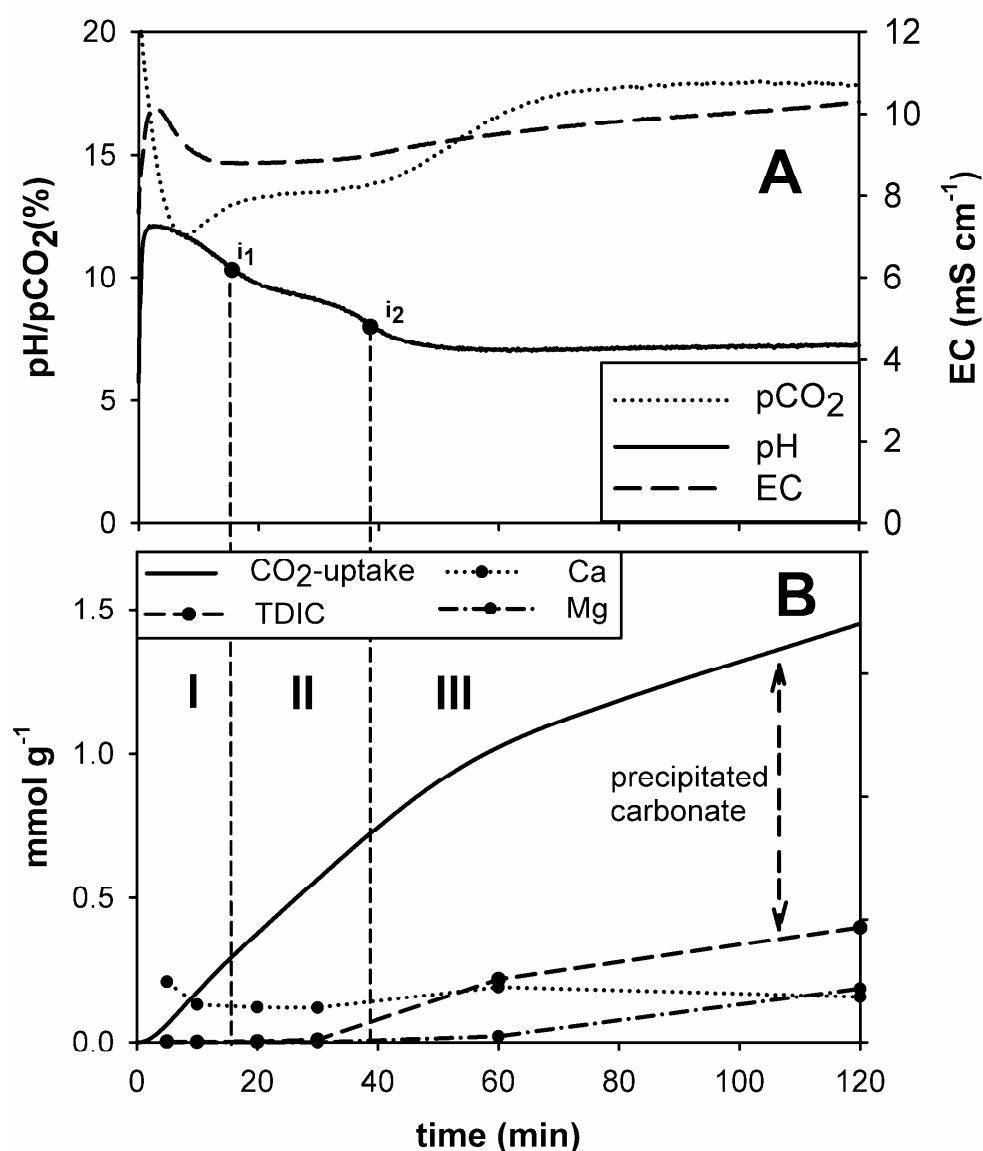
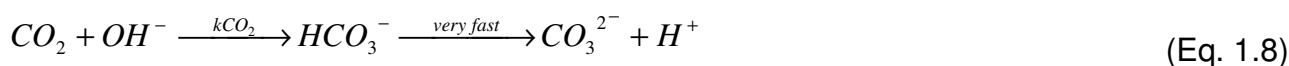


Figure 1.2: Reaction progress in fly ash experiment with water and CO₂ (s/l-ratio = 75g L⁻¹; initial pCO₂ = 0.02 MPa; stirring rate = 300 rpm). -A: pH, pCO₂ and EC.-B: total uptake of CO₂, precipitated amount of carbonate, TDIC and dissolved contents of Ca and Mg per gram fly ash.

Carbonation seems to be fast relative to the transfer of gaseous CO₂ into the aqueous phase since no build-up of TDIC in this initial phase was observed. At the present high pH values however (> 9) the CO₂ transfer is predominated by the reaction path described in Eq. 1.8. The forward rate constant k_{CO_2} given in literature is $8.5 \cdot 10^{-3} \text{ L mol}^{-1} \text{ s}^{-1}$ (Stumm & Morgan, 1996), resulting in higher rates than observed in our study at pH 12 ($0.026 \text{ mmol L}^{-1} \text{ s}^{-1}$):



Phase II is dominated by the carbonation reaction that consumes alkalinity and drives the pH towards lower values. The onset of HCO₃⁻ formation (as TDIC) at the end of phase II indicates deceleration of the carbonation reaction which is due to exhaustion of the lime pool. The pH of the solution is now buffered by the equilibrium between dissolved CO₃²⁻ and HCO₃⁻ so that the pH rapidly decreases to values below the equivalence point of this buffering system (pH 8.3).

CO₂ uptake in phase III is to a significant extent controlled by the formation of TDIC. Only now, also periclase dissolves (Eq. 1.6) which neutralizes CO₂ mainly as dissolved Mg-bicarbonate.

The pH remains nearly unchanged during this phase suggesting that proton consumption in reaction 5 and proton generation in reaction 7 balance each other under these conditions. The coupled increase of TDIC and Mg²⁺ at the end of the experiments implies that dissolution of periclase controls the CO₂ transfer during this phase. Mg concentrations are almost balanced by the generation of TDIC.

To summarize, the time response of the reaction between CO₂ and fly ashes in aqueous solutions is mainly driven by the rates of alkalinity providing reactions, i. e. dissolution of lime and periclase, and rates of alkalinity consuming reactions, i. e. precipitation of calcite and build-up of TDIC. These reactions control the pH which itself feeds back on the reaction velocities of the individual reactions and on the pathways of the reaction. In the following we will discuss the effect of the process variables on the development of the various process phases and how they control the CO₂ uptake.

Effect of process variables on CO₂ uptake

CO₂ partial pressure. The effect of the pCO₂ on the CO₂ uptake was tested at pCO₂ = 0.01, 0.02, 0.025 and 0.03 MPa. At the lowest pCO₂ the pH never fell below 9 (Figure 1.3). Neither TDIC nor Mg²⁺ could be detected which implies that CO₂ is completely transformed into calcite. At higher pCO₂ values a significant drop of the pH can be observed after 10-20 minutes accompanied by a build-up of Mg²⁺ and TDIC. Calcite still precipitated once phase III (pH < 8.3) had established, although at a significantly lower rate. The total uptake of CO₂ under these conditions was increased from 1.0 mmol g⁻¹ (pCO₂ = 0.01 MPa) to 1.47 mmol g⁻¹ (pCO₂ = 0.025 MPa) due to the coeval precipitation of carbonate and formation of TDIC.

At the highest pCO₂ applied in the experiments (pCO₂ = 0.03 MPa) the lowest pH values were measured. Calcite precipitation finished after only 20 minutes at a pH of approxi-

mately 6.6, reducing the net uptake of CO₂ to 1.4 mmol g⁻¹ after 120 minutes of reaction even though higher TDIC values were observed.

It appears that the supply rate of alkalinity from dissolution of lime is not sufficient to maintain a pH high enough for calcite precipitation at high pCO₂ values, which is due to an increased dissolution rate of CO₂ at higher partial pressure. pH-stat experiments performed in deionized water (pH 9, T=25 °C, stirring rate: 300 rpm) demonstrated that the dissolution rate of CO₂ increased almost linearly from 0.007 mmol L⁻¹ at a pCO₂ of 0.01 MPa to 0.02 mmol L⁻¹ at a pCO₂ of 0.03 MPa.

To summarize, the effect of pCO₂ on CO₂ uptake is twofold. Higher pCO₂ values lead to a temporal shift of the pH regime that significantly affects the pathways of CO₂ uptake. The uptake rate is generally enhanced at higher pCO₂ due to the higher dissolution rate of CO₂. Above a threshold of pCO₂ = 0.025 MPa a pH establishes (< 6.9) that suppresses calcite formation during phase II and thus reduces the amount of CO₂ sequestered.

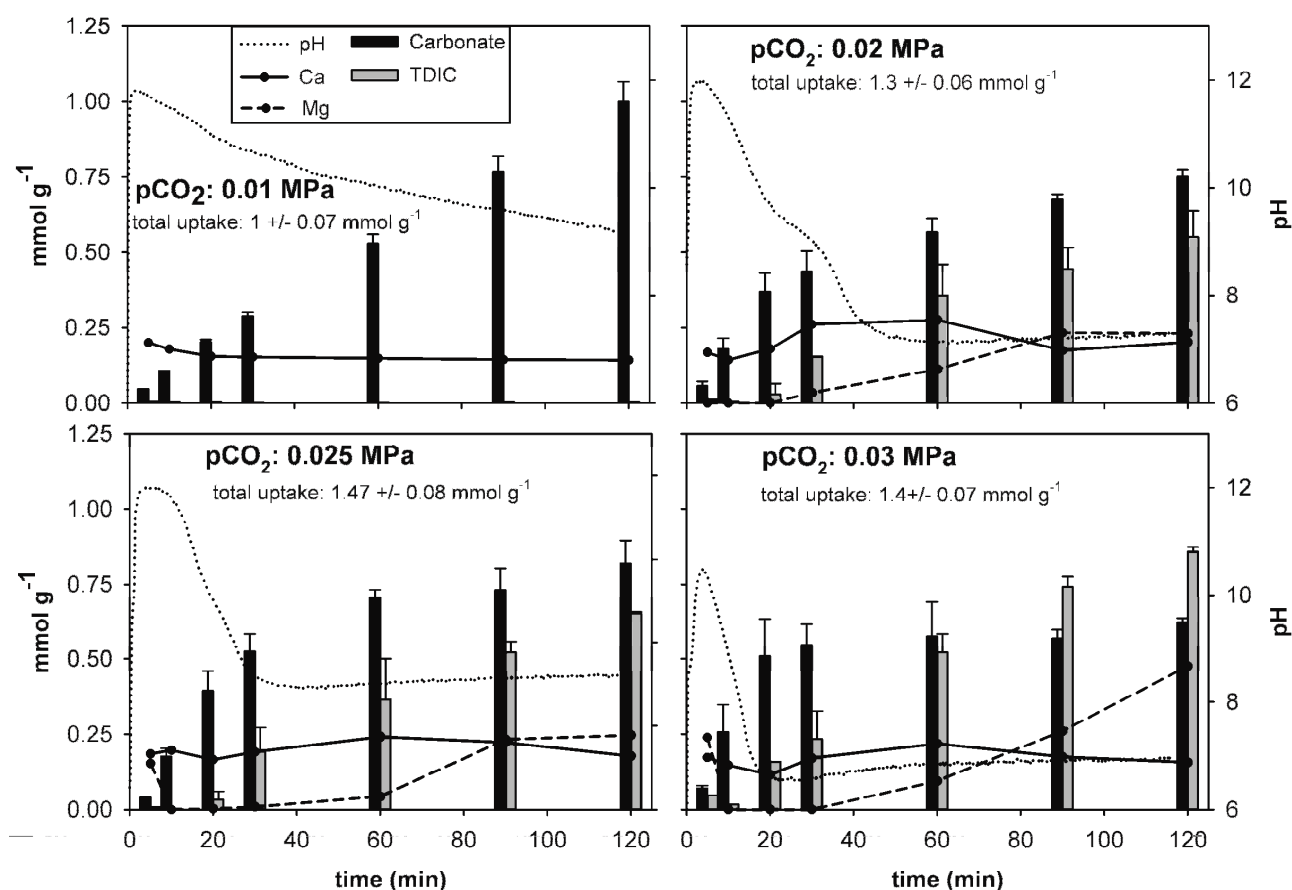


Figure 1.3: CO₂-transfer (millimoles per gram fly ash) into carbonate and TDIC as a function of pCO₂ (s/l = 75 g L⁻¹; T = 25 °C; stirring rate = 450 rpm; gas flux = 1 L min⁻¹). Experimental accuracy was calculated based on replication of experiments at least twice.

Solid-liquid-ratio. Variation of the s/l-ratio strongly affects the pH by the amount of OH⁻ ions released from the alkaline mineral compounds. The more fly ash is available, the longer lasts phase I, as indicated by the minimum of EC (Figure 1.4-Top).

At the lowest s/l-ratio (25 g L⁻¹, pCO₂: 0.01 MPa, Figure 1.4-Top) the highest degree of calcite precipitation was observed with 2.5 mmol CO₂ neutralized per g fly ash and nearly 40 % of the total Ca released from the fly ash compounds, even though calcite precipitation was not yet finished.

Lower s/l-ratios seem to generally increase the Ca release rate and the rate of the CO₂ uptake due to a dilution effect. The larger the volume of water the larger is the solubility of the Ca and Mg bearing mineral phase and the capacity to dissolve CO₂. On the other hand, absolute uptake rates of CO₂ are increased with higher s/l-ratios due to a stronger pH buffer effect (data not shown) resulting in an enhanced dissolution rate of CO₂. The CO₂ uptake per gram fly ash and the time response of the system are therefore almost similar for 50 and 75 g L⁻¹ of suspended ash.

Stirring Rate. The total uptake of CO₂ increased from 0.7 mmol g⁻¹ at 300 rpm to 1.6 mmol g⁻¹ at 600 rpm after 120 minutes with 23 % of Ca converted mainly into calcite at this rate (Figure 1.4-bottom).

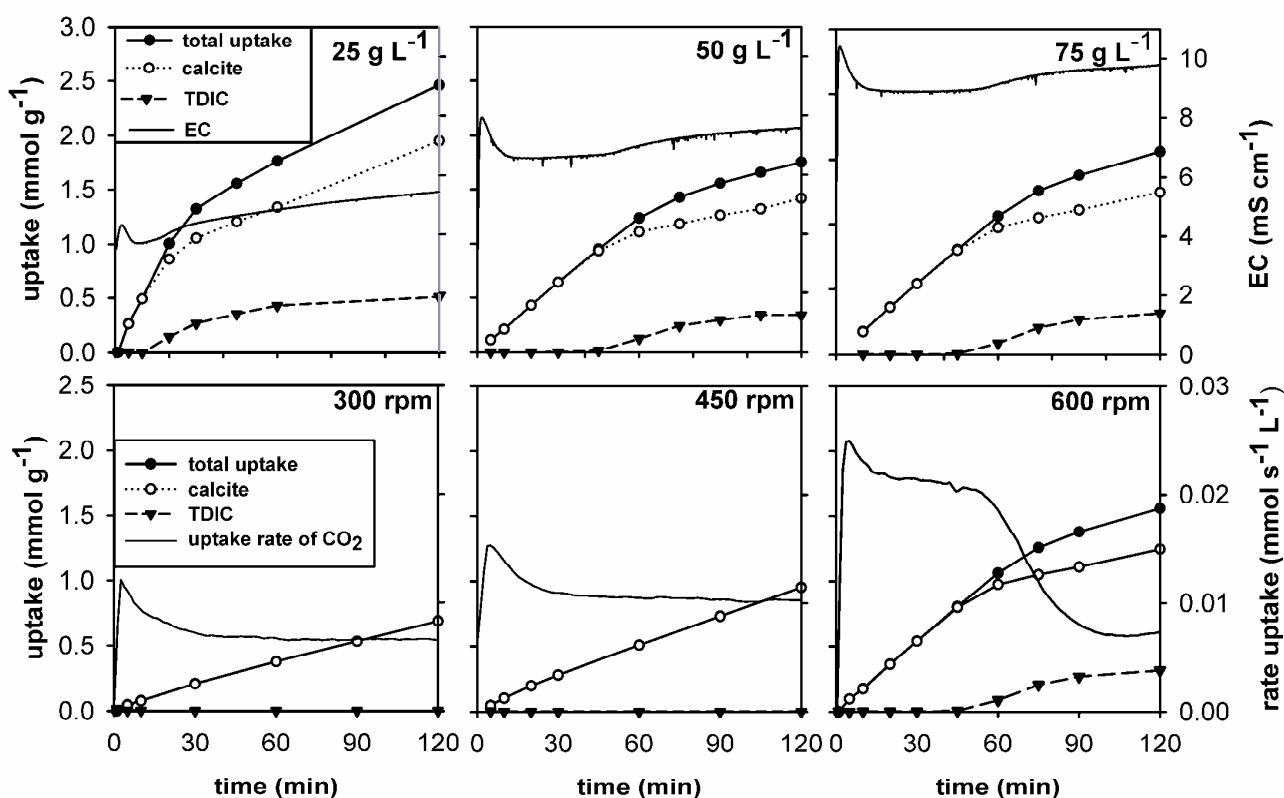


Figure 1.4: Dependence of CO₂ transfer at 25 °C and pCO₂ = 0.01 MPa on –Top: s/l-ratio (stirring rate 600 rpm) and –Bottom: stirring rate (s/l-ratio 75 g L⁻¹).

The rates of CO₂ uptake ($\text{mmol s}^{-1} \text{L}^{-1}$) remained constant during the whole experiment at the lower stirring rates (300 rpm and 450 rpm) after a sharp increase in the first seconds. The constant uptake rates were accompanied by a linear increase of the amount of CO₂ sequestered as calcite. The system remained in phase I and II during the whole experimental time ($\text{pH} > 9$). At 600 rpm the reaction shifts from phase II to phase III after ~ 60 minutes as indicated by the onset of TDIC formation and reduced uptake rates of CO₂ due to reduced calcite formation.

CO₂ uptake rates measured during the period of carbonation in all experiments ($0.007 \text{ mmol L}^{-1} - 0.021 \text{ mmol L}^{-1} \text{ s}^{-1}$) correspond to the dissolution rates of CO₂ as determined during independent pH-stat experiments to test the effect of the stirring rate on CO₂ dissolution in water at pH 10. In these experiments, CO₂ dissolution rates were found to increase from $0.007 \pm 0.001 \text{ mmol s}^{-1} \text{L}^{-1}$ at 300 rpm to $0.019 \pm 0.001 \text{ mmol s}^{-1} \text{L}^{-1}$ at 600 rpm, which is due to the reduction of the size of the gas bubbles mixed into the aqueous phase by the stirring activity and a subsequent increase of their surface area. The match between CO₂ uptake rates and CO₂ dissolution rates implies that the latter process is the rate limiting step during phase I.

The high initial uptake rates of CO₂ seem to be limited by the transport of CO₂ to the mineral surface that can be enhanced with increasing stirring rate (Liu & Dreybrodt, 1997).

Temperature. Figure 1.5 illustrates the effect of a temperature increase from 25 °C to 75 °C on the CO₂ uptake. The higher the temperature, the longer the pH remains buffered by caustic alkalinity, which we interpret to be due to two effects: Raising the temperature on the one hand increases the dissolution rate of the basic mineral compounds (Vermilye, 1969) and on the other hand decreases the solubility of CO₂ in water (Liu & Dreybrodt, 1997). The increase of the CO₂ uptake with temperature can therefore mainly be attributed to the rising formation of carbonate and extension of phase I and phase II (see pH, Figure 1.5). At 75 °C, mainly calcite precipitation accounts for the uptake of CO₂ with more than 95 % of the totally released Ca converted into calcite after 2 hours of reaction.

The rate of calcite precipitation at 75 °C has nearly doubled ($\sim 0.05 \text{ mmol s}^{-1} \text{L}^{-1}$) compared to values observed at 25 °C ($\sim 0.03 \text{ mmol s}^{-1} \text{L}^{-1}$). More than 50 % of the total Ca content of the fly ashes had been converted into calcite after 120 minutes. Rising concentrations of dissolved Al (maximal 10 mmol L^{-1}) at 75 °C are observed and indicate the onset of the dissolution of less soluble Ca compounds (in particular brownmillerite) contributing to the increased Ca-conversion. Thus, enhanced carbonation is mainly due two factors: i) the enhanced release of Ca from the mineral compounds at higher temperature

and ii) the increased rate of calcite precipitation at higher temperature (Buhmann & Dreybrodt, 1985).

In order to determine the maximum CO₂ sequestration potential at 75 °C, experiments were conducted until the pCO₂ at the outflow reached the value at the inflow of the reactor (data not shown). After 270 minutes of reaction (s/l-ratio: 50 g L⁻¹, pCO₂: 0.01 MPa, stirring rate: 600 rpm), an uptake of 5.2 mol CO₂ per kg fly ash (~ 0.23 kg CO₂ per kg fly ash) was achieved. More than 75 % of the available Ca was converted into calcite, 90 % of the total uptake could be related to the precipitation of calcite, and almost 90 % of the neutralizing capacity determined as ANC (6 meq g⁻¹) was consumed by the reaction with CO₂.

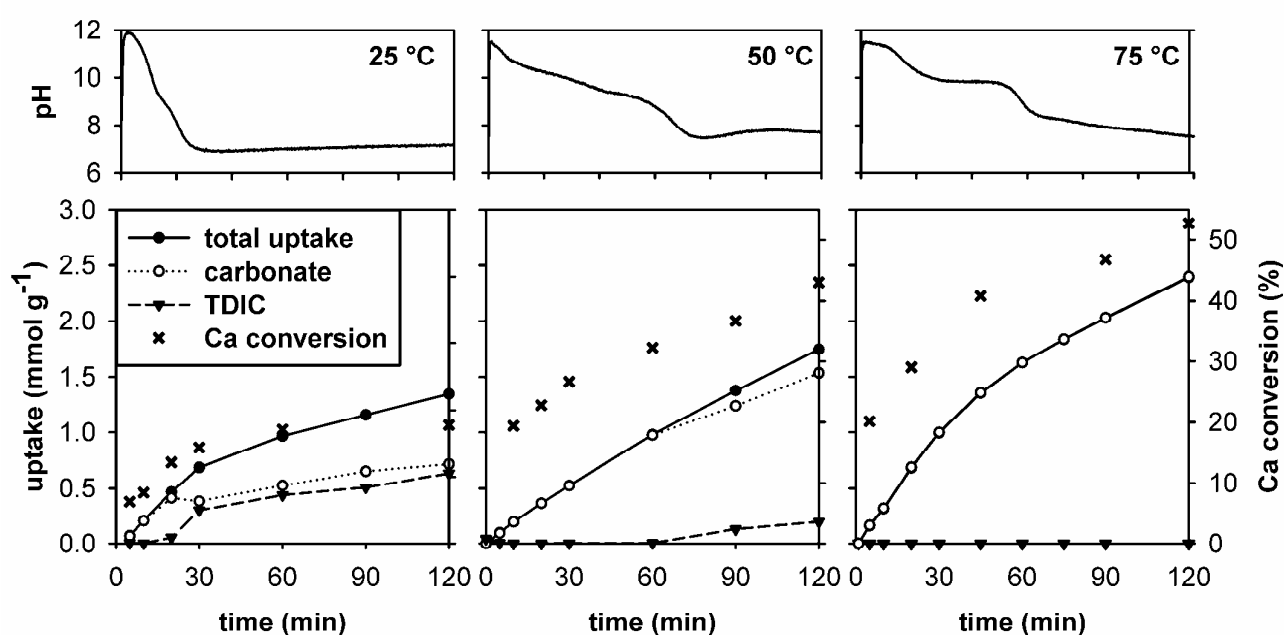


Figure 1.5: Dependence of CO₂ transfer on temperature (pCO₂ = 0.02 MPa, stirring rate 600 rpm, s/l-ratio 75 g L⁻¹). -Top: time course of pH, -bottom: CO₂ transfer. Note that the total uptake of CO₂ at 75 °C is identical to the amount of carbonate precipitated.

1.4 Implications for a technical realization

The maximum conversion of 5.2 moles of CO₂ per kg fly ash (≈ 0.23 kg kg⁻¹) obtained at 75 °C demonstrates the potential of alkaline fly ashes to sequester CO₂. This value accounts for a CO₂ sequestration capacity of nearly 3.5 million t of CO₂ in Germany alone based on the available lignite fly ash, which corresponds to 2 percent of the CO₂ emissions from lignite power combustion (175 million t a⁻¹, (DIW, 2005)).

Our results have outlined the geochemical framework for the technical use not only of lignite ashes for CO₂ sequestration but also of alkaline combustion residues in general. Although the process chain has been elucidated for low s/l-ratios only, it is reasonable to as-

sume that the general principles can be also used at higher ratios, e. g. the so-called semi-dry process route (Baclocchi et al., 2006). In order to provide a rapid uptake at a time scale of minutes, it is necessary to keep the reaction in phase I with the highest CO₂-uptake rates. Establishing a balance between alkalinity providing and consuming reactions is therefore a prerequisite to achieve the adequate pH values, which can be best obtained at enhanced temperature and by maximizing the dissolution rate of CO₂. Contrary to our experimental systems, where CO₂ dissolution was rate limiting, this process can be significantly accelerated in technical systems which will minimize the residence time in a reactor plant.

It appears that the maximum rates of carbonation and formation of dissolved Mg-bicarbonate occur at different pH values. This pool could be made available for mineral trapping if the kinetic restrictions for precipitation of Mg-carbonate can be overcome, e. g. by running the processes at higher temperature (> 50 °C) and higher s/l-ratio (Hänchen et al., 2008).

Acknowledgement

We thank M. Heider and D. Kuenkel for technical assistance and M. Bauer for valuable discussions. M. Back was supported by the German Ministry of Education and Research (BMBF, grant 03G0614A).

Supporting Information Available

The experimental setup, details on the used methods to determine the CO₂-transfer, SEM pictures taken from the lignite fly ashes, grain size analysis and mineralogical composition calculated by Rietveld analysis.

1.5 Supporting Information

Section A: Experimental setup

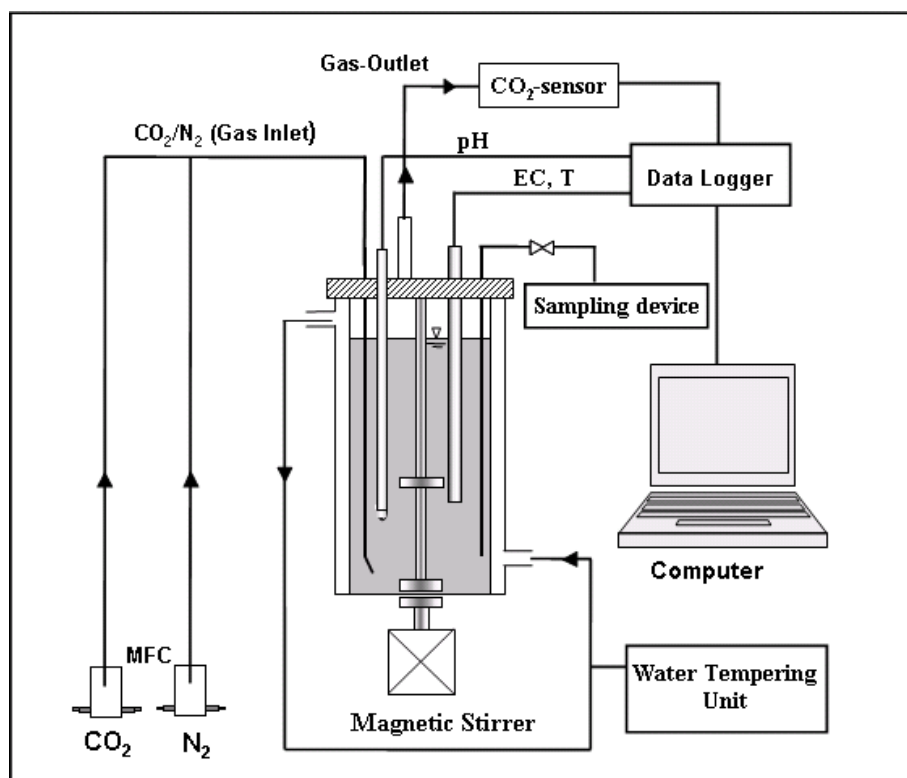


Figure 1.6: Experimental setup: Reactor system with CO₂ flow-through

Section B: Accuracy of the methods used for determination of the total uptake of CO₂, TDIC and carbonate precipitation

The accuracy of the approach to derive the CO₂-uptake from IR-sensor measurements (see experimental section, (Eq. 1.1)) was tested in a set of pH-stat experiments (titration with NaOH) at variable pH and stirring rates. The total uptake of CO₂ in such experiments is related to the formation of TDIC only, which can be determined by the headspace method, (see experimental section). Figure 1.7 shows a high correlation between both methods as indicated by the slope of the linear regression being close to unity. However, a slight offset of ~ 6.5 mmol is observable which we assume to be due to the inertia of the IR-sensor. During the first seconds of the reaction high concentration gradients of CO₂ occur that lead to a slight underestimation of the CO₂-uptake by the sensor technique. Uptakes were corrected for this offset.

In contrast, the headspace method appears to slightly underestimate TDIC at high CO₂ uptake. High CO₂ uptake corresponds to high CO₂ concentrations in the vials after acidification. The resulting absolute gas pressures in the vials exceeded atmospheric values and

were not accounted for when converting measured partial pressures into concentrations using Henry's Law. We tried to minimize these effects by reducing the volume of the injected solution at high concentrations to ensure that the concentration of CO₂ measured in the headspace did not exceed 0.05 atm.

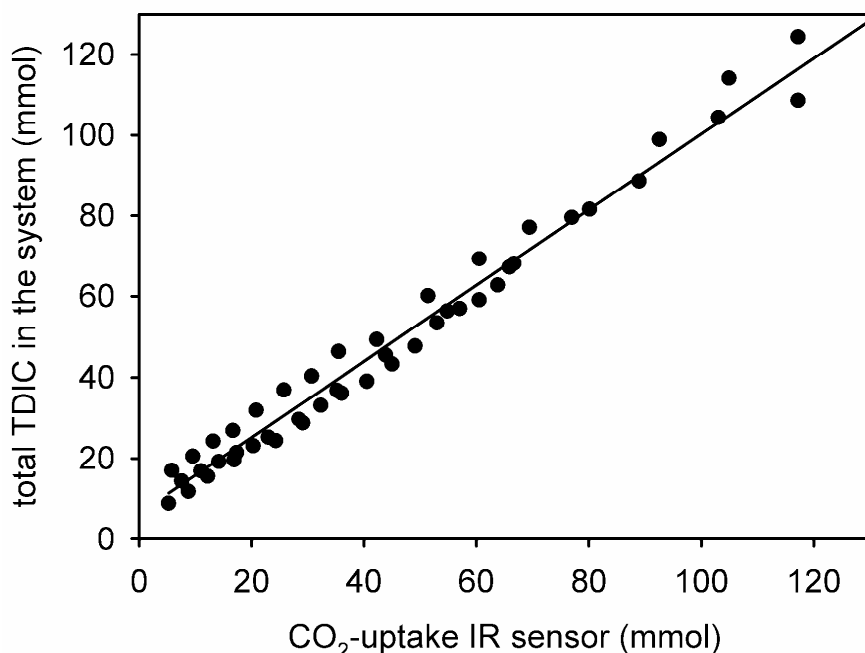


Figure 1.7: Plot of calculated CO₂ uptake derived from IR sensor measurements versus TDIC concentrations derived from headspace measurements. Process parameters were varied between pH 7-10, stirring rates of 300-700 rpm at a constant temperature of 25 °C and a initial pCO₂ of 0.01 MPa.

The amount of precipitated carbonate was calculated as the difference between total uptake as measured with the IR sensor and the TDIC concentration. The precision of this approach was tested by comparing the results with analytical measurements after acidification of 1-10 mg of carbonated solid samples.

The amount of carbonate was calculated using Eq. 1-S. taking into account the change of mass of the total solid phase due to mineral dissolution and the carbonation process:

$$\Delta(\text{CO}_2) = n(\text{carbonate}) \downarrow = c(\text{CO}_2) \times (m_0 - m_{\text{diss}} + m_{\Delta\text{Carb}}) - c(\text{CO}_2)_0 \cdot m_0, \text{ or}$$

$$c(\text{carbonate}) \downarrow = \frac{c(\text{CO}_2) \cdot (m_0 - m_{\text{diss}}) - c(\text{CO}_2)_0 \cdot m_0}{1 - c(\text{CO}_2) \cdot M(\text{CO}_2)}, \text{ with} \quad (\text{Eq. 1-S})$$

$\Delta(\text{CO}_2)$ = total amount of CO₂ (mmol) precipitated as carbonate

$c(\text{CO}_2)$: concentration of CO₂ of reacted ash (mmol g⁻¹),

$c(\text{CO}_2)_0$: mean concentration of CO₂ measured after acidification of unreacted ash (mmol g⁻¹) based on 5 replicates,

m_0 : initial mass of used fly ash (g),

m_{diss} : weight loss of fly ash (g) due to dissolution of fly ash minerals in water (e. g. lime) as being calculated from the change of chemical composition of the solution,

$M(\text{CO}_2)$: molar mass of CO_2 (44 mg mmol^{-1}),

and $m_{\Delta\text{Carb}} = n(\text{carbonate}) \cdot M(\text{CO}_2)$.

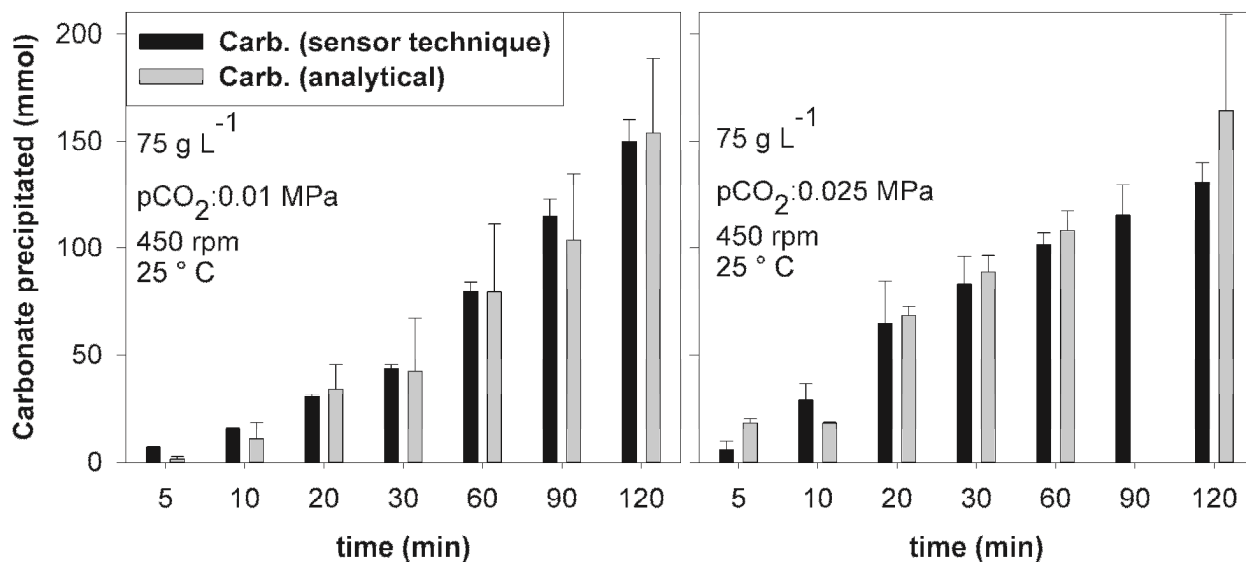


Figure 1.8: Comparison of the amounts of precipitated carbonate calculated as the difference between IR-sensor-derived CO_2 uptake and TDIC, with analytical results obtained after acidification of samples (Eq. 1-S) for two fly ash experiments.

Both methods provided comparable results. However, the variability of the analytical approach based on Eq. 1-S was distinctly higher probably due to a lack of representative sampling of the solid phase from the suspension. We therefore decided to derive the amount of precipitated carbonate from sensor measurements. Standard deviations shown in the figures in the article are calculated from at least two replicates of the experiments.

Section C: SEM-pictures of lignite fly ash

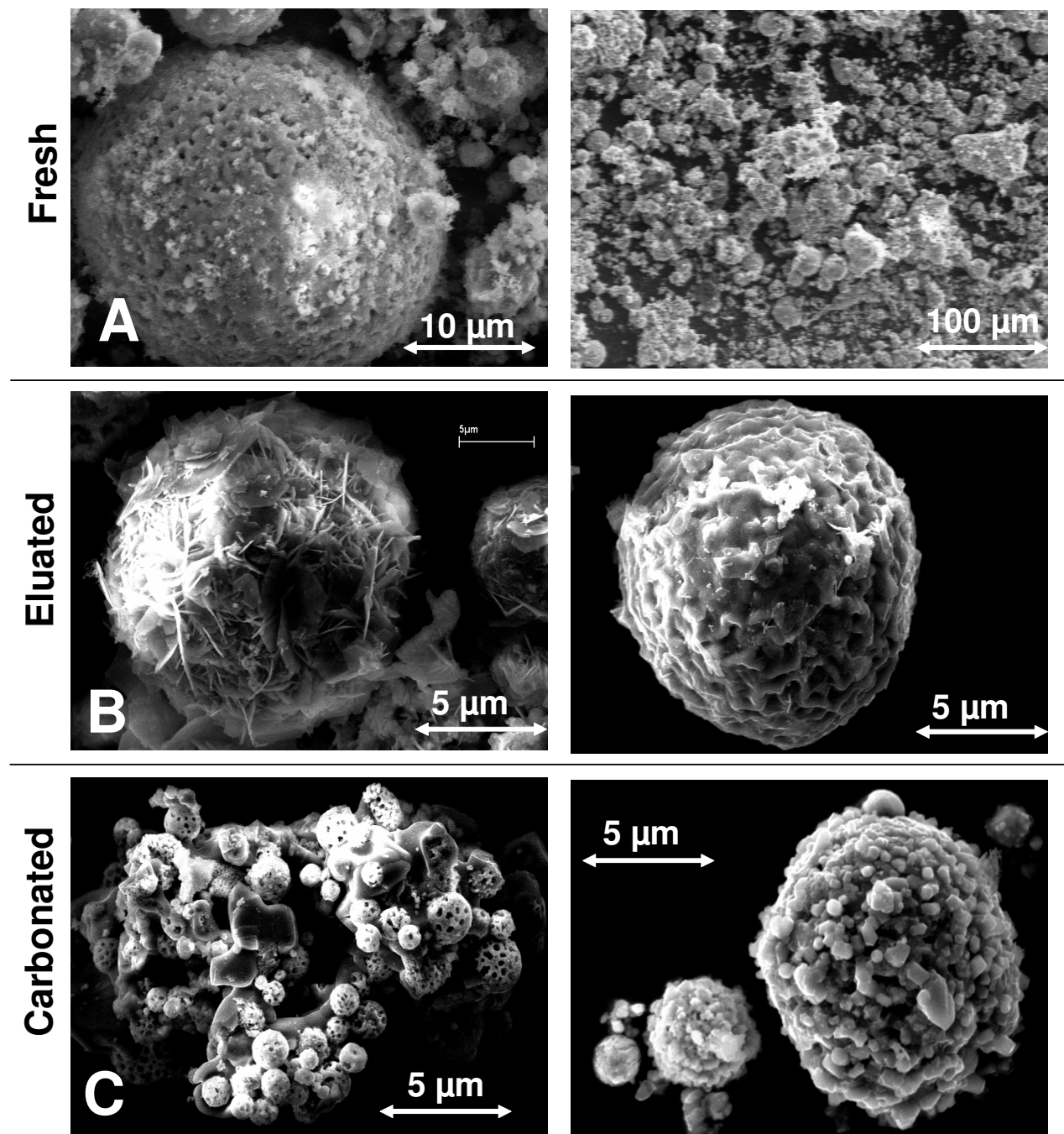


Figure 1.9: SEM pictures of fresh ash (A), eluated fly ash after 120 minutes (B) and carbonated ash after 120 minutes of reaction (C)

Section D: Grain size analysis

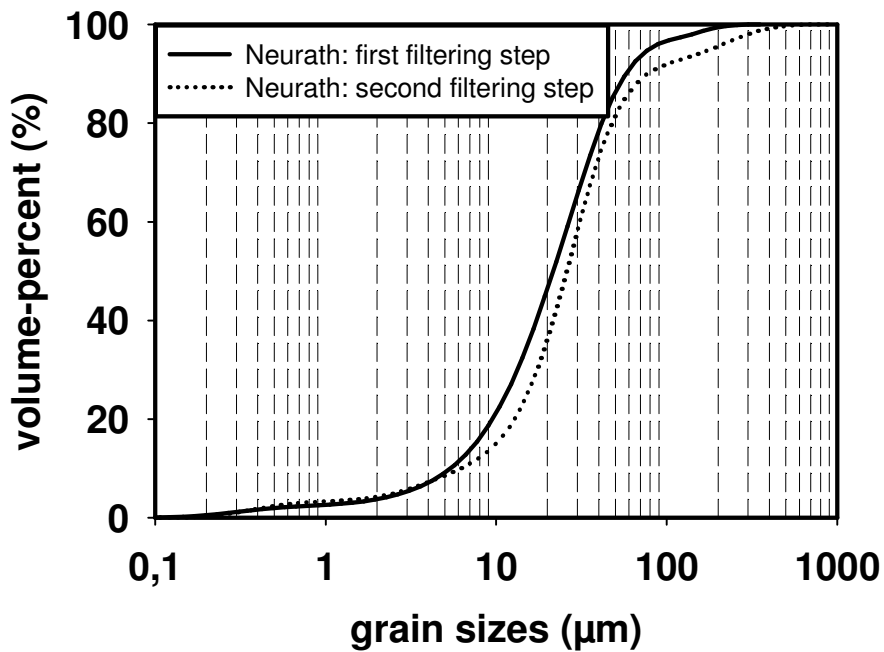


Figure 1.10: Grain size distribution of the fresh lignite fly ashes measured with laser diffraction.

Section E: Mineralogical composition (XRD, Rietveld analysis)

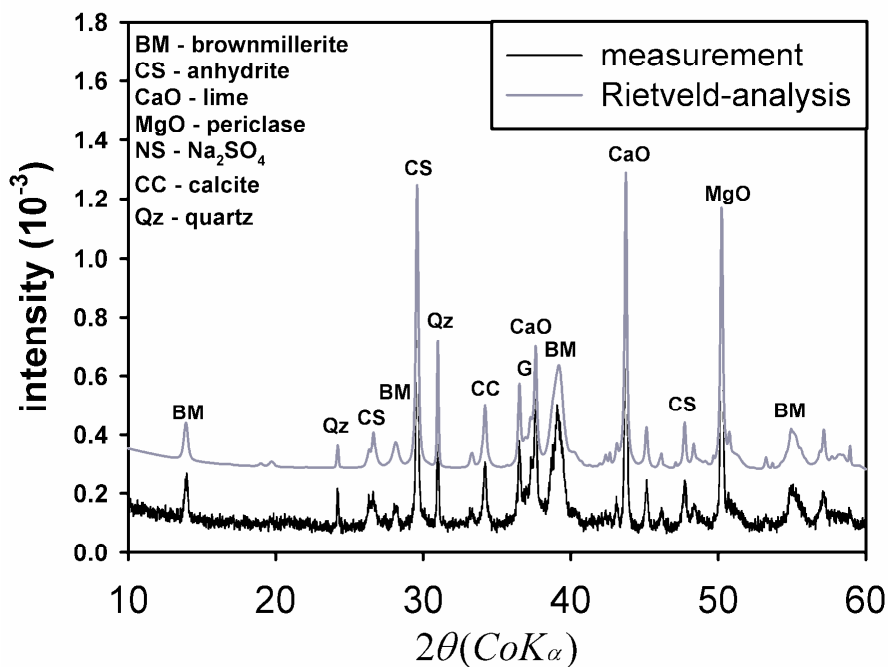


Figure 1.11: X-ray diffractogram of the investigated brown coal fly ash (black) and calculated diffractogram (grey) based on Rietveld analysis

Chapter 2

SEQUESTRATION OF CO₂ AFTER REACTION WITH ALKALINE EARTH METAL OXIDES CaO and MgO

Published in similar form as:

M. Back, M. Bauer, H. Stanjek & S. Peiffer (2011) Sequestration of CO₂ after reaction with alkaline earth metal oxides CaO and MgO, *Applied geochemistry* 26 (7), 1097-1107.

2 Sequestration of CO₂ after reaction with alkaline earth metal oxides CaO and MgO

Back, Martin¹, Bauer, Markus¹, Stanjek, Helge², Peiffer, Stefan¹

The uptake of carbon dioxide by CaO and MgO in aqueous solution has been studied in batch experiments at different temperature in the range from 15 °C - 75 °C, stirring intensities and solid-liquid ratios (0.0125 mol L⁻¹ – 0.125 mol L⁻¹) in order to identify the kinetic controls and limitations. Both minerals are constituents in many combustion residues and their carbonation is considered as an option for CO₂ sequestration.

Generally the uptake of CO₂ by metal (hydr)oxide suspension increased with higher turbulence due to better gas/water exchange and higher temperature due to enhanced rates of mineral dissolution and carbonate precipitation. The reaction of CaO and MgO with CO₂ in solution occurred at distinctly different pH values. While in the CaO systems a pH between 12.8 (0.1 mol L⁻¹) and 11.7 (0.0125 mol L⁻¹) established, suspensions with MgO only reached maximum pH values of ~10.3 even though the mineral surface area was larger in these assays (140 m² L⁻¹ for MgO compared to 7.5 m² L⁻¹ for CaO). This difference in reaction pH affected the transfer of CO₂ from the gas into the liquid phase as well as dissolution rates of the minerals themselves.

Maximum CO₂ uptake rates were 0.027 mmol L⁻¹ s⁻¹ for the CaO containing experiments at pH 12.8. CaO dissolution was fast and calcite precipitation occurred instantaneously at all tested temperatures and concentration levels. Thus, CO₂ dissolution was step limiting the overall carbonation reaction. Under otherwise similar conditions maximum CO₂ uptake rates were lower for the MgO system. Mg carbonate precipitation was slower than calcite precipitation and was depending strongly on the different boundary conditions, in particular temperature and the degree of supersaturation. Temperatures greater than 50 °C were required for assays with low dissolved Mg²⁺ and CO₃²⁻ concentrations in order to precipitate Mg carbonate in the form of hydromagnesite (Mg₅(CO₃)₄(OH)₂ * 4H₂O)). Below 50 °C

¹ Department of Hydrology, University of Bayreuth, BayCEER, D-95440 Bayreuth, Germany

² Clay and Interface Mineralogy, RWTH Aachen University, D-52065 Aachen, Germany

the use of high concentrations of Mg and carbon species were necessary to initialise precipitation of magnesium carbonate as nesquehonite (MgCO₃ * 3H₂O).

This has implications for the application of mineral carbonation in an aqueous system as a means of carbon capture and storage. Ca rich materials can be utilized efficiently and almost independently of reaction regime if an optimum supply of CO₂ is provided. In contrast specific conditions are required to use the CO₂ binding potential of alkaline Mg minerals, as T > 50 °C or high concentrations are required for Mg carbonate precipitation.

2.1 Introduction

Sequestration of CO₂ as CaCO₃ or MgCO₃ is discussed as one option in carbon capture and storage (CCS) technology in order to mitigate the increase of CO₂ in the atmosphere (Gerdemann et al., 2007; Huijgen, 2003; Lackner et al., 1995). Sources of Ca²⁺ and Mg²⁺ can either be natural minerals, such as olivine (Giammar et al., 2005; Wolff-Boenisch et al., 2006), or alkaline minerals contained in alkaline residue materials, such as ashes (Back et al., 2008; Huijgen et al., 2005; Huntzinger et al., 2009, Iizuka et al., 2004; Stolaroff et al., 2005; Teir et al., 2007). Calcium and magnesium resource materials by far exceed the amount of fossil fuels and theoretically have the potential to sequester the complete world-wide CO₂ emissions (Lackner et al. 1995). However, due to the often required pre-treatment, such as mining and grinding, only a fraction of this material pool could actually be utilized in a cost and energy efficient way for mineral CO₂ sequestration (Huijgen et al., 2006c).

Contrary to natural minerals, alkaline residual materials containing Ca and Mg minerals are highly reactive towards CO₂ resulting in the formation of carbonates. In a previous study concerning the carbonation of lignite fly ashes in aqueous solution (Back et al., 2008) at CO₂ partial pressures between 0.01 MPa and 0.03 MPa we observed fast dissolution of the Ca contained in solid phases, leading to the instantaneous precipitation of calcite already at low temperatures (25 °C). Dissolution of alkaline Mg minerals in the fly ashes on the other hand was much slower at this temperature and caused the formation of dissolved magnesium bicarbonate only.

In reaction systems containing gas, aqueous, and solid components the overall reaction can be limited by processes especially at the boundary layers, such as transport through the gas/water interface, mineral dissolution or mineral precipitation. To date, only little attention has been paid to the impact of different reaction conditions on these processes,

such as the effect of dissolved CO₂ on the dissolution of alkaline earth metal oxides (at alkaline pH), or on the subsequent transformation into carbonate species.

The formation of hydrated Mg carbonates (nesquehonite (MgCO₃ * 3H₂O) and hydromagnesite (Mg₅(CO₃)₄(OH)₂ * 4H₂O)) has been observed at temperatures below 60 °C, but the precipitation of stable magnesium carbonates is often inhibited at low supersaturations (Pokrovsky et al., 1999). The conditions for precipitation of such phases at low-temperature alkaline conditions are still not fully understood and need to be resolved in the context of CO₂ sequestration strategies.

Dissolution rates of the Ca and Mg in oxides/hydroxides, lime CaO, slaked lime Ca(OH)₂, periclase MgO and brucite Mg(OH)₂ are generally controlled by the degree of undersaturation and thus increase with decreasing pH (Vermilye, 1969). But also ligand exchange reactions may affect dissolution kinetics. Experiments on brucite dissolution (Pokrovsky and Schott, 2004; Vermilye, 1969) suggest that surface metal hydroxylation weakens the mineral structure at the surface, increases the rate of ligand exchange at the metal center and thus favors the generation of dissolution-active sites. The role of dissolved inorganic carbon species for both the dissolution and precipitation processes has not been studied to date.

Understanding the controlling processes and elucidating the requirements and conditions necessary for fast CO₂ binding by mineral carbonation is of paramount interest for any technical application as a means for CCS. Investigations on the mechanisms of crystallization of different carbonates provide valuable information for the carbonation potential of natural mineral feedstock material, like ultramafic rocks (Béarat et al., 2006; Giammar et al., 2005; O'Connor et al., 2002). As Ca- and Mg-(hydro)oxides are also important alkaline reacting minerals in many waste materials, data on their dissolution and precipitation behavior is essential for the utilization of these materials for CO₂ storage. Experience with these pure phases under aqueous conditions is also necessary to optimize waste carbonation as a technical process under ambient conditions in a wet scrubbing system.

Our experiments were designed to gain principal information about the reactivity and reaction mechanisms of CO₂ with pure alkaline Ca and Mg phases. We have set up an experimental study investigating the reactions of CaO and MgO with CO₂ in aqueous suspensions at low-temperatures (25 °- 75 °C) and low partial CO₂ pressures (0.01 MPa), which is a value typical for flue gas of common combustion processes. With this study we aim to 1) determine the influence of dissolved carbonate on the dissolution kinetics and mechanisms of CaO and MgO, 2) elucidate the conditions at which Mg carbonate precipi-

tation is preferential to the formation of dissolved Mg bicarbonate complexes and 3) understand the overall limiting factors of CO₂ transfer into an alkaline aqueous solution in order to obtain maximum CO₂ binding. This allows us to draw conclusions for the optimal setup and process scheme in a more complex technical system where alkaline materials of a more complex mineralogy are used.

2.2 Materials and methods

The following p.a. grade chemicals were used in the experiments: CaO (Riedel-de Haen), MgO (Fluka), NaHCO₃ (Fluka). Single-point BET surface area measurements using a porosimetry system (Micromeritics ASAP 2010) revealed an area of $28 \pm 1 \text{ m}^2 \text{ g}^{-1}$ for MgO and $2.7 \text{ m}^2 \text{ g}^{-1}$ for the CaO powder, respectively. Particle size distribution was determined by a Malvern Mastersizer 2000 after dispersion in Na₄P₂O₇ using an ultrasonic bath. The particles in CaO and MgO powders were mostly smaller than 100 μm, and the maximum in the grain size distribution was in the 6.3 - 20 μm fraction for CaO but in the 20 – 63 μm fraction for MgO. The MgO sample consisted of ~ 99 wt.-% periclase, whereas the CaO sample consisted of ~ 87 wt.-% lime and ~13 wt.-% slaked lime (XRD with Rietveld analysis, see below for details). This might be due to water uptake during storage of the CaO powder. This mineralogy is considered in our results/discussion section and we think the sample thus rather reflects partly hydrated ash samples. CO₂ of certified gas phase concentration was used for sensor calibration and experiments.

Experimental setup

All experiments were carried out in a 3.7 L laboratory glass reactor (ALF, Bioengineering) equipped with a heating jacket (temperature: 15 °- 75 °C), magnetic stirrer (stirring velocity: 300 - 600 rotations per minute, rpm), and an automatic titration system (pH stat). Sensors for pH, electric conductivity (EC) and temperature (Mettler Inlab; WTW) were placed inside the reactor (Figure 2.1). Prior to starting each experiment the vessel was charged with 2 L of de-ionized water and equilibrated with CO₂ through a continuous gas stream. This CO₂ and N₂ gas flux through the gas tight reactor was controlled by mass flow controllers (MKS Instruments, Type 258C), allowing for an independent variation of total gas flow (up to 0.2 - 2 L min⁻¹) and gas phase pCO₂ (0.005 - 0.03 MPa). The mass flow controllers were tested periodically with a bubble counter. An IR sensor (Vaisala, GMP221,), with a response time t_{63} of 20 s was used to measure pCO₂ in the gas in- or outflow. Samples of the suspension or water phase inside the reactor during the experiment could be obtained through a valve with a syringe. After the experiment was completed the suspension

was left unstirred for 10 min to allow solid phase sedimentation. Then the water was removed, the residual slurry was sampled, freeze-dried and used for XRD analysis.

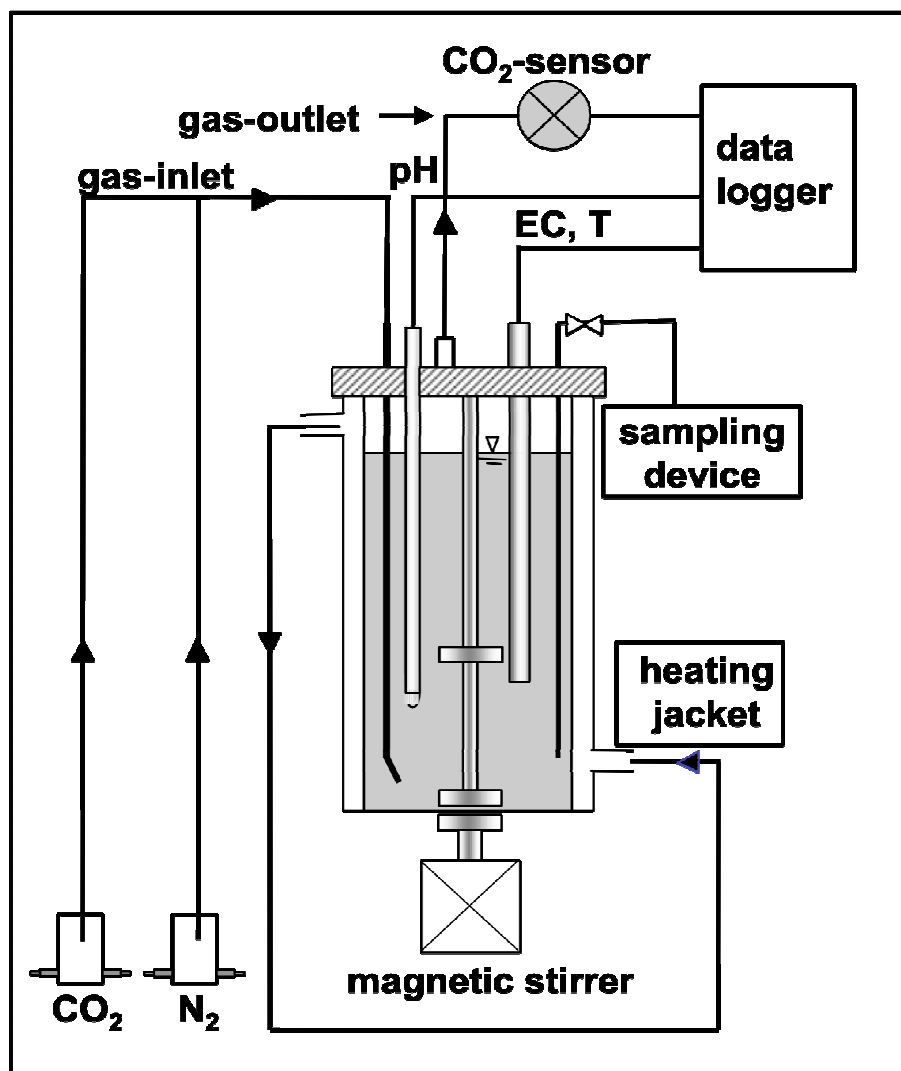


Figure 2.1: Aqueous batch reactor with stirrer, heating mantle, continuous CO₂ flow, sensors

Measurements and calculations

The pH, EC and T inside the reactor as well as CO₂/N₂ gas fluxes and pCO₂ in the gas outflow were recorded continuously every 10 s throughout the experiments. The gas flux and the input/output CO₂ concentrations were used to calculate CO₂ uptake rate and cumulative CO₂ uptake of the system with the ideal gas law (Eq. 2.1). For each measurement time interval of $t = 10$ s the molar CO₂ loss from the gas stream was calculated (Eq. 2.2 + Eq. 2.3). The obtained moles of CO₂ loss were normalized to acquire a CO₂ uptake rate (Eq. 2.4). The cumulative CO₂ uptake per g solid at a certain time integrates the CO₂ uptake in all previous time steps (Eq. 2.5).

$$p \cdot V = n \cdot R \cdot T \quad (\text{Eq. 2.1})$$

$$V_{in/out} = Q_{gas} \cdot t \quad (\text{Eq. 2.2})$$

$$c_{uptake} = c_{in} - c_{out} = ((p_{CO_2in} \cdot V_{in}) - (p_{CO_2out} \cdot V_{out})) \cdot (R \cdot T)^{-1} \quad (\text{Eq. 2.3})$$

$$\text{Rate}_{uptake} = n_{uptake} \cdot (t \cdot V_{solution})^{-1} \quad (\text{Eq. 2.4})$$

$$CO_{2uptake} = \left(\sum (n_{uptake}) \cdot m_{alkaline\ phase} \right)^{-1} \quad (\text{Eq. 2.5})$$

with:

p = pressure [MPa]

V = volume of gas or solution [m³]

c = molar amount [mol]

R = gas constant [8.314 J mol⁻¹ K⁻¹]

T = temperature [K]

Q = gas flux (m³ s⁻¹)

t = Time [s]

pCO₂ = CO₂ partial pressure in [MPa]

Rate_{uptake} = uptake rate [mol · (s·L)⁻¹]

CO_{2uptake} = cumulative uptake [mol · g⁻¹]

m = mass (g)

Collected aqueous phase samples were passed through a nylon filter with a pore width of 0.45 μm. Ca and Mg concentrations of one subsample of the filtrate were determined by ICP-OES (Varian Vista-Pro) after acidification with 1 vol.-% of HNO₃ s.p..

A second subsample was used to measure the amount of total dissolved inorganic carbon (TDIC, Eq. 2.6). For this purpose the sample aliquot was transferred into N₂ purged gaschromatography autosampler vials and acidified with 6N HCl. After vigorous mixing to equilibrate gas and water phase the headspace concentration of CO₂ was analyzed by a gaschromatograph (Hewlett Packard). Due to the low pH the measured amount of CO₂ in the headspace can be used to quantify the TDIC content in the aqueous phase sample according to (Eq. 2.7 + Eq. 2.8 + Eq. 2.9).

$$TDIC = CO_3^{2-} + HCO_3^- + H_2CO_3 + CO_2(aq) \quad (\text{Eq. 2.6})$$

$$c(TDIC_{sample}) = c(IC_{water,vial}) + c(IC_{gas,vial}) \quad (\text{Eq. 2.7})$$

$$c(IC_{gas,vial}) = (pCO_{2gas,vial} \cdot V_{gas,vial}) (R \cdot T)^{-1} \quad (\text{Eq. 2.8})$$

$$c(IC_{water,vial}) = K_H \cdot pCO_{2gas,vial} \cdot V_{water,vial} \quad (\text{Eq. 2.9})$$

with:

c = molar amount [mol]

$p\text{CO}_2$ = CO₂ partial pressure in [MPa]

V = volume [L]

R = gas constant [8.314 atm L mol⁻¹ K⁻¹]

T = temperature [K]

K_H = Henry law constant [$10^{-1.41}$ mol L⁻¹ atm⁻¹]

The mass transfer of CO₂ into solid metal carbonate was calculated as the difference between the total uptake of CO₂ and TDIC. The accuracy of the methods concerning the CO₂ transfer is discussed in detail in Back et al. (2008).

Solid samples were freeze-dried and homogenised to determine the mineralogical composition by X-ray powder diffraction (XRD) using a Huber 423 goniometer with scans run from 2° to 110° (2 θ , Co K α), increments of 0.018° and 10 seconds counting time per step. Quantitative phase analysis based on the Rietveld technique was performed with the program BGMN (Bergmann and Kleeberg, 1998).

Geochemical modelling was performed using the computer code PHREEQC (Parkhurst and Appelo, 1999) Because the ionic strength was generally below 0.1 the Davies equation (Davis and Kent, 1990) was applied for the calculation of activity coefficients by using the MINTeq database (Allison et al., 1990).

Saturation indices (SI) of the mineral phases were calculated by comparing the chemical activities of the dissolved ions of the mineral with their solubility product (K_{SP} , as exemplified for CaO in Eq. 2.10)

$$SI_{CaO} = \log\left(\frac{[Ca][OH]^2}{K_{SP_{CaO}}} \right) \quad (\text{Eq. 2.10})$$

Sets of experiments

CaO and MgO reaction in CO₂-containing water (Set A)

The carbonation reaction of the two alkaline earth metal oxides CaO and MgO occurs at different velocities and under different conditions. In order to determine the important dissolution and precipitation reactions and evaluate the control mechanisms separate carbonation experiments were run with either CaO or MgO at $T = 25$ °C, $p\text{CO}_2 = 0.01$ MPa, $Q_{\text{gas}} = 2$ L min⁻¹ under stirring at 600 rpm. Experiments were started by adding the solid phase powder (CaO or MgO; $c = 0.05$ mol L⁻¹) to the CO₂ saturated solution.

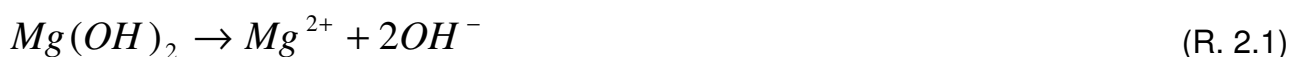
Aqueous phase samples were taken in intervals during the experiment and solid phases were sampled at the end of an experiment. Solubility product and PHREEQC-model calculations, using measured aqueous phase concentrations (e.g. pH or Ca resp. Mg concentrations) were carried out to analyze and interpret the obtained results. XRD analyses were performed on the reaction products to interpret changes in the mineral phase assemblages.

Carbonation of CaO and MgO in water under varying reaction conditions (Set B)

During CaO and MgO carbonation several factors affect the reachable CO₂ uptake rates. Therefore, we ran carbonation experiments with CaO or MgO, similar to those described above, in which either the stirring rate (300 rpm – 600 rpm), solid to liquid ratio (0.0125 mol L⁻¹ – 0.125 mol L⁻¹) or temperature (25 °C – 75 °C) was varied.

Controls on MgO dissolution rate (Set C)

We estimated the in situ dissolution kinetic of MgO by performing pH-stat experiments (pH 8-10) both in deionized water and in solutions containing NaHCO₃ (0-50 mM) to test the effect of dissolved carbonate. The chosen pH range was 8.5, 9, 9.5, 9.75 and 10. After N₂ purging, the solution was readjusted to the desired pH value and MgO powder was added. The pH of the suspension was then kept constant by adding HCl (2 M or 0.2 M) using the autotitration system. The dissolution kinetics were characterized through the initial rates of H⁺ addition/H⁺ consumption, which directly correspond to the rate of Mg²⁺ release into the solution over time (R. 2.1).



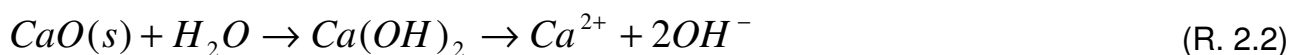
Controls on CO₂ transfer kinetics by stirring and pH (Set D)

A CO₂ exchange process between gas and water phase is a combination of physical dissolution, hydration and dissociation reactions. Especially the first two reactions strongly depend on the stirring intensity and pH. In order to evaluate their relative importance under in situ conditions in our batch systems, pH stat assays were run at different pH values (7 to 12) or different stirring rates (450 and 600 rpm). The solution pH was controlled applying the autotitration system, which added the required amount of NaOH solution (2 M or 0.2 M) to the system through a septum using a canule. As CO₂ and NaOH were introduced into the reactor at the opposite side (CO₂ at the bottom, NaOH near the surface) and as aqueous phase was stirred vigorously any substantial CO₂ uptake by the NaOH solution seems unlikely.

2.3 Results and Discussion

Reaction of CaO/Ca(OH)₂ suspensions with CO₂

The reaction progress of CaO/Ca(OH)₂ during the reaction with water and CO₂ is shown in Figure 2.2 (set A experiment). The CO₂ uptake experiment was marked by an abrupt change of solution pH after approximately 23 minutes of reaction (Figure 2.2-a). The initial period (first 23 minutes) is also characterized by the absence of TDIC and the fast increase of pH, EC and c(Ca²⁺), suggesting the fast dissolution of the alkaline material (CaO, Ca(OH)₂, see R. 2.2). The suspension also showed a fast increase of CO₂ uptake rates from the gas phase up to a maximum of 0.027 mmol s⁻¹ L⁻¹ (t = 5 - 10 min; pH ~ 12.3) and, consequently, a high CO₂ uptake. The high uptake rates are attributed to the instantaneous onset of calcite precipitation (R. 2.3) as the solid phase carbonate content increased and Ca²⁺ concentrations (associated with the rapid drop of EC) decreased.



After ~ 23 min of reaction pH dropped quickly and a minimum in EC was reached. The CO₂ uptake rate strongly decreased and the amount of the solid carbonate phase remained constant. The aqueous speciation was dominated by Ca²⁺ and HCO₃⁻ at low supersaturation with respect to calcite (SI slightly above zero). The inflection point at pH = 8.3 reflects the endpoint of the titration of CO₃²⁻ alkalinity by the precipitation reaction. The uptake of CO₂ was now related to the formation of TDIC and dissolved Ca (~ 4.5 mmol L⁻¹) until a constant pH of 6.8 (denoting equilibrium with calcite) was established after approximately 80 minutes.

After a fast increase the ion activity product (IAP) of Ca²⁺ and OH⁻ reached a constant value of log (IAP) = -4.92 ± 0.03 at pH 12.7 after ~ 5 minutes which is close to values reported for the solubility of portlandite (log (K_{SP}) = -5.325) at 25 °C (Allison et al., 1990; Duchesne and Reardon, 1995; Nordstrom et al., 1990). This observation is in accordance with previous findings that show the portlandite layer on the lime mineral surface to be the reactive species controlling CaO solubility (R. 2.2, Ritchie and Xu, 1990; Wogelius et al., 1995). As Ca(OH)₂ was the reactive Ca phase, we suggest the transformation from lime into Ca(OH)₂ of the original samples did not substantially affect overall reaction.

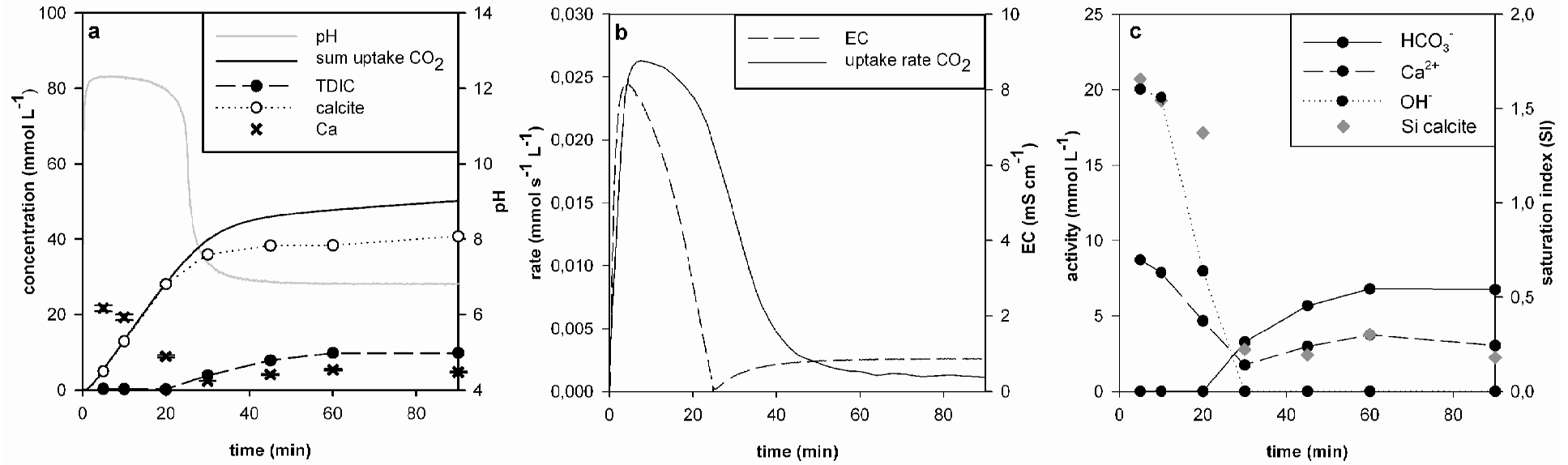
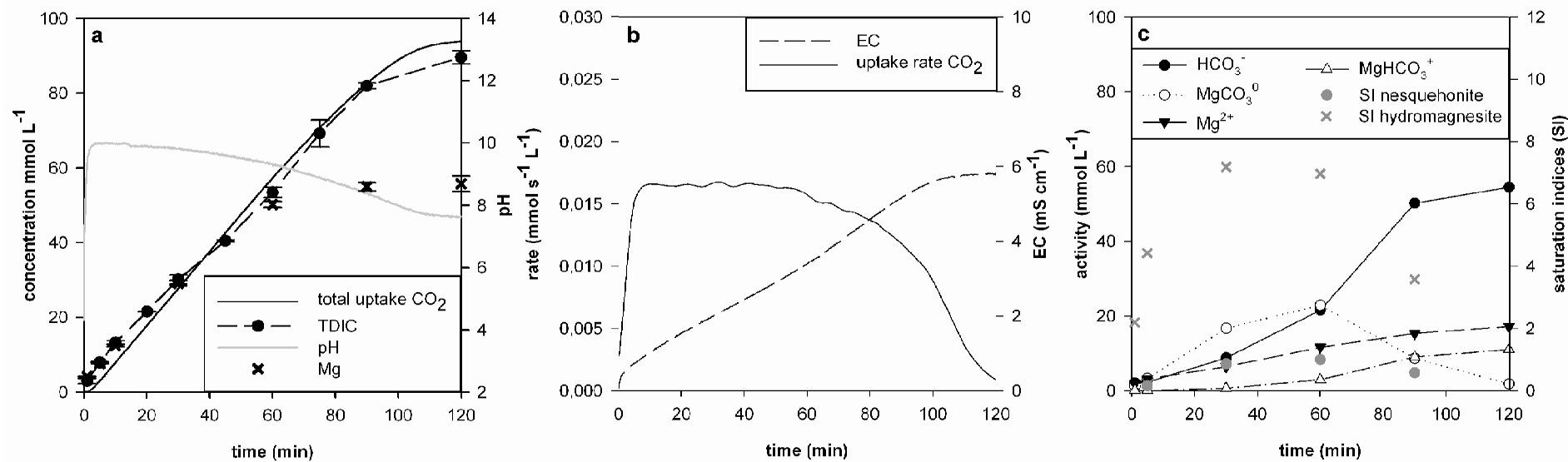


Figure 2.2: Set A: Reaction progress of CaO/Ca(OH)₂ with CO₂ in aqueous solution (25 °C, pCO₂ = 0.01 MPa, stirring rate = 600 rpm): a) pH, c(TDIC), c(Ca), cumulative CO₂ uptake, solid phase calcite content (all mmol L⁻¹); b) uptake rate of CO₂ (mmol L⁻¹ s⁻¹) and solution EC (mS cm⁻¹); c) solution speciation modelled with PHREEQC based on the measurement of pH, TDIC and Ca concentration

Reaction of MgO suspensions with CO₂

Compared to CaO/Ca(OH)₂ suspensions the reaction of MgO/Mg(OH)₂ with CO₂ was slower and took place over a longer period of time (Figure 2.3, set A experiment), even though the initial molar amounts of alkaline material added were identical. In the presence of MgO an initial pH of ~ 10.8 was reached already after 2 minutes, indicating solubility equilibrium. Subsequently, TDIC concentrations and EC increased almost linearly. The amount of formed TDIC was consistent to the amount of Mg released after ~ 60 minutes of reaction, when MgO has been nearly totally consumed. The CO₂ uptake rate remained almost constant (~ 0.016 mmol s⁻¹ L⁻¹ for the shown experiment) during this time period.

The log (IAP) calculated with Mg²⁺ and OH⁻ concentrations was -9.8 ± 0.03 at pH 10.8, which is lower than the solubility product of periclase with log (K_{SP}) = -6.49, but larger than log K_{SP} = -11.2 of brucite at 25 °C (Allison et al., 1990). The solubility of MgO is thus about five orders of magnitudes lower than that of CaO (K_{sp} = -4.92), which is reflected by the pH difference between the two oxide suspensions. As a consequence, the supply of caustic alkalinity in form of OH⁻ by MgO is substantially lower. At the start of the experiment, the pH was slightly below equilibrium with Mg(OH)₂ (log (K_{sp}) = - 9.8, cf. above), indicating that, opposite to the experiments with CaO, the supply of CO₂ was not the rate limiting factor for the dissolution process of MgO. During 60 minutes of reaction the pH decreased to 9.3, reflecting that the overall rate of CO₂ dissolution was higher than the rate of dissolution of MgO. As the MgO dissolution velocity is expected to increase with lower pH (Vermilyea, 1969), the increasing net H⁺ production can only be explained by the proceeding consumption of the MgO mineral pool. Once the release of Mg²⁺ stopped after ca. 80 minutes, dissolution of CO₂ in water proceeded until equilibrium with gaseous CO₂ was achieved at pH values of ~ 7.7. Mg speciation changed from MgCO₃⁰ to MgHCO₃⁺ as the predominant species (Figure 2.3-c). No solid phase magnesium carbonates were detectable under the reaction conditions of the shown experiment with MgO (Figure 2.3), although the solution was clearly supersaturated with respect to hydromagnesite (Mg₅(CO₃)₄(OH)₂ · 4H₂O, SI up to 7, Figure 2.3-c) and nesquehonite (MgCO₃ · 3H₂O).



46 **Figure 2.3: Set A: Reaction progress of MgO/Mg(OH)₂ with CO₂ in aqueous solution (25 °C, pCO₂ = 0.01 MPa, stirring rate = 600 rpm): a) pH, c(TDIC), c(Mg) and cumulative CO₂ uptake (all mmol L⁻¹); b) uptake rate of CO₂ (mmol L⁻¹ s⁻¹) and solution EC (mS cm⁻¹); c) solution speciation modelled with PHREEQC based on the measurement of pH, TDIC and Mg concentration**

In order to elucidate the cause for this apparent difference in the reaction of Mg- compared to Ca-(hydr)oxide a number of factors have to be considered. The slower carbonation of Mg phases might have been an effect of initial particle size or surface area. But although more large particles were found, the BET surface area of MgO material (140 m² L⁻¹) was substantially higher than that of CaO (7.5 m² L⁻¹). This suggests that the fundamental differences in the reaction mechanisms of Ca- and Mg-(hydro)oxide with CO₂ were caused by the observed lower reactivity but not the physical limitation of the reactive surface. The dissolution of Mg phases is less rapid and takes place at lower pH values, and the precipitation of Mg carbonates is kinetically less favoured. Both factors strongly affect the velocity and potential for Mg mineral carbonation.

Dissolution kinetics of MgO

The MgO dissolution rate is reported to be two orders of magnitude slower than the dissolution rate of CaO (Casey, 1991). Thus, in experiments with MgO the build-up of alkalinity may be a rate limiting factor. We have therefore studied the dependence of the dissolution kinetics of MgO on both the pH and the concentration of TDIC.

The dissolution rate was mainly controlled by the pH (Figure 2.4, set C experiment) as predicted by previous studies (cf. above). It appears, however, that dissolved NaHCO₃ has a small effect on the dissolution rate, which we assume is due to the formation of a surface complex between surface bound Mg and a carbonate species. The effect seems to be independent of pH. Also, the concentration of NaHCO₃ does not substantially affect the dissolution rate, which we interpret in terms of a saturation of the MgO surface already at the lowest concentration of dissolved NaHCO₃ used in these experiments.

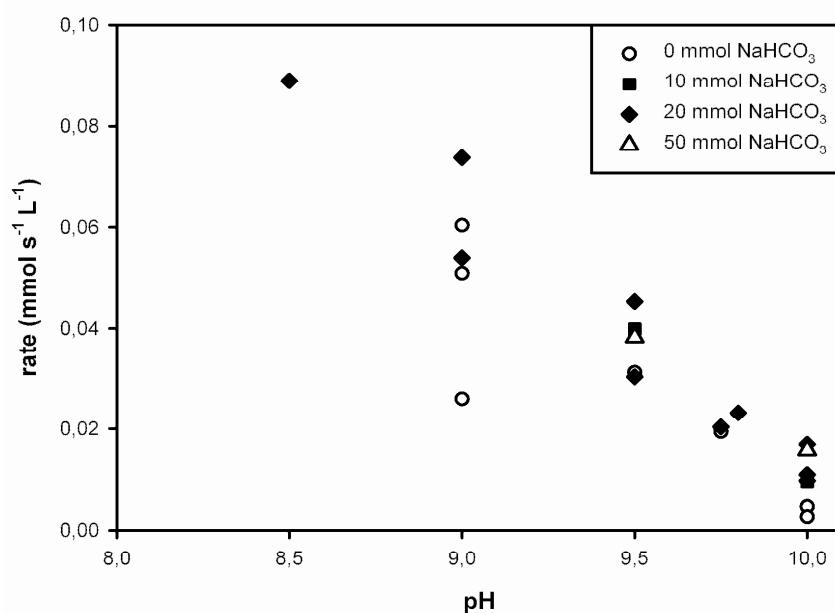
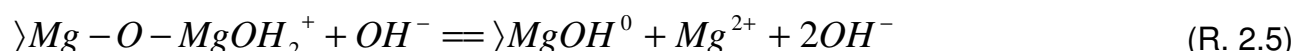


Figure 2.4: Set C: Effect of pH and NaHCO₃ concentration (0 – 50 mmol L⁻¹) on the dissolution rate of MgO in water. The pH was stabilized by automatic titration with 0.1 N HCl: c(MgO) = 0.025 mol L⁻¹, T = 25 °C, stirring rate = 600 rpm

MgO dissolution was previously shown to be affected by ligand interaction with the mineral surface. Proton promoted dissolution controls the dissolution rates of MgO (Vermilye, 1969; Wogelius et al., 1995), and is explained by the one site surface speciation model tested for several surfaces of oxides and silicates (Pokrovsky and Schott, 2004; Sverjensky and Sahai, 1998). The results of Pokrovsky and Schott (2004) furthermore indicate that the dissolution and precipitation kinetics of brucite are mainly controlled by the formation of the surface precursor complex >MgOH_2^+ . The increase of brucite dissolution as a function of H^+ activity can thus be attributed to the protonation of >MgOH^0 sites leading to the formation of >MgOH_2^+ :



which then detaches upon release of an OH^- ion:



In analogy to the surface speciation model proposed by Pokrovsky and Schott (2004) we assume that the reaction of bicarbonate with the mineral surface in the pH range between 8 and 10 occurs as follows. In a first step bicarbonate is adsorbed onto the mineral surface to form a carbonate surface species >Mg-O-MgCO_3^-



The predominance of the species MgCO₃⁰ in the solution (Figure 2.5-II-b) implies that, in a second step, this species detaches from the surface creating a new surface site >MgOH^o:



The OH⁻ ions are again consumed by CO₂ to generate new HCO₃⁻.

Based on this reaction scheme, the overall dissolution rate is proportional to the surface coverage with CO₃²⁻ and protons:

$$dc(\text{MgO})/dt = k_{\text{H}^+} \cdot c(\text{>Mg-O-MgOH}_2^+) + k_{\text{CO}_3} \cdot c(\text{>Mg-O-MgCO}_3^-) \quad (\text{R. 2.8})$$

k_{H^+} and k_{CO_3} being rate constants with $k_{\text{H}^+} \gg k_{\text{CO}_3}$.

The dissolution rate should therefore increase in the presence of CO₂, which goes along with the increasing concentration of TDIC and hence also HCO₃⁻ in the experiments shown in Figure 2.3-c. In contrast the pH was more or less constant. In fact, the rate remains constant during the first 30 minutes and even decreases before dissolution is complete. We therefore assume that the surface of MgO was completely saturated with CO₃²⁻ during the build up of TDIC so that the dissolution rate became independent of the concentration of TDIC. With increasing reaction progress the surface area was shrinking which lead to the observed decrease of the reaction rate (Figure 2.3-b).

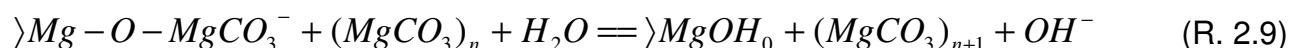
Precipitation of solid carbonate phases

In experiments with CaO, a rapid and complete precipitation of Ca as calcite took place at the conditions of our reference experiment at 25 °C, 0.05 mmol L⁻¹ solid phase and 0.01 MPa pCO₂ (Figure 2.3, set A experiment). In contrast, no formation of Mg-containing carbonate solid phases occurred under the same conditions using the same amount of MgO (Figure 2.3). The precipitation of Mg carbonates (Figure 2.5, set B experiments) required higher temperatures (“high T”, 75 °C). After 180 minutes of reaction (~ 0.96 g/g, Table 1) predominantly hydromagnesite was precipitated. Alternatively, raising initial MgO concentrations (“high MgO”) from 0.05 mol L⁻¹ to 0.125 mol L⁻¹ caused the precipitation of nesquehonite (~ 0.85 g/g after 120 minutes of reaction, Table 1) even though the solution also was strongly supersaturated with respect to hydromagnesite. Magnesite was a minor precipitate (0.003 g/g to 0.02 g/g) in both experiments.

Table 2.1: Effect of an increase in MgO input or T (Set B experiments) on precipitation of magnesium carbonates. Mineral compounds in wt % of the total analyzed solid phase as determined by XRD analysis after MgO carbonation at pCO₂ = 0.01 MPa, stirring rate = 600 rpm; “High MgO”: 25 °C, 0.125 mol L⁻¹ MgO, 180 min; “High T”: 0.05 mol L⁻¹ MgO, 75 °C, 120 min

mineral phase	chemical formula	“High MgO” (wt. %)	“High T” (wt. %)
periclase	MgO	12	1.5
brucite	Mg(OH) ₂	1.5	0
nesquehonite	MgCO ₃ · 3H ₂ O	89	0
magnesite	MgCO ₃	0.3	2
hydromagnesite	Mg ₅ [CO ₃] ₄ (OH) ₂ · 4H ₂ O	0.1	96

In the “high MgO” experiments precipitation of nesquehonite started after ~ 30 minutes at a concentration of dissolved Mg and TDIC concentration of ~ 50 mmol L⁻¹ (Figure 2.5-l) and was accompanied by a temporary increase of the pH (Figure 2.5-l-a). This increase of the pH, which is contrary to the general trend, appears to be caused by kinetic effects related to the precipitation reaction. As has been discussed above, both surface controlled dissolution processes (promoted by H⁺ or HCO₃⁻) release OH⁻, which is rapidly consumed by CO₂. The precipitation reaction appears to accelerate the detachment of the complex MgCO₃^o (R. 2.7): MgCO₃^o is the dominant species during the first 60 minutes with a maximum at about 45 minutes, shortly before precipitation starts (Figure 2.5-l-b). Once a critical degree of oversaturation with respect to nesquehonite is achieved (cf. Figure 2.5-l-b) crystallisation of (MgCO₃)_n seeds starts, which in turn favors the detachment of surface bound MgCO₃ for further growth thereby releasing OH⁻.



Since the precipitation rate depends on the degree of supersaturation, it was initially fast but then, with dropping Mg²⁺ and CO₃²⁻ concentrations, it decreased. Consequently, also the rate of OH⁻ production was higher in the beginning of the precipitation and exceeded that of the OH⁻ consumption by CO₂. Once the supersaturation was reduced, the pH was controlled again by the balance between the release of OH⁻ ions from the MgO surface and the supply of protons from the dissolution of CO₂. This leads again to an uptake of CO₂ as TDIC up to the full depletion of MgO.

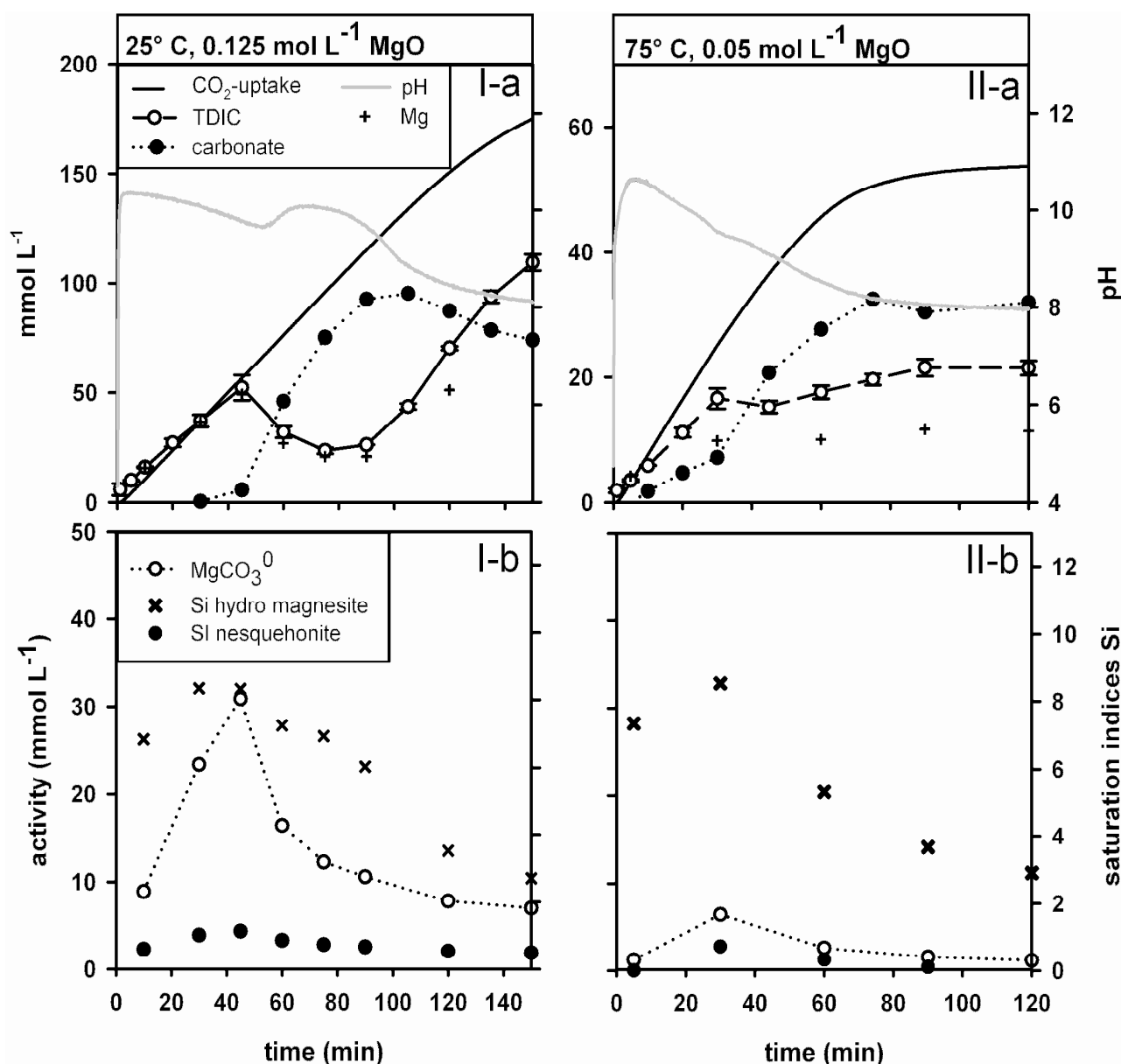


Figure 2.5: Set B: Effect of an increase in (I) MgO input concentrations from 0.05 to 0.125 mol L⁻¹ and (II) temperature from 25 to 75 °C on precipitation of magnesium carbonates: pCO₂ = 0.01 MPa, stirring rate = 600 rpm; a) pH, c(TDIC), c(Ca) or c(Mg), cumulative CO₂ uptake, solid phase carbonate content (all mmol L⁻¹); b) MgCO₃ concentration and saturation indices as calculated by PHREEQC

In the “high T” experiments at 75 °C magnesium carbonate precipitation occurred immediately after the start of the experiments. Hydromagnesite was the predominant carbonate phase detected after the experiment (Table 2.1). This carbonate precipitation in the initial stage of the experiment occurred simultaneously with an increase in TDIC (Figure 2.5-II-a) and, consequently, with a rising SI for Mg carbonates. Saturation was reached after ~ 30 minutes of reaction, leading in increase in Mg carbonate precipitation rate an SI = 8 for hydromagnesite. TDIC in the solution remained constant and all CO₂ uptake from the gas phase directly went into the mineral carbonate fraction during this period. It appears that

the observed change in the rate of carbonate precipitation also lead to a small increase in pH due to R. 2.8, even though the effect was much weaker than in the “high MgO” assays. The concentration of TDIC afterwards remained +/- constant. The transformation into carbonate was almost complete after 80 minutes of reaction (Figure 2.5, ~ 0.90 g/g).

These observations suggest a two-step process. Contrary to experiments at 25 °C precipitation occurs right from the beginning. The Mg²⁺ cation has a highly ionic character and is therefore strongly hydrated at ambient temperatures. Under these conditions either no formation of Mg carbonates occurs or only the precipitation of the Mg carbonate with highest crystal water content and lowest thermodynamical stability, (i.e., nesquehonite, Sayles and Fyfe, 1973) is possible. At higher temperatures, however, the hydration layers are less strongly bound (Hänchen et al 2008) and thus allow for an easier crystallisation and even the formation of low water containing hydromagnesite. Compared to the aggregates of nesquehonite formed at 25 °C (Figure 2.6-a), precipitates of hydromagnesite were fine grained but also characterized by radiating fibrous aggregates (Figure 2.6-b). An analogous morphology was described by Rade (1970) for the hydrated Mg carbonate dypingite Mg₅(CO₃)₄(OH)₂·5(H₂O), which was suggested to be a transient phase during the nesquehonite to hydromagnesite formation (Davis and Kent, 1990). We suggest that in the “high T” experiment nesquehonite forms and might be immediately transformed into hydromagnesite.

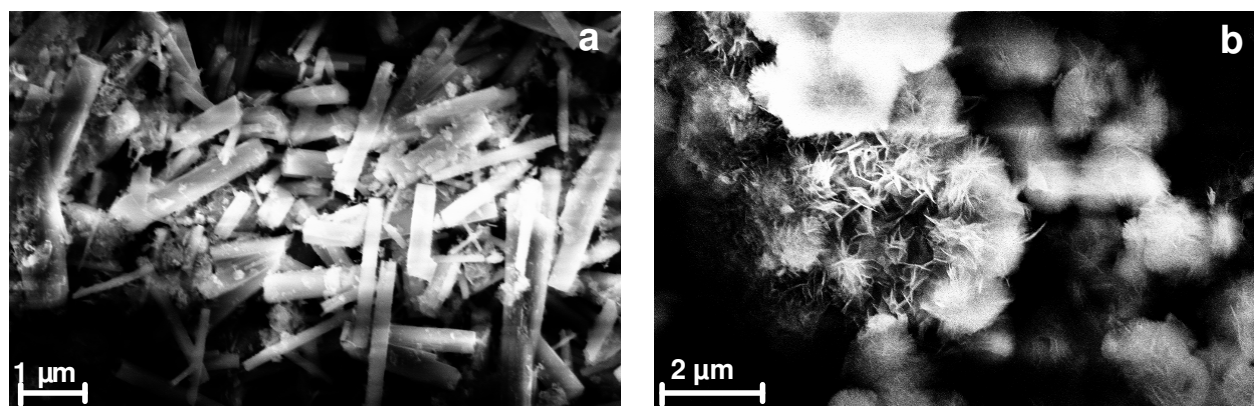


Figure 2.6: Set B: SEM images of the precipitated magnesium carbonates –left: nesquehonite at 25 °C and –right: hydromagnesite after 120 minutes of reaction at a temperature of 75 °C

The transformation of nesquehonite into hydromagnesite between 50 °C and 60 °C has been demonstrated at atmospheric gas pressures in different studies (Davies and Bubela, 1973; Hänchen et al., 2008; Kloprogge et al., 2003). Furthermore, Hänchen et al. (2008) demonstrated by using seeds of nesquehonite that, depending on the operating condi-

tions, hydromagnesite precipitation occurs after an induction period between 2 and 108 minutes.

Controls on CO₂ transfer to the water phase

The previous discussion has demonstrated that the CO₂ uptake during carbonation can be restricted by the surface controlled dissolution of the solid phase Ca and Mg oxides and the temperature dependent precipitation of Ca/Mg carbonate minerals from the suspension. Additionally also the dissolution of CO₂ in the aqueous phase affects the velocity of the overall process. CO₂ transfer from gas to aqueous phase depends on the reaction steps of physical dissolution of CO₂, the hydratisation of CO₂ and dissociation of carbonic acid species. Tests were made in order to find the controlling factors for CO₂ uptake from the gas phase under different conditions.

Effect of stirring

As was expected, CO₂ transfer increased with increasing stirring rate both in pure water (Figure 2.8, set D experiments) and in the suspensions containing CaO or MgO (Figure 2.7). The transfer of CO₂ through the water/gas boundary (physical CO₂ dissolution), is enhanced with increasing turbulence. This is because of the reduction of thickness of the diffusive interfacial layer and due to the formation of more gas bubbles providing higher interface surface area (Dreybrodt and Buhmann, 1991; Dreybrodt et al., 1996). The maximum pH values reached in CaO or MgO suspensions thus decreased with stirring intensity as the input rate of CO₂ and protons to the system increased.

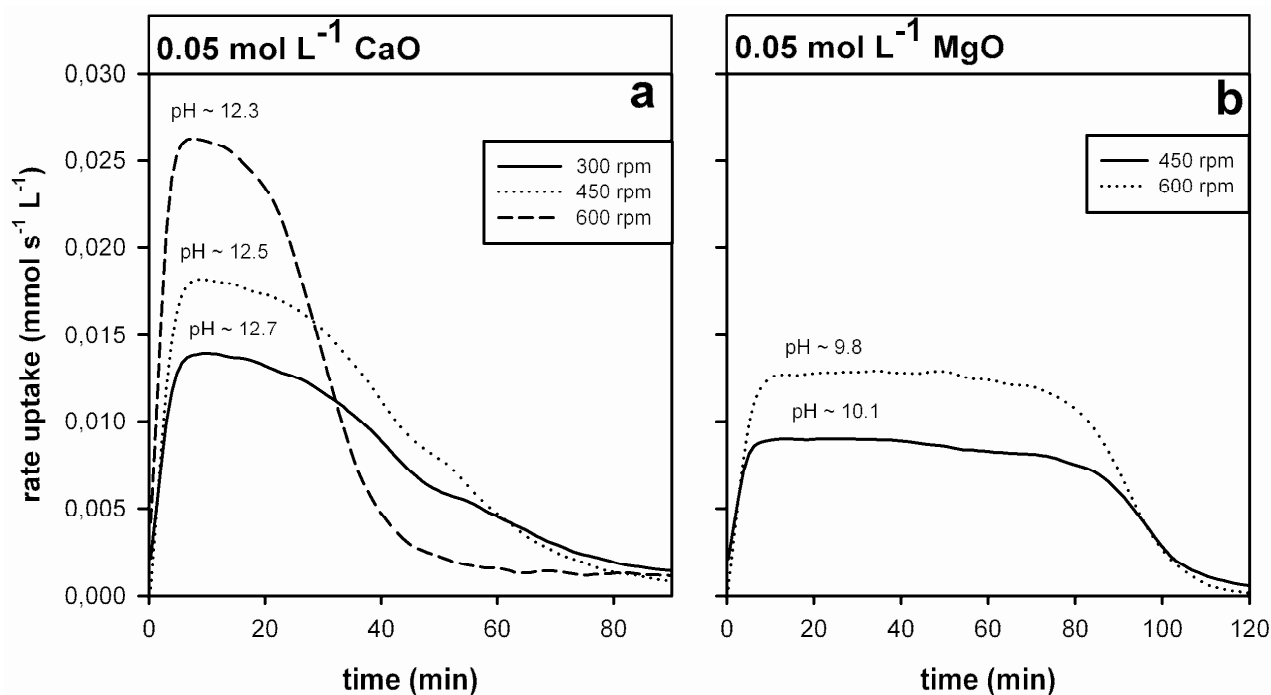
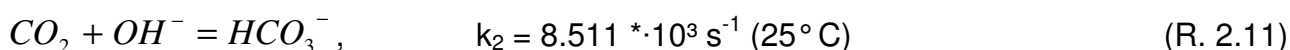
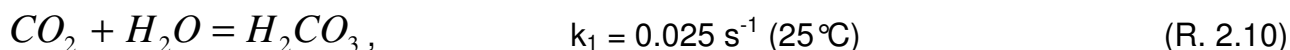


Figure 2.7: Set B: Effect of stirring rate (300 – 600 rpm) on CO₂ uptake rates in CaO (a) or MgO (b) suspension: T = 25 °C, pCO₂ = 0.01 MPa

Effect of pH

The increase of CO₂ uptake with pH in pure water (Figure 2.8) is related to the kinetics of CO₂ dissolution. The hydration of physically dissolved CO₂ molecules is known to be an important rate limiting step for the dissolution of CO₂ (Usdowski, 1982, Stumm/Morgan). At low pH values only the formation of H₂CO₃ takes place (R. 2.10) and the rate of CO₂ hydration is independent of pH (Buhmann and Dreybrodt, 1985; House and Howard, 1984; Kern, 1960). At higher pH additionally the direct formation of HCO₃⁻ (R. 2.11) becomes relevant (Pinsent et al., 1956). The rate of this reaction is pH dependent and increases exponentially for pH > 9 (Pinsent et al., 1956).



Our results did not show this exponential increase for our system, which we attribute to the limitation of diffusion of gaseous CO₂ through the water film. Maximum uptake rates (0.027 mmol L⁻¹ s⁻¹) were similar in experiments with pure water compared to carbonation experiments with CaO and MgO (Figure 2.7) at the corresponding pH values. This suggests that the kinetics of CO₂ transfer through the gas-water interface may control the overall CO₂ uptake rate of CaO/MgO suspensions rather than mineral dissolution itself.

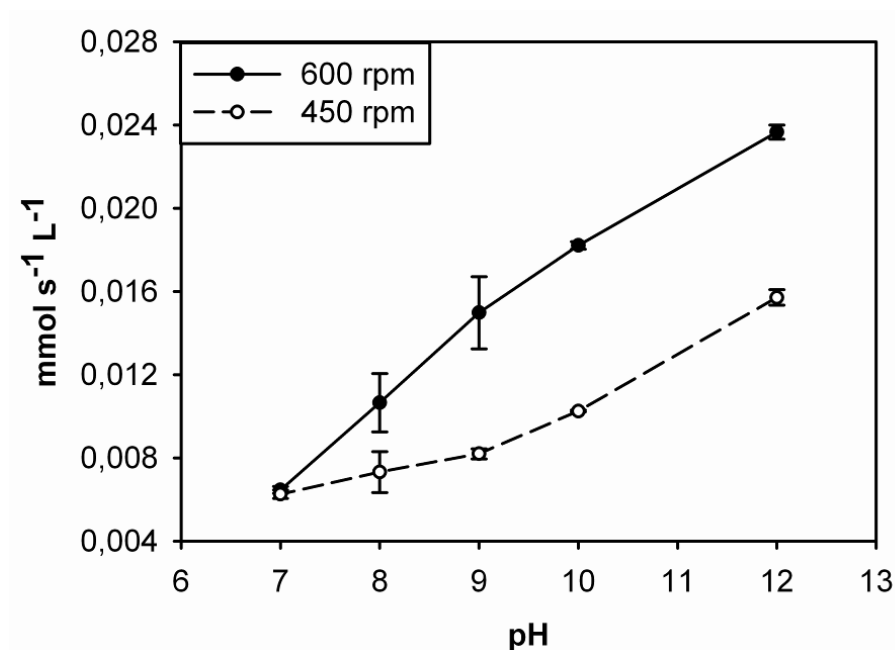


Figure 2.8: Set D: CO₂ dissolution rate in de-ionized water at different stirring rate (300 – 600 rpm) and pH (7 – 12). The pH was stabilized by automatic titration with 0.1 N HCl: T = 25 °C, pCO₂ = 0.01 MPa

Effect of solid-phase concentration

An increase of the solid-phase concentration (Set B experiments) lead to an increase in CO₂ uptake rate and higher maximum pH values for both oxides (Figure 2.9). Both effects reflect the increasing supply of caustic (OH⁻) alkalinity, once saturation with respect to the mineral phase has been achieved. This effect is certainly caused by the larger available mineral surface area at higher solid phase concentrations. Due to their different solubilities the maximum pH values reached and the CO₂ uptake patterns differ for CaO and MgO phases.

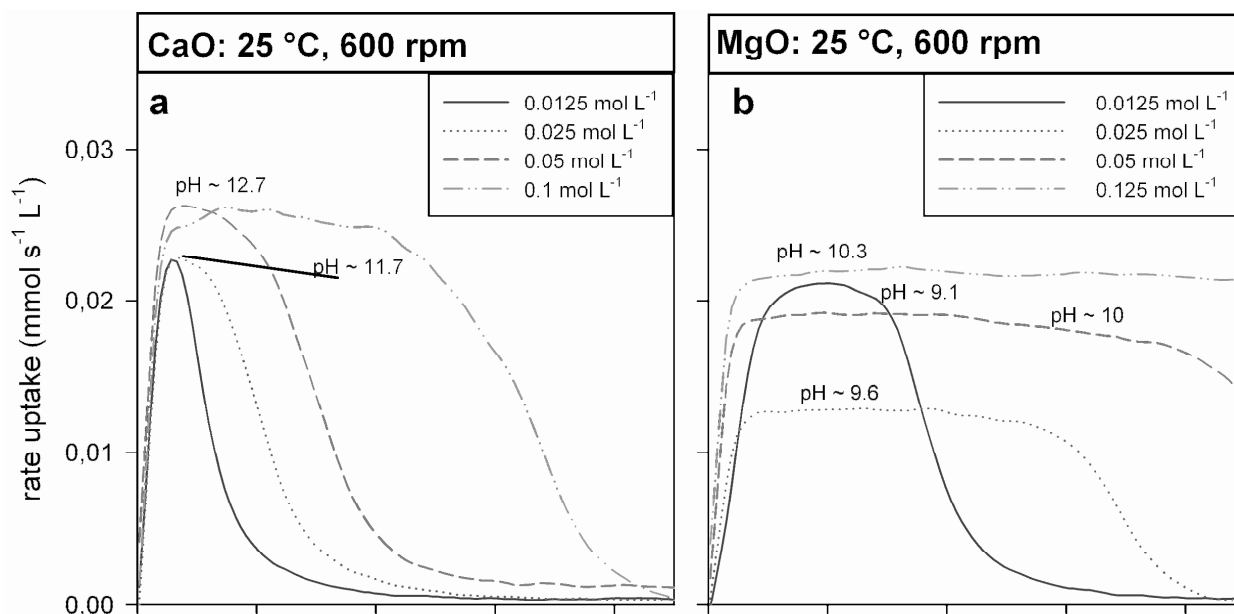


Figure 2.9: Set B: Effect of different CaO or MgO input concentrations (0.0125 to 0.125 mol L⁻¹) on the CO₂ uptake rates and maximum pH values of carbonation experiments: T = 25 °C, pCO₂ = 0.01 MPa, stirring rate = 600 rpm

For different CaO concentrations the CO₂ uptake pattern was similar to that described in Figure 2.2-b. Maximum CO₂ uptake occurred during the initial period of calcite precipitation. The duration of this stage increased linearly from 6.6 minutes at 0.0125 mol L⁻¹ to 60 minutes at 0.1 mol L⁻¹ of suspended CaO-amount. For the tested solid concentrations of 0.0125 and 0.025 mol L⁻¹ an uptake rate of ~ 0.023 mmol s⁻¹ L⁻¹ was observed. At concentrations higher than this value the maximum uptake rate approached a constant value of ~ 0.027 mmol s⁻¹ L⁻¹ at a pH of 12.7 (Figure 2.9-a). This rate corresponds to the maximum value of CO₂ dissolution measured at the same pH in pure water (cf. Figure 2.8), implying that also for these experiments CaO dissolution kinetics were limited by the transfer of CO₂.

Using MgO, the maximum pH value was 10.3 and maximum CO₂ uptake rates of 0.021 mmol L⁻¹ s⁻¹ were reached. Referring to the tested equilibrium pH of MgO of 10.8 (cf. above), the release of Mg²⁺ and OH⁻ was the rate limiting step for the CO₂ uptake also for the maximum tested solid density (amount of mineral phase suspended per volume of water). For the smaller available mineral surface areas, the CO₂ uptake and pH consequently decreased with decreasing MgO-amounts. However, at a MgO concentration below 0.05 mol L⁻¹, the CO₂ uptake remained constant. At this point the effect of the lower pH seems to counterbalance the effect of the smaller available surface area.

Effect of temperature

The effect of temperature (Set B experiments) on CO₂ uptake is different for the two oxides. While a higher temperature enhances CO₂ transfer in the CaO system it has the opposite effect in the MgO system (Figure 2.10).

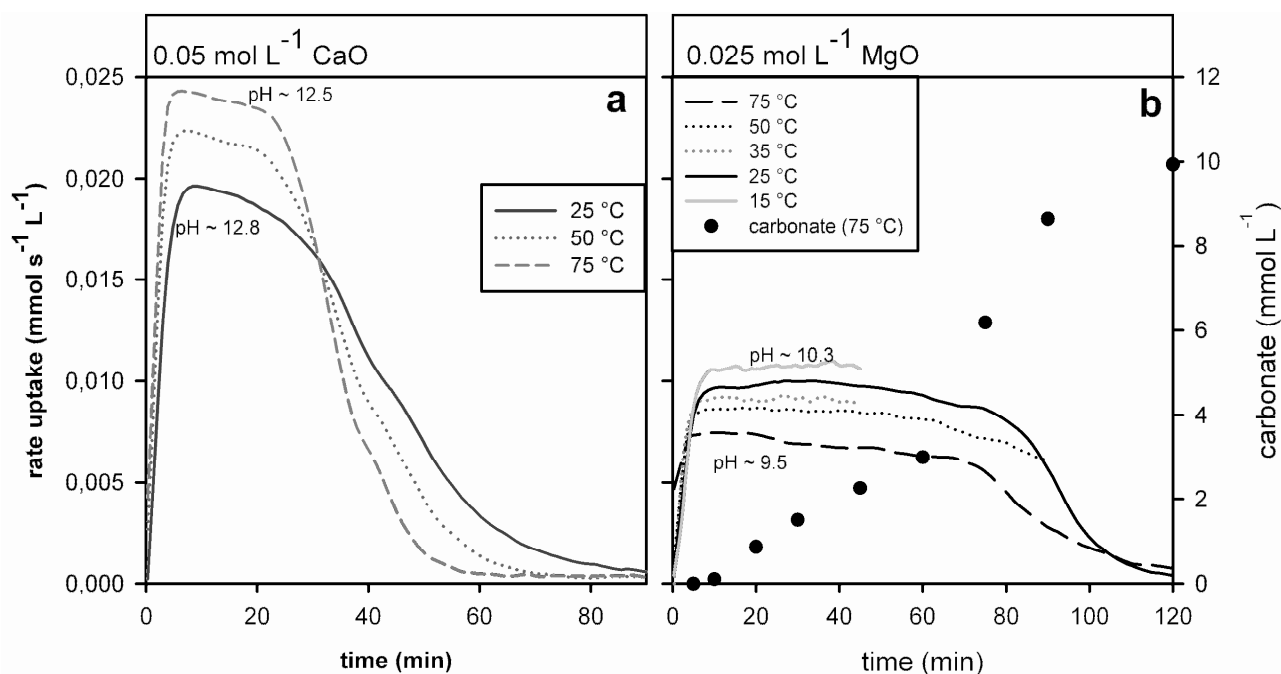


Figure 2.10: Set B: Effect of different temperature (25 to 75 °C) on the CO₂ uptake rates and maximum pH values of CaO or MgO carbonation experiments: $c(\text{CaO}) = 0.05 \text{ mol L}^{-1}$ or $c(\text{MgO}) = 0.025 \text{ mol L}^{-1}$, $p\text{CO}_2 = 0.01 \text{ MPa}$, stirring rate = 450 rpm

Both minerals are characterized by a retrograde solubility with temperature (Robie and Hemingway, 1995). As a consequence, lower pH values were established at the higher temperatures in both mineral suspensions. The dissolution kinetics of both oxides, however, appears to increase with temperature. Maximum rates of CO₂ uptake are reached distinctly earlier in the 75 °C-experiments compared to lower temperatures-experiments (Figure 2.10).

The precipitation rate of calcite is known to increase with temperature (Dreybrodt and Buhmann, 1991). After 30 minutes of reaction $\sim 30 \pm 0.75 \text{ mmol L}^{-1}$, $37.8 \pm 1 \text{ mmol L}^{-1}$ and $40 \pm 0.75 \text{ mmol L}^{-1}$ calcite was precipitated for 25 °C, 50 °C and 75 °C, respectively. Calcite precipitation thus increased with rising temperature, which is in accordance with the observed higher CO₂ uptake rates and the lower suspension pH due to higher H⁺ supply rate. It can be assumed that the increase of the TDIC removal by the precipitation reaction amplified the concentration gradient of CO₂ between the gaseous and the liquid phase at higher temperature and thus may have lead to the observed enhancement of CO₂ uptake.

In contrast, no precipitation of Mg carbonates had been observed in the temperature range between 15 °C and 50 °C using 0.025 mol L⁻¹ MgO. Mg carbonate precipitation only occurred at 75 °C right from the start of the experiment and even increased after ~ 60 minutes of reaction. At the low pH established by the lower solubility of MgO at this temperature, the dissolution rate of CO₂ in water may have dropped to a value that explains the observed decrease of the CO₂ uptake rate in spite the precipitation of solid phase. Compared to the CaO-system, the rate of Mg carbonate precipitation in the MgO-system is substantially lower than the total uptake of CO₂ of the MgO suspension. This means that the gradient of CO₂ between the gaseous and the liquid phase is less affected by the increasing temperature.

2.4 Conclusions

In summary our experimental observations showed a number of processes and conditions which influence the rate and the products of the carbonation of pure mineral CaO- and MgO-carbonation.

The carbonation of CaO happens fast, occurs at high pH values > 12 and is controlled at the mineral surface by the dissolution of Ca(OH)₂. In our CO₂ experiments a CaO mineral surface area of about 7.5 m² L⁻¹ was necessary to reach the saturation pH of 12.8 (25 °C, 600 rpm, pCO₂: 0.01 MPa). As long as Ca(OH)₂ is available CO₂ uptake by the system is high and leads to the simultaneous precipitation of CaCO₃. In contrast, under similar conditions MgO carbonation is a slower and much more complex process. The attained pH values, CO₂ uptake rates and carbonation velocities were substantially lower, which is due to the lower solubility product of the reaction controlling hydroxide Mg(OH)₂. The observed dissolution rates were substantially lower compared to CaO. Lacking or slower carbonate precipitation contributes to this phenomenon as well as slower CO₂ transfer from the gas phase due to lower pH.

Gas phase CO₂ transfer into the aqueous phase can be a carbonation limiting factor, which is controlled by the solution pH, by the available surface area of the gas/water interface and by the gradient at that interface. Total CO₂ uptake was thus maximized by high turbulence and by a steep gas/water CO₂ gradient, as observed at maximum calcite precipitation rates at higher temperatures. In the CaO system, the CO₂ transfer was always the rate limiting step for carbonation. In the MgO experiments, the rate of Mg carbonate precipitation was always lower than the total uptake rate of CO₂ at the chosen process conditions. Consequently, lower uptake rates of CO₂ have been observed at higher tem-

peratures due to lower saturation pH of Mg(OH)₂. However it remains an open question whether temperatures greater than 75 °C will increase the rate of Mg carbonate precipitation to an extent leading again to an enhanced net uptake rate of CO₂.

These findings have a number of implications for a potential technical application of alkaline earth mineral carbonation for CCS, which are important regardless if natural minerals or alkaline waste phases are used. The reaction progress found for the pure minerals shows parallels with the bulk processes observed during carbonation of alkaline wastes, suggesting that CaO and MgO can be used as proxies to estimate alkaline waste reaction with CO₂. Furthermore the laboratory results show that an optimum CO₂ distribution and supply to the reacting suspension is essential to achieve maximum CO₂ uptake rates. This can be managed by providing adequate turbulence and interface area. In order to maximize total CO₂ binding also reaction conditions favouring precipitation of CaCO₃ and Mg carbonates have to be applied, i.e. temperatures > 50 °C. The fast and easily achieved precipitation of Ca carbonates emphasizes that Ca rich materials should be utilized preferentially. Additionally, a process combining the alkalinity donating Mg(OH)₂ dissolution with CaCO₃ precipitation, e.g. by using Ca from other source minerals, might be a feasible option to limit energy demand otherwise required to enforce for Mg carbonate formation.

These findings are valuable information about how to optimize alkaline waste carbonation in an aqueous system. To further improve our understanding of the mechanisms and kinetics of the controlling reactions at the mineral surfaces (dissolution and precipitation), however, improved experimental setup and approved methods for examining the mineral surface chemistry need to be applied. Future work should also focus on establishing a kinetic model, covering the different reactivity of alkaline components to predict the carbonation of different waste materials and to optimize the process design.

Table 2.2: Minor and trace elements of the used powders of CaO and MgO determined by ICP-MS after digestion with hydrofluoric acid.

	CaO (mg kg ⁻¹)	MgO (mg kg ⁻¹)
Al	304	<
Ba	<	6.35
Ca	n.d.	72.2
Cr	<	6.23
Cu	<	7.69
Fe	236	35.93
K	148	31.4
Mg	3278	n.d.
Mn	117	6.05
Na	76.5	1500
Ni	<	13.02
Pb	6.85	<
S	1825	<
Si	443	227
Sr	196	8.53

Acknowledgements

Funding for the research projects CO₂-TRAP and ALCATRAP was provided by the German Ministry of Education and Research (BMBF) through the GEOTECHNOLOGIEN research and development program (grant 03G0614A and 03G0690A). We thank M. Heider, M. Rohr and D. Kuenkel for technical assistance in the laboratory. Thanks also to C. Ockert and the anonymous reviewers for comments and suggestions on the text.

Chapter 3

APPLICATION OF A PHREEQC BASED KINETIC MODEL TO SIMULATE PROCESS AND DYNAMICS OF THE CARBONATION OF ALKALINE MATERIALS BY GAS PHASE DERIVED CO₂ IN AQUEOUS SYSTEMS

3 APPLICATION OF A PHREEQC BASED KINETIC MODEL TO SIMULATE PROCESS AND DYNAMICS OF THE CARBONATION OF ALKALINE MATERIALS BY GAS PHASE DERIVED CO₂ IN AQUEOUS SYSTEMS

Back, M¹; Bauer¹, M and Peiffer, S.¹

Abstract

In this study a simplified model for the carbonation of alkaline waste materials has been set up and tested. The model is based on the PHREEQC program, which was used for thermodynamic calculations. Additionally the possibility of implementing reactions kinetic into the code as BASIC statements was used to predict the reaction progress over time. Experimentally derived specific dissolution rates for CaO/MgO and CO₂ were taken for the model implementation together with the available dissolution/precipitation kinetic of calcite and anhydrite taken from literature. Experimental assays conducted in an aqueous carbonation reactor were used as reference to test the model and evaluate its robustness and sensitivity.

By applying the common rate law of Morse we determined a rate constant k of 0.94 mmol L s⁻¹ with a correspondent rate order of 3.4 for CaO dissolution. MgO dissolution was nearly two orders slower with a rate constant of 0.0011 mmol L s⁻¹ and rate order of 5.3.

The implementation of the used rate law for the dissolution of CaO and MgO was well suited to kinetically model the carbonation process of the alkaline oxides and its progression sequence over time. We could demonstrate that the dissolution and precipitation reactions mainly depend on the saturation state and the pH of the solution.

By testing two related scenarios relevant for carbon capture and storage (CCS), it was shown that MgO derived alkalinity can be used for calcite precipitation. The addition of CaCl₂ as Ca source is preferential due to its high solubility and high reaction affinity to H⁺. By adding CaSO₄ into a solution containing Mg²⁺ and dissolved carbon species, degassing of CO₂ from the suspension is observed mainly due to the drop of the pH and the increase of HCO₃⁻.

¹ Department of Hydrology, University of Bayreuth, BayCEER, D-95440 Bayreuth, Germany

By testing the presented model for the simulation of the carbonation of lignite fly ash. Disparities were mainly observed with respect to the mineral dissolution rates of certain mineral phases and can be mainly assigned to the complex and partially unknown mineral compositions of the residues. The significant higher CO₂ neutralizing capacity, calculated by our simulation, suggests that a large part of reactive CaO and MgO was still incorporated in the mineral matrix of the fly ashes and could not be dissolved at mild process conditions (25 °C).

3.1 Introduction

Reduction of CO₂ emissions into the atmosphere is a key challenge in order to mitigate the anthropogenic greenhouse effect. To these ends technical solutions are investigated to capture CO₂ after combustion of fossil fuels from the power plant flue gases. Typical separation techniques are based on CO₂ pre-concentration, which significantly decrease the efficiency of a power plant (Rubin, 2008). Alternatively CO₂ can be removed directly from the power plant flue gas by reaction with alkaline materials, like minerals or alkaline waste by mineral carbonation (Costa et al., 2007; Huijgen et al., 2006a; Oelkers et al., 2008).

Previous studies showed that CO₂ sequestration by alkaline wastes in aqueous solutions is a rapid process and occurs already at mild process conditions (Back et al., 2008; Back et al., 2011). Reactions and kinetics of CO₂ uptake in alkaline waste suspension were determined experimentally on the basis of the process variables pH, pCO₂, Ca, Mg and total dissolved inorganic carbon (TDIC) using a batch reaction system. The CO₂ neutralizing capacity of different alkaline materials, like fly ashes, oil shales, steel slags, cement kiln, or bottom ash, was carried out to be primarily due to the presence alkaline reacting and easily soluble (hydr)oxides of Ca and Mg like free lime, periclase, portlandite or brucite (Baciocchi et al., 2010; Back et al., 2008; Huijgen and Comans, 2006a; Huntzinger et al., 2009; Uibu et al., 2009). Depending on the process conditions this resulted in the formation of solid phase carbonates (calcite, vaterite, Mg carbonates) and the increase of DIC, mainly as Mg carbonate complexes. In the context of CCS, carbonated products can be disposed in landfills or used as additive in building materials, while DIC may be injected into an aquifer as an Alkalinity Containing Solution (ACS) in a consecutive step, both providing possibilities for ultimate CO₂ storage.

Using pure mineral powders of CaO and MgO minerals with CO₂ in laboratory systems, the direction and velocity of these processes could be reproduced and evaluated (Back et al., 2011).

Physico-chemical model calculations are valuable tools to improve our understanding of processes and controls in natural or anthropogenic systems, predict reaction for not tested conditions or materials and to support a technical realization. Due to the importance of dissolution and precipitation processes in the context of mineral carbonation mainly thermodynamic equilibrium models were previously used for reproduction of technical assays (Montes-Hernandez et al., 2009; Uliasz-Bochenczyk and Mokrzycki, 2006) as well as natural (weathering) system (Astrup et al., 2006; Meima, J.A. and Comans, R.N.J. 1999). Also

flow models (ASPEN, METSIM) were used to simulate the continuous mineral carbonation process in technical systems (Lekakh et al., 2008; Huijgen et al., 2006a). The geochemical model code PHREEQC (Parkhurst and Appelo, 1999) was applied to estimate the dissolution and precipitation of various solid phases in technical carbonation application (Gitari et al., 2006; Montes-Hernandez and Perez-Lopez, 2009; Perez-Lopez et al., 2008; Uliasz-Bochenczyk and Mokrzycki, 2006) in order to predict CO₂ uptake processes and potentials. Were these models successfully applied?

Any model dealing with the carbonation of alkaline minerals in natural or waste materials in an aqueous reaction system has to deal with several individual processes (as pointed out by Uliasz-Bochenczyk and Mokrzycki, 2006, Fernandez et al, 1999; Rendek et al., 2006). The thermodynamic constants of these processes are mostly well known and available in one of the standard PHREEQC databases. For many reactions even constants for high ionic strength conditions are provided (Pitzer, 1979):

- Diffusion of CO₂ into the suspension
- Solvation of CO₂(gas) into CO₂(aq) and formation of H₂CO₃
- Dissociation of H₂CO₃ into HCO₃⁻ and CO₃²⁻ under H⁺ release
- Dissolution solid phases releasing Ca²⁺, Mg²⁺ and caustic alkalinity
- Nucleation and precipitation of Ca or Mg carbonates (e.g. calcite, vaterite, magnesite, nesquehonite)

Little attention was up to now paid to modelling the kinetic of the carbonation procedure, even though they are crucial for any application on industrial scale. The carbonation reaction of an amount of alkaline material is a dynamic process. All of the above mentioned processes take place in parallel, but the different Ca or Mg sources dissolve sequentially (Back et al., 2008). Also, the stability of products depends on the actual reaction conditions, e.g. as precipitation of MgCO₃ is kinetically inhibited and occurs only at higher temperatures and supersaturation compared to calcite formation (Hänchen et al., 2008). Mg based alkalinity may be used, however, for calcite precipitation if other Ca sources are available. Potential Ca rich solutions are brine solutions in the vicinity of Ca bearing rocks and sediments. As an example, a huge amount of oil and gas production a huge amount of saline wastewater containing dissolved Ca is produced annually and could be also used for carbonation reaction (Soong et al., 2006). Furthermore, the injection of CO₂ or alkalinity rich solutions into aquifers containing soluble Ca minerals (e.g. anhydrite) may represent a further option for mineral trapping. By the initiation of dissolution of these minerals the wa-

ter becomes enriched in calcium ions. Consequently precipitation of calcium carbonate occurs, provided that sufficient alkaline buffering capacity is available (Kühn, et al., 2009).

The objective of this study was to set up and test a simplified model for the carbonation of alkaline waste materials. The model was based on the PHREEQC program, which was used for thermodynamic calculations. Additionally the possibility of implementing reactions kinetic into the code as BASIC statements was used to predict the reaction progress over time. Experimental assays conducted in an aqueous carbonation reactor were used as reference to test the model and evaluate its robustness and sensitivity.

In the first step the model thermodynamic constants and rate expressions were determined for in situ conditions in the reactor and have been compared available literature values.

Studies of pure end-member divalent metal oxides are however very timely and scarce. Certainly due to the high reactivity of CaO and MgO, only a few studies exist offering the kinetic rate constants measured at acid pH conditions (pH 1 and pH 2, Casey and Ludwig, 1996; Oelkers, 2001, Vermilye, 1969), varying by up to 10 orders of magnitude. We therefore performed dissolution experiments under nitrogen atmosphere as a function of the saturation state of CaO and MgO using our batch reactor system.

In the second step these constants were included in the model and their quality tested by comparing experimental and modelled data for the carbonation of pure CaO and MgO. In the last step the evaluated model was applied to three more complex systems and sequestration scenarios. In these we estimated the effect of different additional Ca²⁺ sources (CaCl₂, CaSO₄) on carbonation and especially on the utilization of MgO derived alkalinity.

Alkaline residue materials contain, unfortunately, a variety of different Ca and Mg bearing minerals and glassy spheres including different cement phases (CSH), anorthite, brownmillerite, gehlenite, anhydrite, calciumsilicates, aluminosilicates and apatite. Furthermore, constituents of silicon (quartz, cristobalite, tridymite, opal), aluminium (mullite, corundum, alunite) and iron (Fe(II)- and Fe(III)- hydr(oxides) and sulphates) are typically contained in these materials (Enders, 1995; Vassilev et al., 1999). Also, the reaction pathway leads to more unusual products (e.g. vaterite and bassanite) or to metastable phases (e.g. ettringite) for which thermodynamic data is lacking. One of our main goals was thus to investigate how the heterogeneous composition of the fly ashes affects the overall CO₂ transfer with respect to the carbonation process. Based on the determined mineral composition of lignite fly ashes used for laboratory carbonation experiments (Back et al., 2008) we com-

pared the results to a simplified model system including a representative amount of CaO and MgO, anhydrite, calcite and NaSO₄.

The model provides a first tool to identify reaction controls and find preferential process conditions and promising types of alkaline materials for carbonation. The model also might be a useful tool for predicting the kinetics and water composition of the system, supporting the process of designing and dimensioning a technical carbonation system.

3.2 Materials and methods

Experimental section

All experiments were carried out in a 3.7 L reactor facility (ALF, Bioengineering) equipped with a heating jacket, magnetic stirrer, an automatic titration system, temperature sensor, and electrodes for pH and electric conductivity (EC). Gas flow through the gastight reactor was controlled by mass flow controllers (MKS Instruments, Type 258C). During reaction pH (Mettler-Toledo electrode), EC including temperature (WTW), and the output pCO₂ (Vaisala GMP221 IR-sensor) were recorded continuously. Additionally the suspensions were sampled periodically and filtered (nylon filter: 0.45 μm). Depending on experiment the filtrates were analyzed for Ca and Mg (ICP-OES Varian Vista-Pro after acidification with 1 vol.-% of HNO₃ s.p.) and TDIC (GC, Hewlett Packard, headspace after acidification). Solid samples were taken after an experiment, freeze-dried and homogenised to determine the mineralogical composition by X-ray diffraction (XRD) and X-ray fluorescence (XRF). The CO₂ uptake of the system was determined from the set gas flux, known input and measured output CO₂ concentrations. A more detailed description of methods and calculations is provided in (Back et al., 2011).

The following p.a. grade chemicals were used in the experiments: CaO (96-100.5 wt.-%, Fluka), MgO (>> 98 % calcined substance, Fluka), NaCl (Fluka), CaCl₂ (Fluka), NaHCO₃ (Fluka). The single-point BET surface area measurement using a porosimetry system (Micromeritics ASAP 2010) revealed an area of 28 ± 1 m² g⁻¹ for the MgO and 2.7 m² g⁻¹ for the CaO powder. The MgO sample consisted of ~ 99 wt.-% periclase, whereas the CaO sample was made up of ~87 wt.-% lime and ~13 wt.-% portlandite (XRD analysis). CO₂ of certified gas phase concentration was used for sensor calibration and experiments. Lignite fly ashes from a lignite coal powerplant (Neurath, Germany) were used in this study. The fly ashes were collected from the first filtering step of connected electrostatic precipitators and stored in containers sealed from ambient air. Residual coal particles >250 μm were

separated from the ashes by sieving. The used anhydrite (Sangerhäuser, Thuringia, Germany) was grinded to grain sizes < 63 µm by a disc mill.

Determination of in situ CO₂ dissolution kinetics

The transfer of CO₂ from the gas phase into the water phase under in situ conditions of the used reactor system was determined at different pH values (7 to 12) and stirring rates (300 to 600 rpm). To initiate the experiments the reactor vessel was filled with de-ionized water. During equilibration with the applied pCO₂ at different pH values and stirring velocities the gas phase CO₂ was monitored in the outflow and TDIC was measured in the solute phase over time. These methods were used to calculate the reactor specific in-situ dissolution rate of CO₂ at different stirring rates (Back et al., 2008). Solutions pH was kept constant by adding HCl (2 M or 0.2 M) using the autotitration system.

Determination of in situ CaO and MgO dissolution rate constants

For CaO and MgO dissolution rate measurement, deionized water was degassed for 30 min at pH 4. After addition of the solid mineral phase the increase in EC, reflecting the increase in dissolved Ca²⁺ or Mg²⁺ concentration (Supporting Info, Figure 3.14), was recorded and used for reaction-rate determination.

The common rate law for the dissolution of minerals was used, which depends on the saturation and on the mineral surface (Eq. 3.1 - Eq. 3.3, (Morse and Berner, 1972b)). The experimentally determined dissolution rate was plotted against saturation (1-Ω). Using a nonlinear regression analysis to minimize the RMSE between measurement and model (CoStat (Simons, 2001)) the reaction order n and the reaction rate constant k were determined. Assuming the particle morphology of the CaO and MgO powders as ideal spheres, the dependence order of the surface area x was fixed as 3 during our regression analysis according to Eq. 3.3.

$$R_f = \frac{dmCaO}{dt} = k (S(t)) \cdot (1 - \Omega)^n \quad (\text{Eq. 3.1})$$

R_f: reaction rate (mol m² s⁻¹)

S(t): surface area per Liter (see below)

Ω: saturation with respect to the mineral phase (IAP/K)

n: reaction order

k: rate constant (mol L s⁻¹)

$$S(t) = \frac{A_{initial}}{V_{initial}} \cdot \left(1 - \frac{n(CaO_{conversion}(t))}{n(CaO_{initial})} \right)^x \quad (\text{Eq. 3.2})$$

with,

S: surface area per Liter ($\text{m}^2 \text{L}^{-1}$)

A: initial surface area (m^2)

V: volume of solution (L)

n: amount of mineral (mol)

x: dependence order on surface area

$$R = k \cdot \frac{A}{V_{\text{initial}}} \cdot \left(1 - \frac{n(\text{CaO}_{\text{conversion}}(t))}{n(\text{CaO}_{\text{initial}})} \right)^3 (1 - \Omega)^n \quad (\text{Eq. 3.3})$$

CO₂ uptake (carbonation) experiments by alkaline materials

In order to test the model calculations with the implemented rate constants against real data experiments were conducted with pure mineral phases or lignite fly ash (see Table 3.1). For these experiments the laboratory reactor was filled with 2 L of deionized water, brought to the experimental temperature and saturated with CO₂ at the desired pCO₂ and gas flux conditions. Then pure mineral phases, such as CaO, MgO, CaCl₂ and CaSO₄ or mixtures of these materials, were added to the solution.

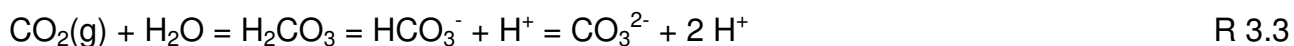
In the MgO-CaCl₂ experiment the reactor was filled with a 0.136 mol L⁻¹ CaCl₂ solution and brought to the experimental conditions (see Table 3.1). At the starting point of the experiment 0.05 mol L⁻¹ of MgO have been added.

In the MgO-anhydrite experiment we added 0.05 mol of anhydrite to the MgO suspension after being reacted with CO₂ for 120 minutes.

In the experiment using lignite fly ash 50 g L⁻¹ have been suspended into the water and have been reacted with CO₂ in aqueous suspension for 120 minutes.

Modelling section

The PHREEQC computer code uses thermodynamic constants to calculate the aqueous element speciation in equilibrium, accounting for acid/base reaction, redox transformations, complexation, solid dissolution/precipitation or gas dissolution. Thermodynamic equilibrium constants for many reactions are provided by model databases but can also be included from external sources. Reaction kinetics can be implemented by using a BASIC interpreter. For each reaction with time dependence a separate BASIC program is required in the input file, which must specify the reaction variables, such as reaction order n and rate constant k. To simulate the carbonation of alkaline phase mineral dissolution, CO₂ dissolution and mineral precipitation (Reaction 3.1 to 3.5) were modelled for every time step in dependence on the actual saturation conditions. Dissociation of H₂CO₃ was considered as fast and always in equilibrium.



In situ rate constants were determined by the above mentioned experiments for the dissolution of CO_2 in water and dissolution kinetics of CaO and MgO . The precipitation of Mg carbonates is complex and not yet fully understood (Back et al., 2011), which is why conditions allowing for the formation of magnesite, hydromagnesite, nesquehonite were avoided in the experiments and thus did not have to be simulated. Well-known rate coefficients, such as the dissolution/precipitation kinetic of calcite (Plummer et al., 1978) and the dissolution kinetic of anhydrite/gypsum (Jeschke et al., 2001) are taken from literature. The expressed rate law of calcite dissolution/precipitation (Plummer et al., 1978) was already translated into the PHREEQC code by (Parkhurst and Appelo, 1999) and could be used in this model. Because the ionic strength was generally below 0.1 the Davies equation (Davis and Kent, 1990) was applied for the calculation of activity coefficients by using the MINTEQ database (Allison et al., 1990).

The quality and validity of the model setup and the determined rate and equilibrium parameters was tested against the results of carbonation experiments. The data from a sequence of laboratory assays was used for that purpose, which were carried out in the aqueous laboratory reactor. The mineral phase complexity of experiments and simulations was increased stepwise. In the first step only pure phases of Ca (hydr)oxide or Mg (hydr)oxide were used. Secondly, a mixture of Ca and Mg (hydr)oxide was carbonated, followed by systems including CaCl_2 or CaSO_4 .

Finally, we attempted to simulate the observed carbonation process of mineralogically much more complex alkaline waste suspensions. From XRD analysis we know that the used fly ash suspension (50 g L^{-1} lignite fly ash from Neurath power plant) contain initially $\sim 0.15 \text{ mol L}^{-1}$ lime, 0.2 mol L^{-1} periclase, $\sim 0.03 \text{ mol L}^{-1}$ calcite, and $\sim 0.06 \text{ mol L}^{-1}$ anhydrite (Back et al., 2008). These phases and the minerals quartz (0.03 mol L^{-1} , inert) and Na_2SO_4 , (0.03 mol L^{-1} , completely soluble) can all be easily accounted for in the normal model setup. Additionally, however, brownmillerite ($\text{Ca}_2(\text{Fe}_{1.634}/\text{Al}_{0.366})_2\text{O}_5$, $0.06\text{-}0.1 \text{ mol L}^{-1}$), several silicates (microcline, gehlenite, quartz, Ca-Si hydroxides, $\sim 0.04 \text{ mol L}^{-1}$) and a considerable pool of amorphous material ($> 15 \%$ w/w) could be identified in the lignite fly

ash. Little to no thermodynamic and kinetic data for the minerals is available, so that their reactivity and contribution to CO₂ binding was unclear.

The model was first tested against the data from experiments with pure mineral phases and solution composition. Later reactions in less well defined alkaline waste suspensions were simulated (CaO, MgO, mixed phase carbonation, see Table 3.1).

In situ rate constants were determined by the above mentioned experiments for the dissolution of CO₂ in water and dissolution kinetics of CaO and MgO (CaO, MgO, CO₂ dissolution, see Table 3.1). The precipitation of Mg carbonates is complex and not yet fully understood (Back et al., 2011), which is why conditions allowing for the formation of magnesite, hydromagnesite, nesquehonite were avoided in the experiments and thus did not have to be simulated. Well-known rate coefficients, such as the dissolution/precipitation kinetic of calcite (Plummer et al., 1978) and the dissolution kinetic of anhydrite/gypsum (Jeschke et al., 2001) are taken from literature. The expressed rate law of calcite dissolution/precipitation (Plummer et al., 1978) was already translated into the PHREEQC code by (Parkhurst and Appelo, 1999) and could be used in this model. Because the ionic strength was generally below 0.1 the Davies equation (Davis and Kent, 1990) was applied for the calculation of activity coefficients by using the MINTeq database (Allison et al., 1990).

Table 3.1: List of experiments

experiment	solid phase	T °C	CO ₂ %	rpm	remarks
CaO dissolution	CaO	25	0	600	
MgO dissolution	MgO	25	0	600	
CO ₂ dissolution	none	25	10	300-600	pH stat 7-12
CaO carbonation	CaO	25	10	600	
MgO carbonation	MgO	25	10	600	
mixed phase	CaO/MgO	25	10	600	
MgO-CaCl ₂	MgO/CaCl ₂	25	10	600	
MgO-anhydrite	MgO/CaSO ₄	25	10	600	
lignite	fly ash	25	10	600	

3.3 Results and Discussion

Determination of rate constants and model setup

Determination of experimental CO₂ dissolution kinetics

We measured the dissolution kinetics of CO₂ in the aqueous phase at constant pH for different stirring velocities. After a short period (< 5 minutes) of pH stabilization, the TDIC concentrations in the solution increased linearly and the CO₂ uptake from the gas phase

was constant over time. Apparently, the dissolved amount of CO_2 was near equilibrium with respect to the pCO_2 for the chosen pH and stirring conditions. Each addition of NaOH during the titration thus leads to a short pH increase and re-dissolution of CO_2 until the equilibrium pH with respect to the pCO_2 is reached again. These conditions are also consistent with those in our carbonation experiments as soon as saturation with respect to CaO and MgO is achieved in the initial stage of mineral dissolution.

Since both, the dissolution rate of CaO and MgO as well as the CO_2 dissolution rate increase together with the agitation velocity (see also Back et al., 2011), we only performed pH-stat-experiments with the maximum value of 600 rpm for the model implementation (Figure 3.1). The in situ CO_2 dissolution rates determined show an almost linear increase with pH (Figure 3.1) but were substantially slower than expected from literature for high pH values. We attribute this phenomenon to the limitation of diffusion of gaseous CO_2 through the water film. The available gas-water interface area is thereby determined by the number and dimension of emerging gas bubbles in the system, mainly as a function of the agitation velocity.

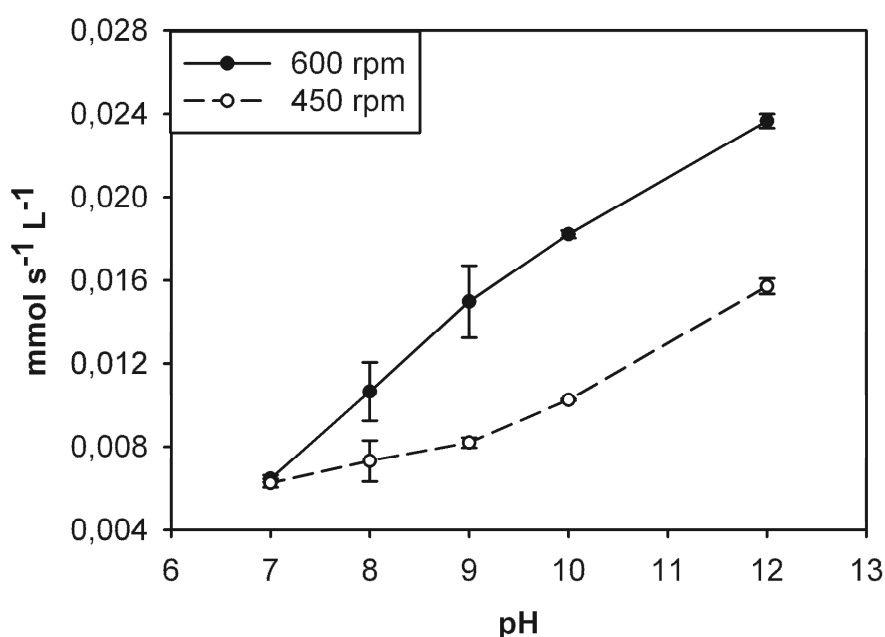


Figure 3.1: The dissolution kinetic of CO_2 in water valid for our experimental setup as a function of stirring rate and pH at close to equilibrium conditions of CO_2 . The standard derivation was calculated by comparison of the measured CO_2 -uptake (sensor technique, see method section) and increase of TDIC in solution (headspace method) versus time

Determination of the CaO dissolution rate constant

In CaO dissolution experiments constant Ca^{2+} and OH^- (as estimated through pH and EC) concentrations established ~ 5 min after mineral addition to the water phase (Figure 3.2). At that time the ion activity resulted in a $\log \text{IAP} = -4.92 \pm 0.03$ at 25°C and was therefore slightly above the solubility product for portlandite ($\log K_{\text{SP}}: -5.325$; Duchesne, 1995; Nordstrom, 1990; Allison, 1990).

CaO dissolution rates were determined for the initial release of Ca^{2+} and OH^- during the first 8 minutes of reaction until saturation with respect to CaO was attained at a pH value of ~ 12.8 (Figure 3.2).

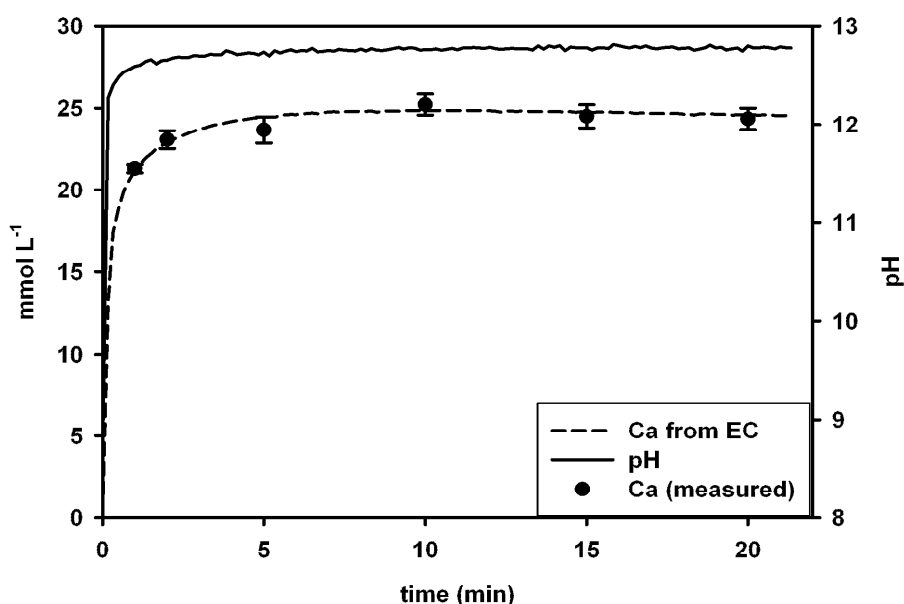


Figure 3.2: CaO dissolution experiment at 25°C at nitrogen atmosphere for a suspended amount of 0.05 mol L^{-1} CaO at constant stirring of 600 rpm.

Based on the experimental data illustrated in Figure 3.2, a nonlinear regression analysis was performed to calculate the variables n (rate order) and k (rate constant). The calculation resulted in a rate order n of 3.4 with a corresponding reaction rate of $0.94 \text{ mmol L s}^{-1}$ and a residual error of 0.0074 (Figure 3.3).

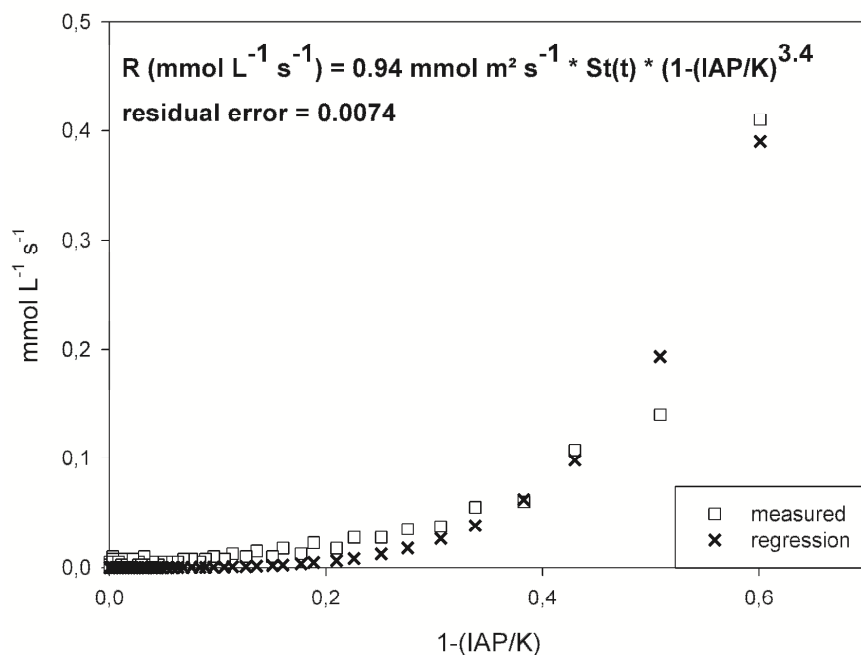


Figure 3.3: Rate model for the dissolution of CaO (0.05 mol L^{-1}) at 25°C under nitrogen atmosphere and constant stirring of 600 rpm.

The dissolution process of CaO is supposed to be constricted on the breaking up of the Ca–oxygen bonds and replacing these with proton–oxygen bonds. Many workers have shown that the rate of oxide mineral dissolution is mainly influenced by the interactions with adsorbed hydrogen and dissolved hydroxyl ions in the solution (Casey and Ludwig, 1996). In general, the dissolution of single (hydr)oxides proceeds via metal for proton exchange reactions (often called protonation), breaking metal–oxygen bonds and replacing these with proton–oxygen bonds (Furrer and Stumm, 1986). Considering proton promoted dissolution as the rate determining process, a n -th order dependence on the activity of the protonated surface species is often observed (Stumm and Morgan, 1996). However, pH values greater than 10 are reached within seconds in our experiments, supposing that the changing effect of protonation is certainly negligible after this point. We suppose, the high dissolution kinetic of CaO far from equilibrium certainly leads to a loss of reliability according to the determination of the exact value of n and the characterization of the dissolution mechanism, respectively. Without offering a mechanistic explanation with respect to the calculated reaction order we have used the parameters for model implementation from the regression analysis (Figure 3.3) as the most adequate numerical solution.

Testing of CaO and CO₂ dissolution rate values: Model vs. experiments

Figure 3.4 shows the results from a carbonation experiment by suspending 0.05 mol L⁻¹ CaO into the water at 25 °C and a pCO₂ of 0.01 MPa. This experiment has been also described in detail in Back et al. (2008).

The reaction progress is marked by an abrupt change of the solution pH after approximately 23 min of reaction. The initial period (first 23 min) is characterized by the fast increase of the pH and dissolved Ca due to the dissolution of CaO. Maximum CO₂ uptake rates are observed during this period (not shown here) and the absence of TDIC is explained by the instantaneous precipitation of calcite. In the second period after 23 minutes of reaction the CO₂ uptake rates significantly decrease together with the pH of the process solution. At this time the pool of CaO is totally consumed and mainly converted into calcite. The following small increase of TDIC and Ca denotes equilibrium with respect to calcite and pCO₂ at pH values of ~ 6.

Together with the available kinetic data of calcite dissolution/precipitation (Plummer et al., 1976) we applied the determined kinetic data of CO₂ and CaO dissolution (see above) to simulate the experimental time course (Figure 3.4). The simulation results match quite well to the laboratory data with respect to the time course of the pH, dissolved Ca concentration and the amount of precipitated calcite. A slight difference between the experiment and the simulation is the amount of TDIC in the first period of the reaction. Calcite precipitation in the simulation is controlled by the SI of calcite and the dissolved amount of CO₂. As an explanation we suggest that the precipitation of calcite in the laboratory experiments might be pre-dominantly surface controlled and might be therefore determined by the transportation of CO₂ to the mineral surface of CaO.

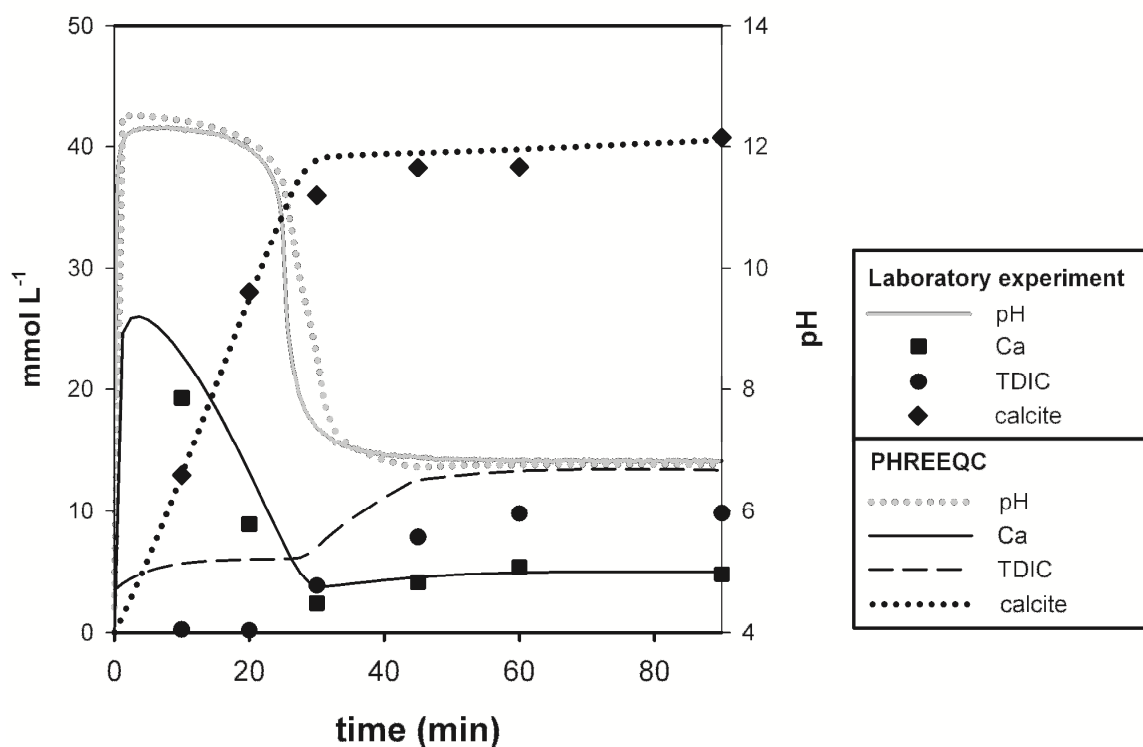


Figure 3.4: Comparison of results from laboratory experiments with simulation results performed with PHREEQC ($x=3$, $n=3.4$, $k=0.94 \text{ mmol m}^{-2}\text{s}^{-1}$) for the reaction between CO_2 ($p\text{CO}_2$: 0.01 MPa) and CaO (0.05 mol L^{-1}) suspended in water at a temperature of $25 \text{ }^\circ\text{C}$ and constant stirring of 600 rpm.

Determination of the MgO dissolution rate parameters

The dissolution kinetics of MgO was determined in analogy to those of CaO (Figure 3.5). After 6 minutes of suspending MgO into the water at $25 \text{ }^\circ\text{C}$ and under constant stirring (600 rpm) log IAP values for MgO/MgOH₂ of -9.8 have been observed. These are lower than the saturation product of periclase ($\log K_{\text{SP}} = -6.49$) but above that of brucite ($\log K_{\text{SP}} = -11.2$, Allison, 1990) and by a factor of five lower than the IAP for CaO/Ca(OH)₂ (see above). However, maximal values of dissolved Mg were reached already after 6 minutes of reaction suggesting equilibrium with respect to MgO. Until the end of the experiment after 20 minutes of reaction, a slight decrease of the Mg concentration was observed. We attribute this effect of hydroxylation of the MgO surface as proposed by (Wogelius et al., 1995) leading to the formation of a hydroxide surface structure. The lower solubility of the Mg hydroxide, respectively brucite, is supposed to explain the decrease of the Mg concentration during the onset of the experiment.

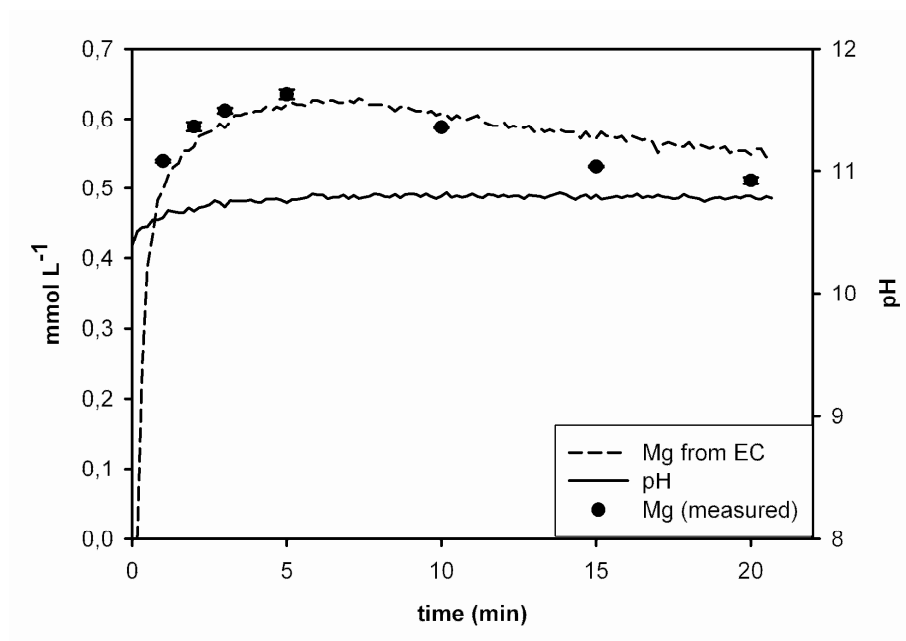


Figure 3.5: MgO dissolution experiment at 25 °C at nitrogen atmosphere for a suspended amount of 0.05 mol L⁻¹ MgO at constant stirring of 600 rpm.

The progression of the pH and the Mg concentration during the first 6 minutes of reaction was used to calculate the rate constant k and reaction order n of MgO dissolution, as already described for CaO (see above).

Compared to CaO dissolution the calculated rate constant k for MgO dissolution is nearly three orders of magnitude lower ($k = 0.0011 \text{ mmol m}^2 \text{ s}^{-1}$) with a correspondent rate order of 5.4 (Figure 3.6).

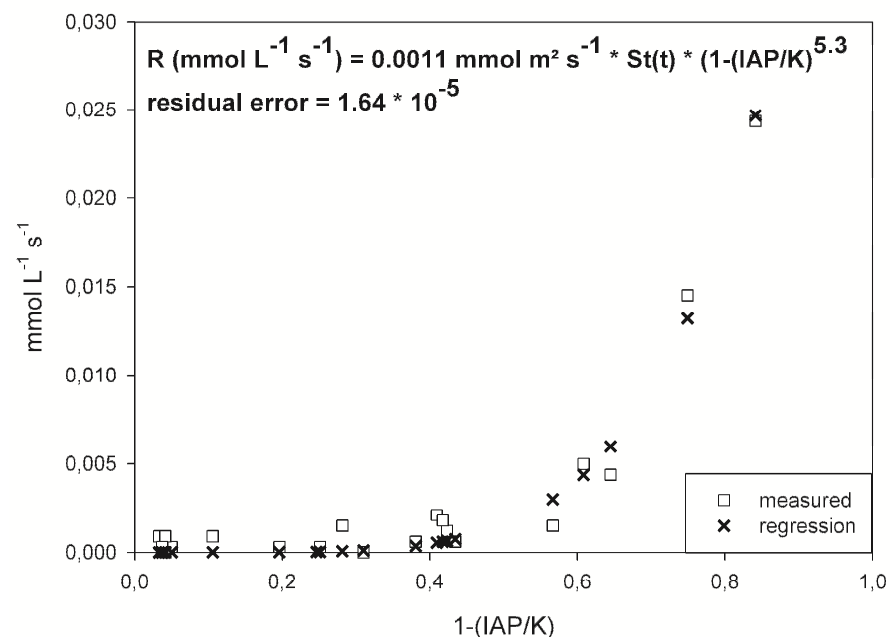


Figure 3.6: Rate model for the dissolution of MgO (0.05 mol L⁻¹) at 25 °C under nitrogen atmosphere and constant stirring of 600 rpm.

Testing of MgO and CO₂ dissolution rate values: Model vs. experiments

The determined kinetic data of MgO dissolution was correspondently used to simulate the reaction of MgO suspended in water at 25 °C and a pCO₂ of 0.01 MPa (Figure 3.7).

Compared to CaO/Ca(OH)₂ suspensions the reaction of MgO/Mg(OH)₂ with CO₂ is slower at initial pH values of 10.8 after 2 minutes, indicating solubility equilibrium with respect to MgO. The almost linear increase of TDIC concentration equals the release of dissolved Mg to the process solution as far as MgO has been nearly totally consumed after ~ 60 minutes of reaction. After the consumption of the MgO pool the increase of TDIC proceeds up to a final value of 0.1 mol L⁻¹ after ~ 100 minutes of reaction at an equilibrium pH of ~ 7.6. No carbonate precipitation has been observed at the chosen process conditions, whereas two mols of CO₂ have been neutralized per one mol of MgO.

The reaction progress of the laboratory experiment is reproduced by the PHREEQC simulation quite well. However, a smoother course of the pH curve is observed in the laboratory experiment and may indicate that our model assumptions on surface control do not exactly meet the actual conditions.

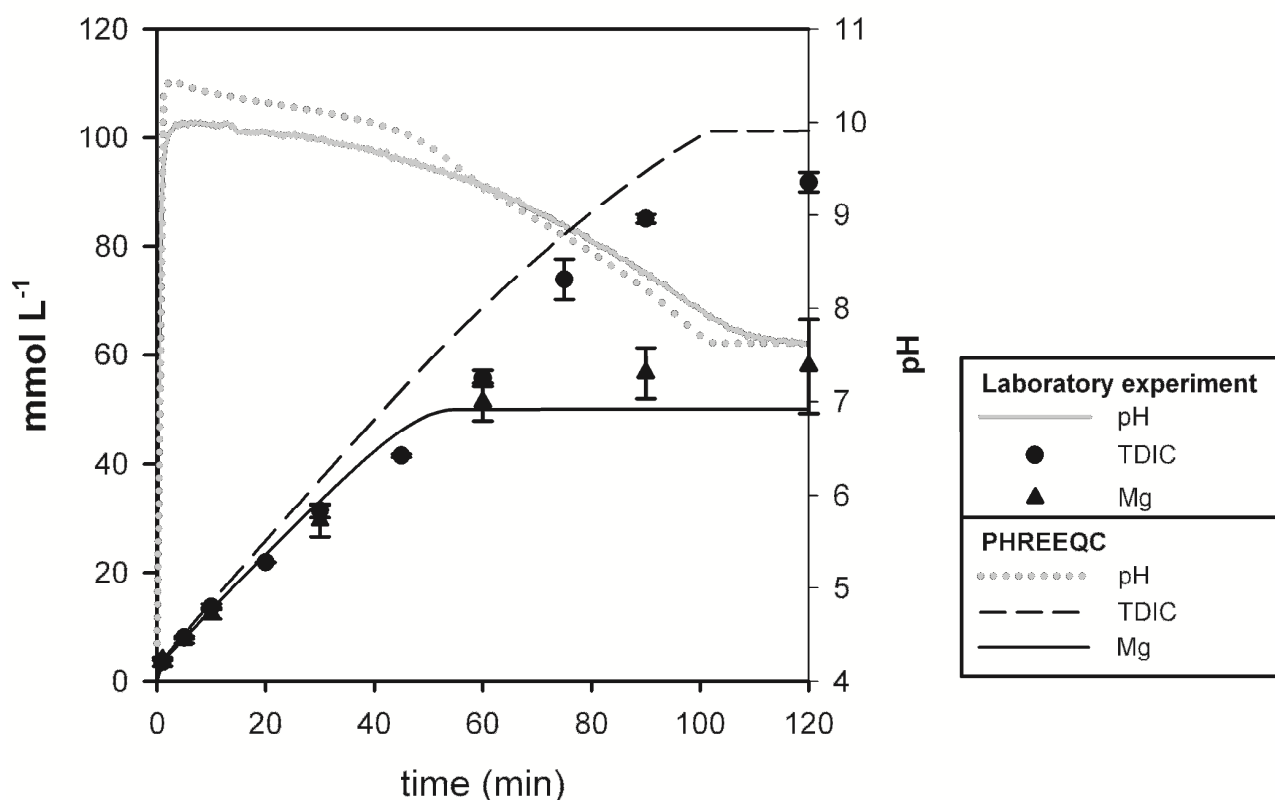


Figure 3.7: Comparison of results from laboratory experiments with simulation results performed with PHREEQC for the reaction between CO₂ and a suspensions of MgO of 0.05 mol L⁻¹

Simulation of the carbonation in systems with multiple mineral phases

As shown above the composed model was well able to simulate the carbonation process and its progression over time for different alkaline minerals separately. Carbonation processes in nature or in technical system, however, mostly take place in more complex systems containing a variety of different mineral phases. In order to evaluate the model performance for these more complex multiphase systems we carried out laboratory carbonation experiments and corresponding simulations.

Conditions were chosen, which represent scenarios relevant in the context of mineral carbonation and CCS. Scenario I) depicts the sequence of reactions occurring during CO₂-sequestration a mixture of Ca and Mg (hydr)oxides, which are substantial contributors to CO₂ uptake of alkaline residues. Scenario II and III) evaluate the possibilities of using MgO derived alkalinity for the carbonation of Ca added as CaCl₂ containing solution and solid CaSO₄. These are relevant processes occurring in brines, typically rich in Ca²⁺, or anhydrite containing aquifers, into which MgO and CO₂ rich suspensions are transferred. Since the precipitation of Mg carbonates is often kinetically inhibited, brine or anhydrite are potential Ca sources and might be used to sequester CO₂ in form of calcite. Scenario IV) attempts to simulate alkaline waste material carbonation.

Scenario I: Carbonation of a CaO/MgO mixture

The carbonation process of CaO/MgO mixture in aqueous suspension has been described in detail elsewhere (Back 2010), and is illustrated for a suspension with 0.05 mol L⁻¹ of Ca resp. Mg (hydr)oxide in Figure 3.8. The initial period of the reaction is controlled by the quick dissolution and saturation with respect to CaO/Ca(OH)₂ at pH values of ~ 12.8 and calcite precipitation. As soon as the mineral pool of Ca (hydr)oxide is consumed (~ 20 minutes in the shown experiment), the dissolution of MgO starts and the pH is stabilized at values of ~ 10.3 denoting saturation with respect to MgO. A built-up of the concentrations Mg and C species occurs until MgO is dissolved after ~120 minutes of reaction.

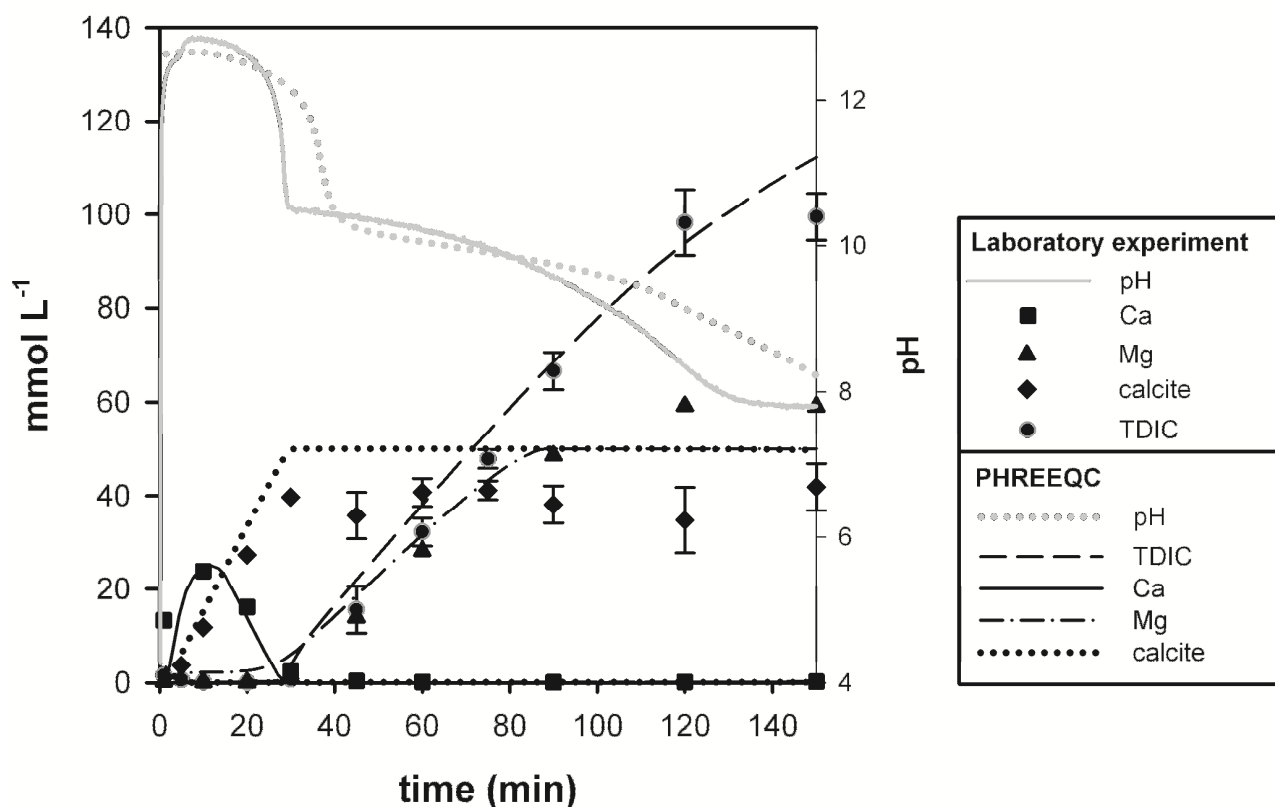


Figure 3.8: Comparison of results from laboratory experiments with simulation results performed with PHREEQC for the reaction between CO₂ and a suspensions of CaO and MgO both of 0.05 mol L⁻¹

The sequence of reactions could be reproduced well by the developed PHREEQC model using the previously determined rate parameters. The pH development as well as the changes in dissolved species (Ca²⁺, Mg²⁺, DIC) and equilibrium phases (CO₂, CaO, MgO) can be predicted over time and in the appropriate concentration range. The model provides additional information about the carbonation process, which is not directly visible in the aqueous phase data. In addition, the simulation directly shows the saturation index (SI) of the minerals CaO, MgO and calcite and illustrates that their dissolution and precipitation depends on the saturation state and the pH (Figure 3.9-A). The whole process initially is limited by CO₂ uptake and carbonic acid formation, which has a lower rate than CaO dissolution. The solution was soon almost saturated with respect to CaO (SI_{CaO} > -1), nonetheless the high rate constant allowed for the quick dissolution of this phase (Figure 3.9-B). MgO dissolution, however, took place mostly at SI < -2, so at stronger undersaturation (Figure 3.9-A+B). This reflects the slower release rate for this mineral, resulting in longer reaction time for similar amounts and a gradual pH decline. In this stage CO₂ uptake rate was above mineral dissolution rate, thus the system was limited by Mg²⁺ and OH⁻ release.

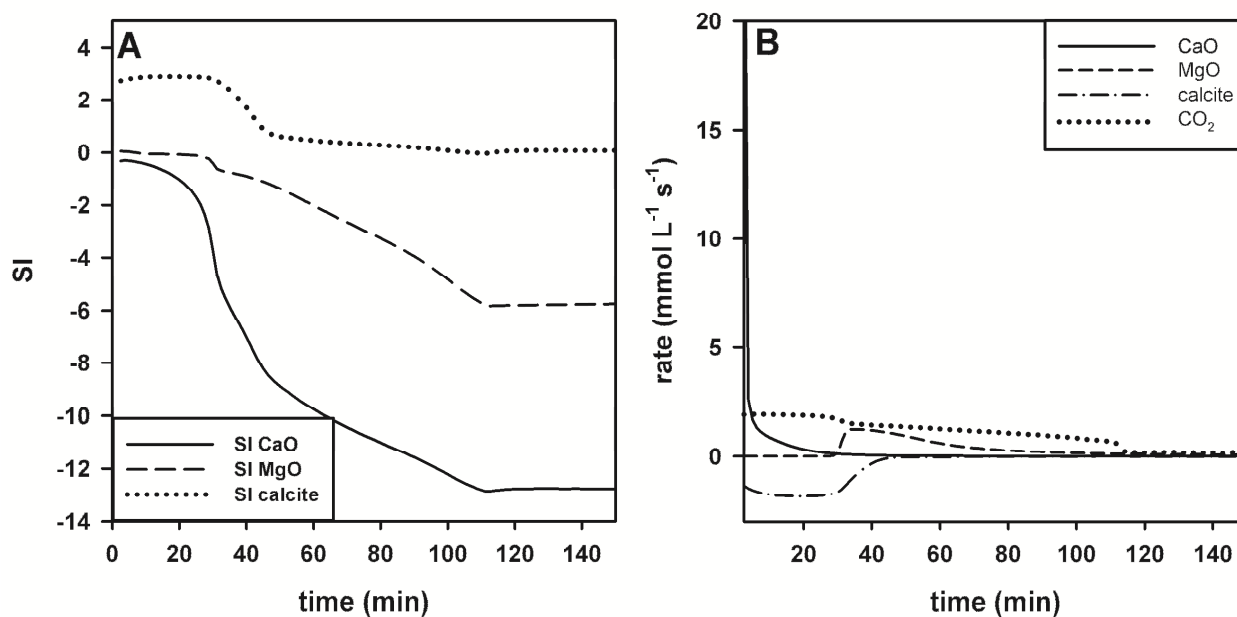


Figure 3.9: Simulation with PHREEQC for the reaction between CO_2 and a suspensions of CaO and MgO both of 0.05 mol L^{-1} . -A: Comparison of calculated SI values of CaO, MgO and calcite. -B: Dissolution kinetics of CaO, MgO and CO_2 compared to rate of calcite precipitation.

Scenario II: Using MgO derived alkalinity for CO_2 sequestration in Ca rich solution

Both laboratory experiment and simulation results demonstrate that the MgO based alkalinity is immediately consumed due to CO_2 dissolution and calcite precipitation (Figure 3.10-II). The amount of calcite precipitated matches approximately the amount of Mg^{2+} released over the whole course of the experiment. Thus, only a small fraction of CO_2 neutralized in the suspension is bound as HCO_3^- , as also shown by low TDIC values. Berner (1975) showed in a series of precipitation experiments that the presence of Mg^{2+} disturbs the precipitation of calcite, but this was apparently not the case for the conditions in our experimental approach.

The results show the applicability of the PHREEQC model for predicting the reaction sequence and velocity of CO_2 binding in an aqueous MgO/CaCl_2 system. The reaction was considerably fast and limited by the CO_2 provision to the system only at the very beginning, after ~ about 5 min the MgO dissolution step became rate controlling.

A difference between laboratory observations and simulation results was found for the patterns of pH and CO_2 uptake over time (Figure 3.10-A). The PHREEQC model suggest lower maximum pH and CO_2 uptake values and a more gradual and slower decline than the experiments. We attribute this to the fact that the applied CO_2 dissolution rate model (Results section 1, see Figure 3.1) depends on pH and stirring velocity but not on the CO_2

concentration gradient between water and gas phase. Calcite precipitation however increases this gradient due to the fast consumption of CO_2 . (Back et al., 2008) and thus causes an increase in dissolution rate of CO_2 and consecutively also in the dissolution rate of MgO . High pH values between 9 and 10 are therefore observed during this period.

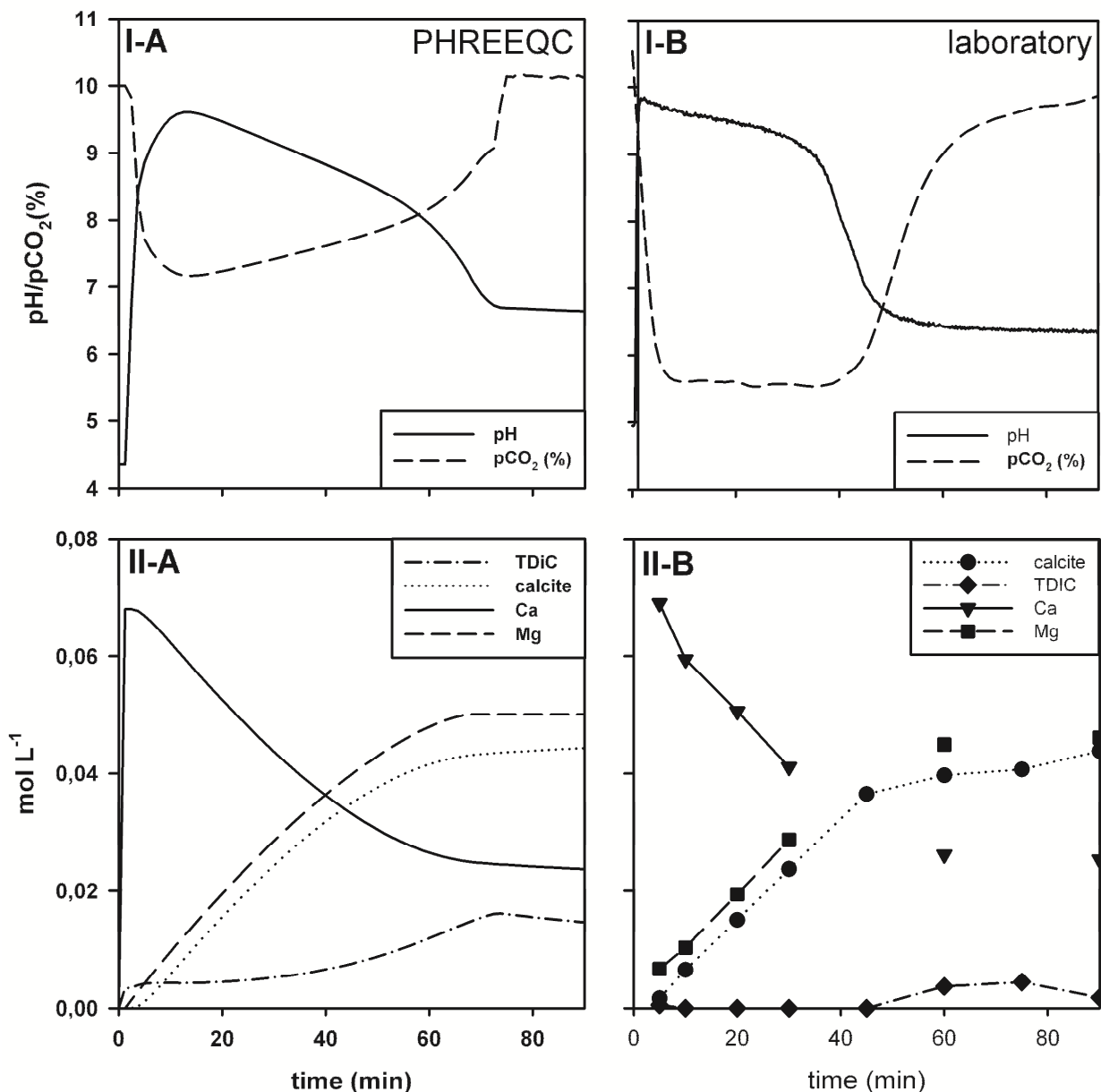


Figure 3.10: $0.05 \text{ mol L}^{-1} \text{ MgO}$ are suspended in a solution containing $0.136 \text{ mol L}^{-1} \text{ CaCl}_2$ at a $p\text{CO}_2$ of 0.01 MPa , $25 \text{ }^\circ\text{C}$ and constant stirring of 600 rpm .

Scenario III: Using MgO derived alkalinity for CO₂ sequestration with anhydrite

This scenario reflects the reaction of a TDIC, Mg²⁺ and MgO rich solution at high pH with solid phase anhydrite, functioning as Ca source material. The MgO suspension (0.05 mol L⁻¹) was first brought to reaction for 120 min with CO₂ at 0.01 MPa. In analogy to the pure phase experiments described above (results part I), within the first 90 – 100 min MgO dissolves completely and Mg²⁺ and TDIC are accumulated to constant values of ~ 0.05 mol L⁻¹ dissolved Mg and ~ 0.1 mol L⁻¹ dissolved inorganic C (ratio 1 Mg : 2 TDIC) at pH ~ 7. The PHREEQC model illustrates that carbon species are mainly present as HCO₃⁻ at this point, so two bicarbonate ions are required to balance one Mg²⁺.

The addition of 0.05 mol L⁻¹ anhydrite into the solution after 120 min brings the system into disequilibrium and initiates several processes. Mg²⁺ concentration remained constant at a value of 0.05 mol L⁻¹ throughout the experiment but Ca²⁺ and SO₄²⁻ started to appear in the solution due to the slow but continuous anhydrite dissolution. Sulphate release continued until the end of the experiment to ~15 mol L⁻¹ (Figure 3.11-II-A). Initially also EC and TDIC increased, but after ~150 min, CaCO₃ precipitation was triggered (increase in measured calcite) resulting in an EC drop, low Ca²⁺ concentrations and decreasing TDIC values. At the same time an increase in the pCO₂ of the gas outflow was observed with values above gas input pCO₂ was measured. This suggests degassing of CO₂ from the solution.

These findings, even the degassing and the anhydrite dissolution after Jeschke et al. (2001), could be reproduced very well by the PHREEQC model and the derived speciation data can help to interpret the apparent shift in solution chemistry observed after ~150 min. Before, HCO₃⁻ and SO₄²⁻ were charge balanced as aqueous Mg bicarbonate and Ca sulfate complexes. Then the onset of calcite precipitation removes Ca²⁺ and HCO₃⁻ from the solution in the stoichiometry of 1:1, leading to the formation of MgSO₄ (aq) and thus to the partial release of HCO₃⁻ from its aqueous complexes with Mg²⁺ as the pH remains constant.

This is supported by Figure 3.12, showing the development of production/consumptions rates for different species over time after the addition of the anhydrite. While the rates of CaCO₃ precipitation, MgSO₄ (aq) formation and CO₂ degassing increase quickly and remain > 0 throughout the rest of the experiment. Coming along with anhydrite dissolution, the aqueous species TDIC, HCO₃⁻ and MgHCO₃⁺ disappear. The rates of calcite formation and HCO₃⁻ consumption are similar, suggesting CaCO₃ precipitation according to R6 + R7. Additionally, also MgHCO₃⁺ starts to be consumed and to be transformed into MgSO₄ (aq)

as the thermodynamic stability favours the latter species. The degassing of CO₂ thus, seems to be caused by the decrease in pH (R7), the increase in HCO₃⁻ (R8) and the general rise in ionic strength.



In addition the comparison of experimental and PHREEQC simulation results also clearly emphasizes the problem of nucleation to start precipitation. Whereas calcite precipitation occurred almost immediately after anhydrite addition and saturation with respect to calcite in the simulation, its crystallization in the laboratory experiment was clearly delayed (~20 – 30 minutes). This suggests that a critical degree of oversaturation was necessary to start nucleation.

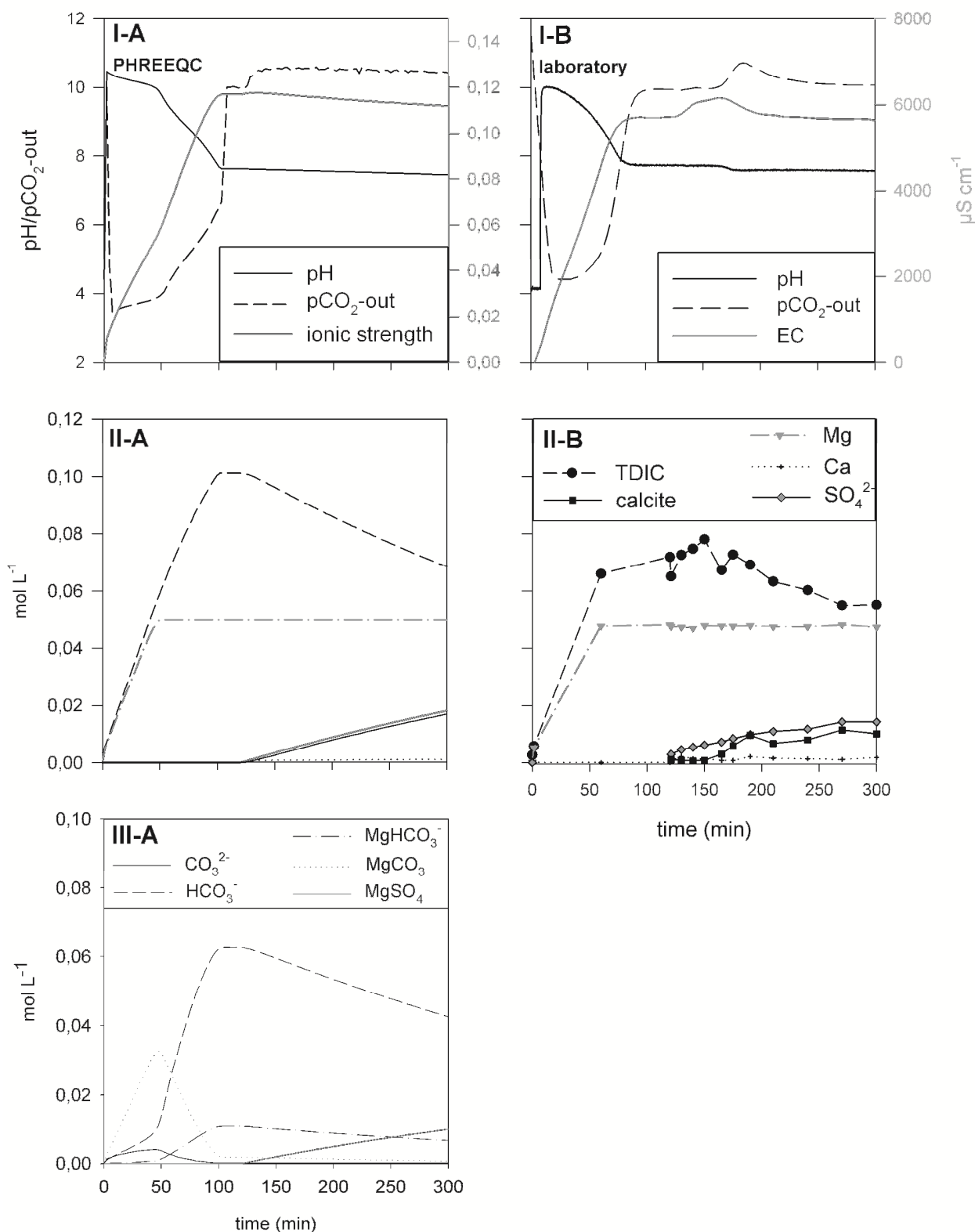


Figure 3.11: Comparison of the PHREEQC simulation (A) and laboratory experiment (B), the reaction of 0.05 mol L⁻¹ MgO at 25 °C, at a pCO₂ of 0.01 MPa and agitation rate of 600 rpm. After 120 minutes of reaction 0.05 mol anhydrite have been added (I: pH, pCO₂, EC; II: total concentration of dissolved TDIC, Ca, Mg, sulphate and amount of precipitated calcite; III: activities of certain dissolved species).

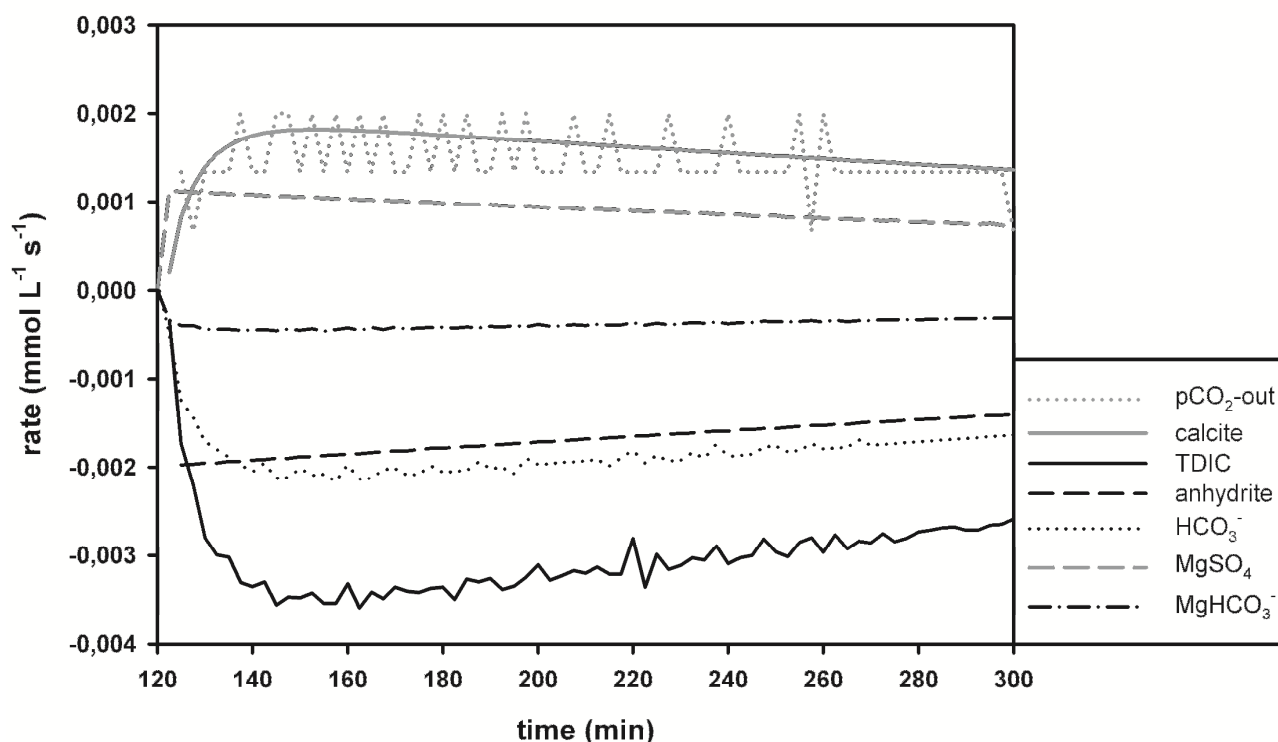


Figure 3.12: Comparison of the calculated activities of dissolved species (HCO_3^- , MgSO_4 , MgHCO_3^-) and total concentrations of TDIC, $\text{pCO}_2\text{-out}$, calcite and anhydrite from PHREEQC simulation after the addition of 0.05 mol L^{-1} anhydrite to the solution containing 0.05 mol L^{-1} MgO at $25 \text{ }^\circ\text{C}$, at a pCO_2 of 0.01 MPa and agitation rate of 600 rpm .

Simulation of lignite fly ash carbonation

As the arranged PHREEQC setup could adequately simulate the kinetics of pure mineral phase reaction with CO_2 using the experimentally derived rate constants, the final step was to model the processes occurring during the carbonation of a lignite fly ash sample with its more complex mineralogy.

The used lignite fly ash, as described by Back et al. (2008), contained highly soluble constituents. Contact with water leads to a rapid release of Ca, Na, SO_4^{2-} and OH^- into the solution and a strong increase in pH up to 12.8 (Figure 1, B). The high pH values measured in the first period of the reaction reflects the caustic alkalinity generated by the dissolution of lime. At the same time dissolved Ca is consumed by calcite precipitation. Once the Ca (hydr)oxide pool is depleted the reaction regime changes, with Mg phases and dissolved carbonate starting to control the pH and the CO_2 uptake. The dissolution of $\text{MgO}/\text{Mg}(\text{OH})_2$ causes the increase in Mg^{2+} concentration charge balanced by TDIC. According to dissolved species analysis the shift from CaO/Calcite controlled to MgO/Mg-TDIC controlled system occurred after 45 to 60 min at pH 8-9.

The initial model comprised the kinetics of CO₂, CaO, MgO, calcite and anhydrite. In correspondence to the experiments carried out with pure CaO and MgO, the simulation of the lignite fly ash carbonation with such a setup shows a very distinct separation of two reaction phases (Figure 1). In the initial period the system is controlled by the fast release of Ca²⁺ and caustic alkalinity from CaO at pH > 12 followed by the MgO buffered period with pH >10. The laboratory results with lignite fly ash, however, show a continual, gradual decrease of the pH from the beginning of the experiment and not a steep drop.

We attribute this difference as a limited and decreasing accessibility of the reactive Ca/Mg (hydr)oxide phases. Only a fraction of these mineral pools was apparently available quickly and easily for mineral dissolution and OH⁻ release under the given conditions. This is confirmed by several observations. First, at the end of the experiment lime and periclase could be still detected in the carbonated product, even though the pH in the suspension had been far below equilibrium values with CaO/Ca(OH)₂ (> 12) resp. MgO/Mg(OH)₂ buffered system (pH ~10.5). Second, if the total XRD determined amounts of CaO or MgO are applied, the carbonation in the model runs takes considerably longer than the time observed experimentally.

The reduction of the mineral surface area during dissolution is accounted for in the model. So the incomplete consumption of the (hydr)oxide pools in the fly ashes must be due to the inclusion of mineral fractions within grains from the beginning and with the formation of calcite coating during the reaction. Both factors explain why the CaO and MgO dissolution rates were substantially lower than expected from the pure phase experiments and why they decrease overtime. The release of species from the solid to the aqueous phase, however, strongly depends on the surface area. The bulk ash contain 10 times more mineral phase (w/w) but the BET surface of the bulk ash (38 m² g⁻¹) was only by a factor of 1.5 higher than that of a MgO powder (28 m² g⁻¹). Both the depletion of reactive minerals at grains surfaces and the formation of coatings must be expected to increase metal ion and OH⁻ diffusion times into the aqueous phase and thus lead to a decrease in carbonation amount and velocity over time (see also Huijgen et al. (2005)). The narrow peak of maximum EC within the first 5 minutes confirms the assumption that only a portion of the detected reactive minerals by XRD is easy available for mineral dissolution.

Simulation and experiment also differed in the pattern of the dissolved sulphate concentration over time. The quickly released amount of sulphate in the experiments (0.05 – 0.06 mol L⁻¹) was nearly twice the value being available from Na₂SO₄ (~0.025 mol L⁻¹, confirmed by ~0.05 mol L⁻¹ initial Na⁺ release) and concentration even increased slightly over

time during the carbonation process. This suggests the presence of another sulphate source, which might be a (amorphous) phase not detected by XRD analysis (e.g. Al-sulphate). Another explanation might be the instantaneous dissolution of finely granulated anhydrite. However, the positive SI values with respect to gypsum ($K_{\text{gypsum}} = 10^{-4.6}$, Appelo and Postma, 1999) and the constant amount of dissolved sulphate only allows the dissolution of a sulphate containing phase only within the first seconds of reaction (Figure 1-III-B). The lower and nearly constant concentration of dissolved Ca compared to our simulation results further indicates that the instantaneous precipitation of Ca containing phase like ettringite, as observed in Table 2, might have occurred. To summarize, the discrepancies between the model and laboratory experiment are mostly explained by the unknown dissolution/precipitation of those mineral phases that were not considered in the model. Neglecting these minerals was on the one hand necessary to keep the simulation code easy to handle. On the other hand mineral composition of the source materials is very heterogeneous with a substantial amount of glass compounds and XRD amorphous material. Determination of the exact mineralogy was therefore impossible and additionally reaction constants for many specific phases are not available.

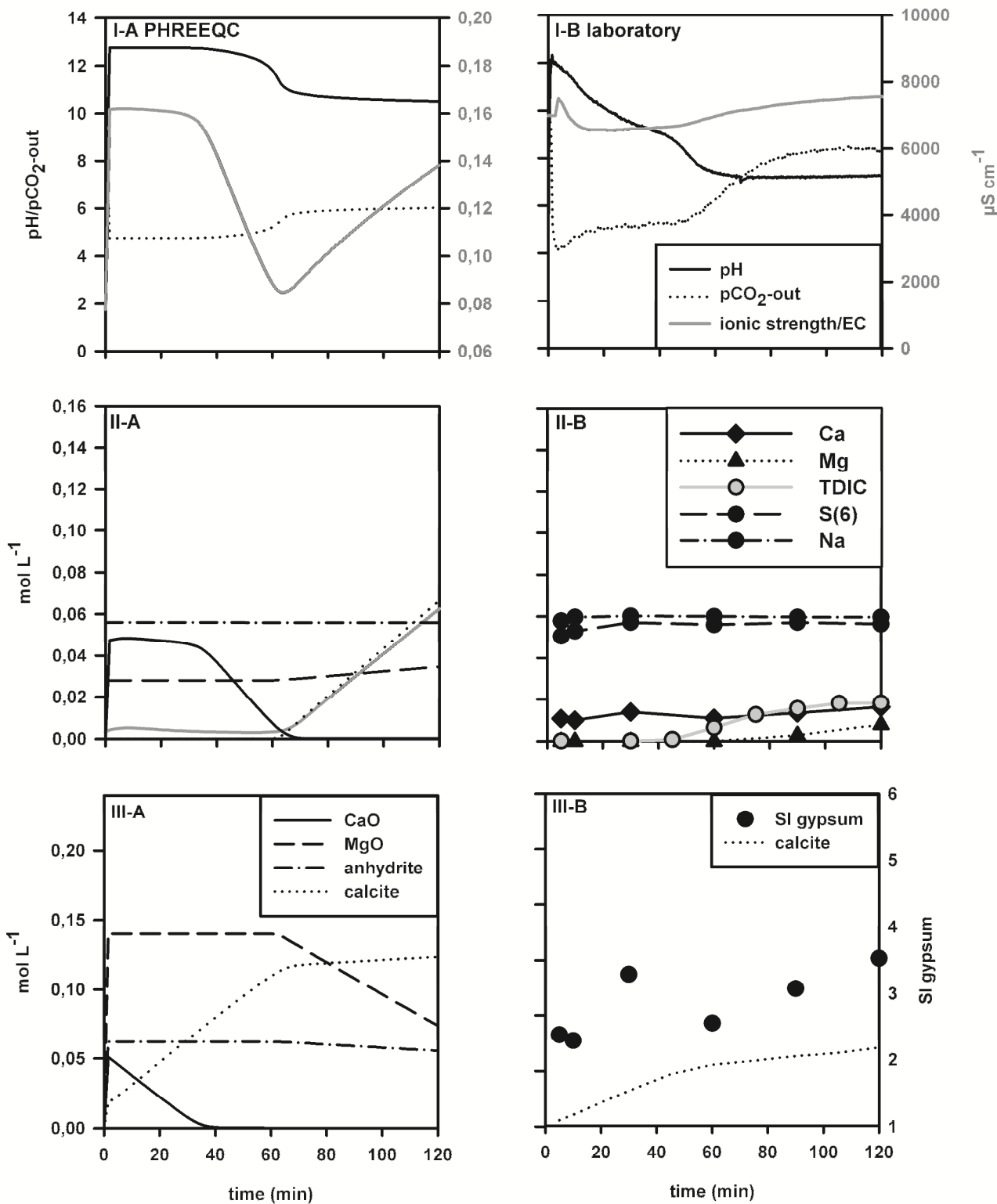


Figure 3.13: Simulation of lignite fly ash experiments (50g L^{-1}) with PHREEQC (A) and comparison with the laboratory experiment (B)

Table 3.2: Relative mineralogical composition of the lignite fly ash before and after 10 minutes of CO₂ treatment (s/l-ratio:75g L⁻¹, pCO₂: 0.02 MPa, stirring rate: 450 rpm, T: 25 °C)

mineral phase (Rietvelt analysis)	chemical formula	wt.-% (unreacted)	wt.-% (CO ₂ treated after 10 min)
brownmillerite	Ca ₂ (Fe _{1.634} ,Al _{0.366}) ₂ O ₅	20.5	20.5
anhydrite	CaSO ₄	13	7
lime	CaO	11.5	3
periclase	MgO	11.5	11.5
Na ₂ SO ₄	Na ₂ SO ₄	5	0
quartz	SiO ₂	3	3
amorph. compounds	-	28.5	42.5
ettringite	Ca ₆ (Al(OH) ₆) ₂ (SO ₄) ₃ 26 H ₂ O	0	3.5

3.4 Conclusions

Overall, the implementation of the used rate law for the dissolution of CaO and MgO was well suited to kinetically model the carbonation process and its progression sequence over time. We could demonstrate that the dissolution and precipitation reactions mainly depend on the saturation state and the pH of the solution. This explains why the dissolution and CO₂ transfer reactions occurs sequentially if both minerals are suspended at the same time.

By testing the scenario of using MgO derived alkalinity for calcite precipitation, the results illustrated that the addition of CaCl₂ as Ca source is preferential due to its high solubility and high reaction affinity to H⁺. The MgO based alkalinity was thus immediately consumed for calcite precipitation. By adding CaSO₄ into the Mg-TDIC solution, the reaction sequence was predominantly affected by the thermodynamic stability of MgSO₄ (aq). Degassing of CO₂ from the suspension was finally observed mainly due to the drop of the pH and the increase of HCO₃⁻. In order to understand the reaction sequence of the tested sequestration scenarios, the simulation was found to be a very useful tool since it allows the exposure of all dissolved species and present mineral phases at each timestep.

Furthermore, the simulating of the carbonation of lignite fly ash delivered important hints for further lack of knowledge, like the extended availability of thermodynamic data of characteristic mineral phases contained in combustion residues. In future work, a better simulation of fly ashes might be attempted through changing the amounts of available mineral (as a fraction of the total XRD determined), through adding “dummy phases” with equilibrium constants and kinetic parameters resembling unknown/amorphous Ca or Mg phases and by including ettringite und brownmillerite thermodynamically into the model. This way the model can even be used not only as a method of troubleshooting but as a

way to identify lacking phases and estimate their thermodynamic/kinetic properties in an inverse modeling procedure.

Acknowledgements

Funding this research was provided by the German Ministry of Education and Research (BMBF, 03G0614A). We thank M.Heider and M.Rohr for technical assistance and M.Kühn and K.Vosbeck for their support regarding the realization of the modeling procedure.

Supporting Information

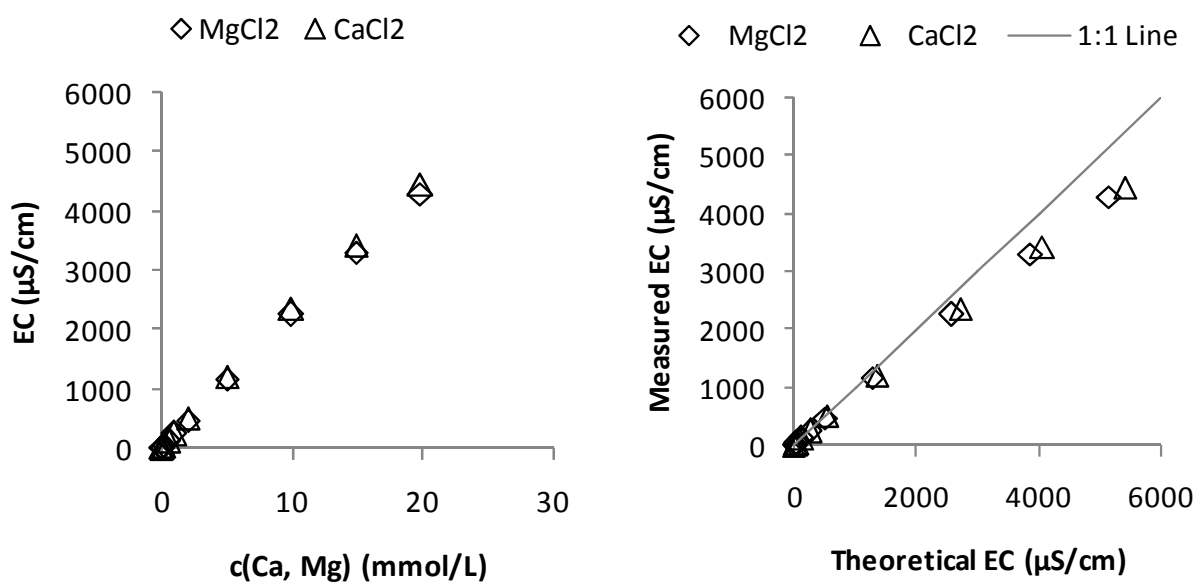


Figure 3.14: Solution concentration in Ca^{2+} and Mg^{2+} vs. measured EC and theoretical EC

Chapter 4

MINERAL TRAPPING OF CO₂ IN OPERATED GEOTHERMAL RESERVOIRS

Published in similar form as:

M. Kühn, C. Clauser, K. Vosbeck, H. Stanjek, V. Meyn, M. Back & S. Peiffer (2009) Mineral trapping of CO₂ in operated hydrogeothermal reservoirs, in M. Grobe, J. C. Pashin, and R. L. Dodge, eds., *Carbon dioxide sequestration in geological media—State of the science: AAPG Studies in Geology* 59, p. 545–552

4 MINERAL TRAPPING OF CO₂ IN OPERATED HYDROGEO THERMAL RESERVOIRS

Michael Kühn¹, Katrin Vosbeck², Volker Meyn³, Martin Back⁴, Christoph Clauser¹, Helge Stanjek², Stefan Peiffer⁴

Storage of carbon dioxide by precipitation of carbon-bearing minerals in geological formations is, on the long run, more stable and therefore much safer than direct storage or solution trapping. Among available options for CO₂ sequestration those are particularly attractive which offer additional economic benefits apart from the primary positive effect for the atmosphere (e.g. enhanced gas or oil recovery), such as the novel approach of storing dissolved CO₂ as calcite in managed geothermal aquifers.

Hydrogeothermal energy in Germany is mainly provided from deep sandstone aquifers by a so called “doublet” installation consisting of one well for hot water production and one well for injection of the cooled water. When cold brines are enriched with CO₂ and injected into an anhydrite bearing reservoir this mineral dissolves. As a result, the water becomes enriched in calcium ions. Numerical simulations demonstrate that dissolved Ca and CO₂ react to form and precipitate calcium carbonate provided that alkaline buffering capacity is supplied from plagioclase in the reservoir rock or by surface water treatment with fly ashes. It is shown that anhydrite dissolution with concurrent pore space increase is important to balance pore space reduction by precipitation of calcite and secondary silicates. Laboratory experiments prove the feasibility of transforming anhydrite into calcite and provide necessary kinetic input data for the modelling.

Suitable geothermal reservoirs exist, which contain sufficient anhydrite as matrix mineral and plagioclase for supplying alkalinity. Mass balance calculations performed with respect to the anhydrite and feldspar content show, that for an assumed operation time of 30 years, the theoretical storage capacity is significant: millions of tons of CO₂ can be trapped as calcite in geological formations used by geothermal heating plants.

¹ RWTH Aachen University, Applied Geophysics, Lochnerstrasse 4-20, D-52056 Aachen, Germany

² RWTH Aachen University, Clay and Interface Mineralogy, Wüllnerstrasse 2, D-52056 Aachen, Germany

³ Institute of Petroleum Engineering, Agricolastrasse 10, D-38678 Clausthal-Zellerfeld, Germany

⁴ University of Bayreuth, Hydrology, Universitätsstrasse 30, D-95440 Bayreuth, Germany

4.1 Introduction

Various available options for the sequestration of carbon dioxide (CO₂) in the subsurface have been proposed and discussed to reduce the amount of anthropogenic CO₂ released into the atmosphere. A possible means of reducing these CO₂ emissions is to inject them into structural reservoirs in deep, permeable geologic formations. The aim of the CO₂Trap project (Kühn et al., 2005) in the framework of the GEOTECHNOLOGIEN special program “Investigation, Utilisation and Protection of the Underground”, is to develop, study and evaluate, alternative approaches for the subsurface deposition of CO₂.

One concept is to sequester CO₂ not only by hydrodynamic trapping within a reservoir, but to convert dissolved CO₂ into the geochemically more stable form of calcite (CaCO₃) in a reaction with calcium obtained from dissolution of sulphates and alkalinity from feldspars or fly ash. In this way, the costs for sequestration in deep saline aquifers can be transformed into a benefit when combined with the production of ecologically desirable geothermal heat. Alternatively, geothermal energy can be made more economical, compared to fossil energy sources, by storing CO₂ and trading of emission certificates.

Due to the geological situation, geothermal energy in Germany is mainly provided from deep aquifers. The common arrangement of boreholes is the well doublet, consisting of one well for hot water production and one well for cooled water re-injection (Figure 4.1). The new concept is to load the cooled water with dissolved CO₂. After re-injection into the reservoir, this cold water becomes enriched in calcium e.g. due to the dissolution of anhydrite (CaSO₄). Subsequently, CO₂ precipitates as calcium carbonate. The following chemical reactions need to be considered with regard to CO₂ storage in geothermal reservoirs:

Due to the decreased solubility of anhydrite with temperature, injecting cold water dissolves the mineral in a region expanding around the well. The concentrations of calcium and sulphate increase in the water with the dissolution of anhydrite:



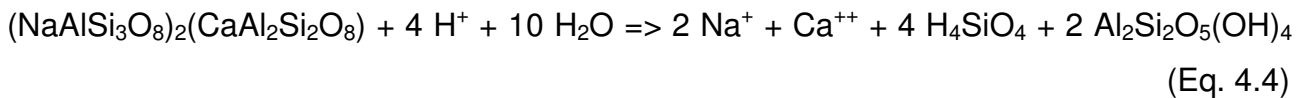
Before re-injection, the produced and cooled brines are enriched with carbon dioxide. As a result carbonic acid is generated:



The overall reaction, the transfer of anhydrite into calcite, describes the favoured reaction path:



From equation (3) it is obvious that a surplus in acid exists which tends to inhibit calcite precipitation in general. However, if the increase in Ca is large enough (equation (1)) or if alkalinity is available to buffer the reaction, the solubility product of calcite is exceeded and CO₂ will be trapped as calcite. Alkalinity can be provided either by surface water treatment with fly ash or in situ through the weathering of feldspars. The reaction of oligoclase to kaolinite is given here as an example:



With regard to the feasibility of this new technology the chemical reactions outlined above requires to find the answer to the following three key questions:

1. Where are suitable geothermal reservoirs which contain anhydrite as matrix mineral?
2. Does the transfer of anhydrite into calcite work at all and what are the reaction rates?
3. What are feasible sources of alkalinity and how fast can they be made available?

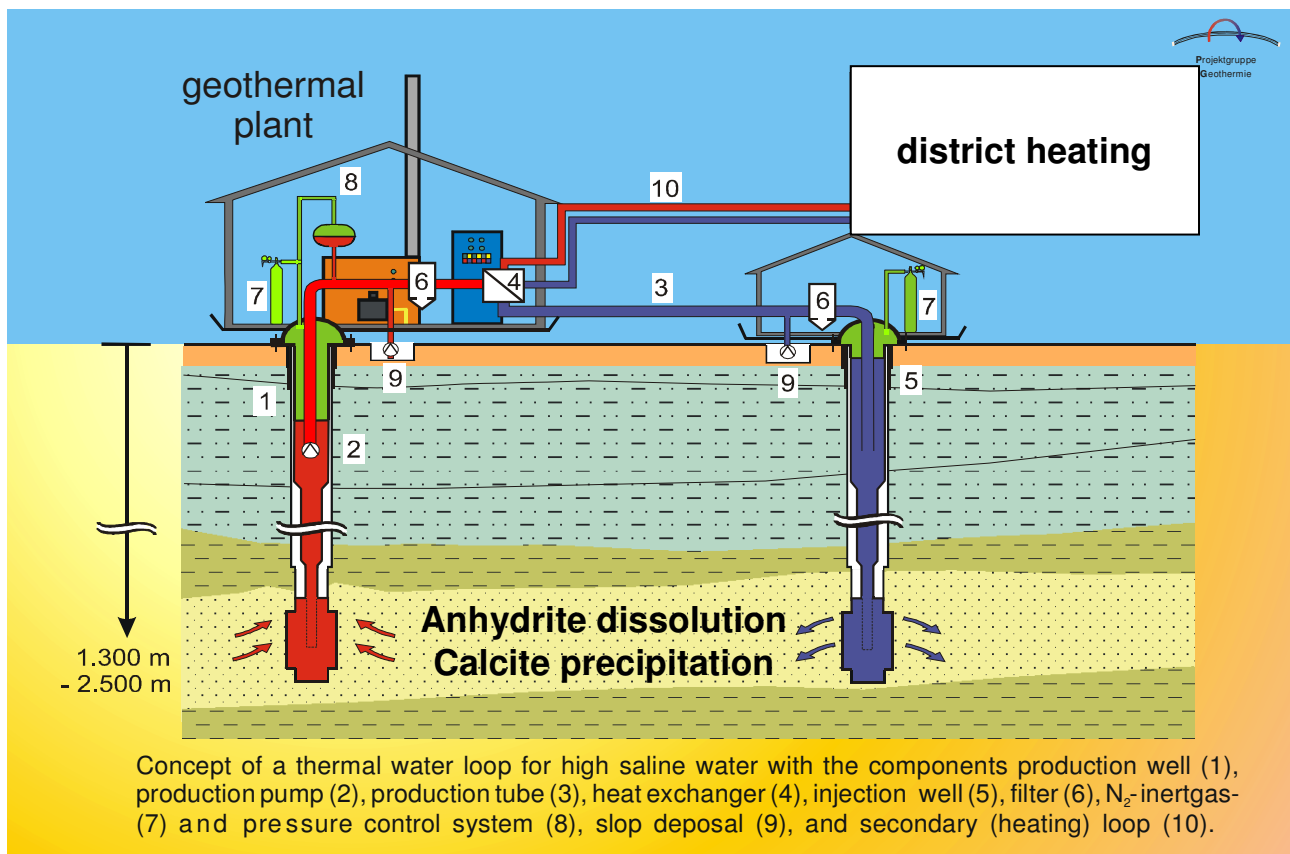


Figure 4.1: Geothermal heating plant with a common bore hole doublet arrangement.

4.2 Suitable geothermal reservoirs

The stratigraphic horizons, suitable for the storage of CO₂, are identified by the analysis of borehole data. They are selected based on the occurrence of anhydrite, adequate thick-

ness of potential storage layers and a pool of petrophysical data. The latter is required to deduce representative input parameters for numeric models.

One candidate site is at Stralsund, situated in Northeast Germany near the Baltic Sea. Here, a geothermal resource was confirmed in previous studies in Buntsandstein layers at a depth of about 1520 m (Kühn et al., 2002a). This site is used here to demonstrate the potential for CO₂ storage by numerical simulations. There are three wells in the target area which measures 12 km by 6 km. They tap the Detfurth sandstone with a thickness between 33 m and 36 m. Drilling profiles and core samples indicate that the reservoir consists of a weakly consolidated, fine to medium feldspatic quartz sandstone. The sandstone contains less than 2 % clay and 4 % - 5 % cement minerals. Determined clay minerals are kaolinite, muscovite, chlorite, illite and montmorillonite (Bartels and Iffland, 2000). The cementation consists mainly of calcite and dolomite with a minor amount of anhydrite (Table 4.1). The highly saline formation water is of the Na-(Ca-Mg)-Cl type with a solute content of 280 g L⁻¹ and a formation temperature of about 58 °C (Table 4.2; Bartels and Iffland, 2000).

Table 4.1: Data for the geothermal site Stralsund.

Reservoir data	
Reservoir volume	220,000,000 (m ³)
Average porosity	24 %
Average permeability	0.54 · 10 ⁻¹² m ²
Pumping rate	100 (m ³ h ⁻¹)
Lifetime of reservoir	30 (years)
Rock mineral phases	
Anhydrite	76.5 (mol m ⁻³)
Feldspars	200 (mol m ⁻³)
Clay minerals	50 (mol m ⁻³)

Mass balance calculations are useful to assess quickly the feasibility of this technology because they do not require large computations. The storage capacity of the potential reservoir at Stralsund was calculated using available data and applying plausible boundary conditions.

The storage capacity of CO₂ in a geothermal reservoir depends on the volume and porosity of the reservoir as well as on the pumping rates. Furthermore, physico-chemical properties of the brine and, most important, the mineralogical composition of the reservoir rock determine the amount of CO₂ which can be trapped in minerals. Our calculation was

based on the situation at Stralsund with the wells 1500 m apart, the reservoir 34 m thick and a porosity of 24 % (average permeability $0.54 \cdot 10^{-12} \text{ m}^2$). Table 4.1 summarizes the reservoir data.

The storage capacity depends on the most restrictive constraints, i.e. the anhydrite and feldspar content and CO₂ in solution. Calculations were performed with respect to the anhydrite content (assuming all anhydrite is transformed into calcite), the feldspar content (assuming that the feldspar dissolves completely and provides alkalinity needed for the transformation) and the solubility of CO₂ in brine (based on the equation of state of Duan and Sun, 2003). The latter defines the amount of CO₂ that can be stored additionally to the CO₂ stored as mineral.

If all anhydrite is transformed into calcite, approximately 0.562 Mt CO₂ (equivalent to 1.27 kg CO₂ per tonne sandstone) can be trapped. This value is seen as a lower limit since the anhydrite content is very low at the geothermal site Stralsund compared to other potential target reservoirs. Provided that not the anhydrite content but the alkalinity source is the limiting factor, 1.1 Mt of CO₂ could be bound by mineral trapping (equivalent to 2.49 kg CO₂ per tonne sandstone). Additionally, 2.2 Mt of CO₂ can be dissolved in the brine.

In order to achieve a zero emission power plant (i.e. equal amounts of CO₂ trapped and emitted during the lifetime of the geothermal plant including construction and demolition) approximately 0.15 Mt of CO₂ (Kayser and Kaltschmitt, 1996) need to be trapped as calcite. From the figures above it is obvious that this goal can be easily reached.

4.3 Transformation of anhydrite into calcite

The transformation of anhydrite into calcite is critical for the feasibility of this new technology. Three aspects of the reaction are particularly important: (1) The acidity produced in the system which limits the reaction. (2) The velocity of the transformation, i.e. the dissolution kinetics of anhydrite and the precipitation kinetics of calcite. (3) Changes in the pore space due to dissolution of anhydrite and precipitation of calcite.

Batch reaction experiments and calculations

In batch experiments in the laboratory, the dissolution kinetics of natural anhydrite was studied far from the conditions of thermodynamic equilibrium (saturation index $SI < -0.4$). The experiments were carried out in a 1 L glass vessel with a lid through which a Teflon-coated stirrer and a conductivity electrode reached into the solution. The stirrer rotated with 350 min^{-1} . At this stirring velocity, no influence on the dissolution rates was observed and the turbulent conditions held all particles in suspension. The temperature was varied

between 20 °C and 40 °C. The following rate law was determined for solutions of low ionic strength:

$$R = 2893 \cdot e^{\frac{-42000}{8.31 \cdot T}} \cdot (1 - \text{IAP}/K_s)^8 \text{ [mol m}^{-2} \text{ s}^{-1}] \quad (\text{Eq. 4.5})$$

with an activation energy of 42 kJ mol⁻¹. T is the absolute temperature, IAP the ion activity product and K_s the solubility product. Dissolution experiments in solutions containing sodium chloride indicate that the addition of 1 g to 5 g NaCl per litre has no influence on the activation energy and the rate constant, but it does change the reaction order from 8 to lower values between 5 and 6.5. Future experiments will focus on the dissolution kinetics of anhydrite close to equilibrium.

In order to study and prove the feasibility of the transformation of anhydrite into calcite additional batch experiments were performed in an Erlenmeyer flask in which 200 g of a 0.16 molar NaHCO₃ solution (pH 8) reacted with 15 g of anhydrite, stirred for different periods of time. The initial pH was varied between 7 and 8 by addition of hydrochloric acid. During the reaction, anhydrite dissolved and the calcium concentration of the solution increased. Because of the high HCO₃⁻ concentration, the solubility product of calcite was exceeded and calcite precipitated. After termination of the experiment the suspension was freeze dried and the mineral phases quantified with X-ray diffraction (XRD). The black dots in Figure 4.2 (right) display the amounts of calcite that were formed during the experiments.

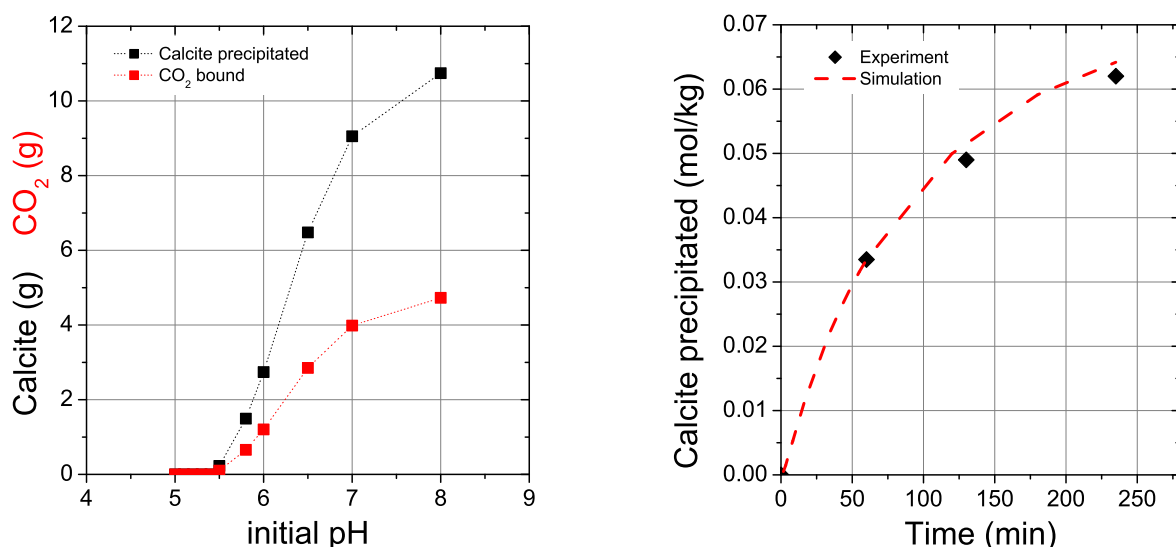


Figure 4.2: (left) Calcite formed and CO₂ bound versus initial pH of solution as modelled with PHREEQC; boundary conditions: mass of solution = 1 kg, 0.16 M NaHCO₃ solution, infinite amount of anhydrite, T = 30 °C, pCO₂ = 1 MPa. (right) Evolution of calcite in suspension during a transformation experiment.

Based on these laboratory experiments, batch reaction calculations with PHREEQC (Parkhurst and Appelo, 1999) were performed, to deduce the limiting pH of the brine and to confirm also theoretically the feasibility of the transformation of anhydrite into calcite. The reaction of anhydrite with the NaHCO₃ solution was studied under varying pH conditions assuming a pCO₂ of 1 MPa and a temperature of 30 °C. Figure 4.2 (left) depicts the amount of calcite formed and of CO₂ bound in calcite depending on the initial pH of the solution. Theoretically, the reaction of interest takes place down to a pH of 5.5. Hence, the transformation is not limited to extremely high pH values but occurs also under boundary conditions that can be achieved with the targeted technology.

In the kinetic simulation using the program PHREEQC, equation (4.5) was applied as rate law for the dissolution of anhydrite, and the precipitation of calcite was described according to Plummer et al. (1978). The red dashed line in Figure 4.2 (right) represents the simulated amount of calcite precipitated, reproducing the laboratory data (black diamonds) very well. Both our experiment and calculations prove that calcite is formed under different boundary conditions.

4.4 Core flooding experiment

Dissolution of anhydrite and growth of calcite can be translated into porosity changes. Following the assumption of equation (4.3) that 1 mole of anhydrite, with a molar volume of $4.59 \cdot 10^{-5} \text{ m}^3 \text{ mol}^{-1}$, is transferred into 1 mole of calcite, with a molar volume of $3.69 \cdot 10^{-5} \text{ m}^3 \text{ mol}^{-1}$, a net increase in porosity is determined of about 20 %. Even though porosity and permeability are closely related properties, a porosity increase does not result necessarily in a corresponding permeability increase. If, for instance, precipitation of calcite occurred primarily in the pore throats the net permeability of the reservoir sandstone might also decrease. To study the relation between porosity and permeability changes in the system a core flooding experiment was performed with original reservoir rock. A sandstone sample cemented with anhydrite was examined at constant, elevated temperature of 70 °C and a pressure of 0.6 MPa in order to determine resulting pore space changes due to the entire process of dissolution and precipitation during CO₂ storage in geothermal reservoirs. The experiment was carried out with such low overpressure because the pressure dependence of the anhydrite solubility at high salinities is only very small. For example it was shown that the solubility of anhydrite at 0.1 MPa coincides well with the one at 10 MPa (Kühn et al., 2002b). The confining pressure was applied to avoid that the water circulates around the core.

The core (length 5.8 cm, diameter 3 cm) was flushed applying a 1 molar sodium carbonate solution for 1700 hours with a constant flow rate of 2 mL per hour (Figure 4.3). Dissolution of anhydrite was determined by measuring the sulphate concentration in the solution at the core outlet (samples were not taken under pressure). In total, about 16 g of anhydrite were dissolved and flushed out of the core. The highest sulphate concentration throughout the experiment, measured at the beginning of the test (about 15 g L⁻¹), corresponds to only 10 % of the thermodynamic equilibrium. Hence, the dissolution reaction never reaches saturation within the sandstone sample. The concentration of calcium (counterion of sulphate in anhydrite mineral) is too small to be measured at the core outlet because most of the calcium is precipitated as calcite within the core.

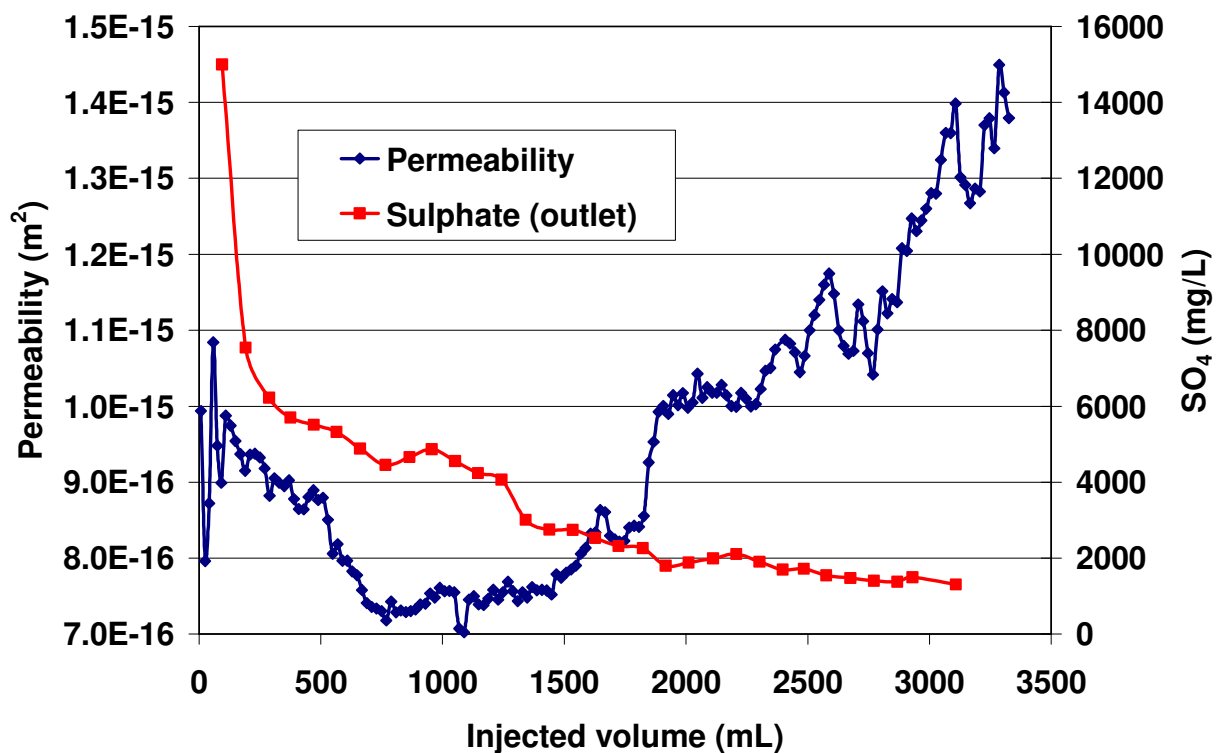


Figure 4.3: Core flooding of a sandstone sample (length 5.8 cm, diameter 3 cm) cemented with anhydrite and flooded with 1 mol L⁻¹ Na₂CO₃ solution at a constant flow rate of 2 mL per hour. Anhydrite is dissolved and detected by the sulphate concentration at the core outlet. The average permeability across the core length increases with time.

Permeability changes of the sample were continuously measured via a capacitive differential pressure gauge. As an important result it was observed that the average permeability of the core increases continuously with flooding time after a short initial period of a slight permeability decrease (Figure 4.3). As expected, the combined reaction of anhydrite dissolution and calcite precipitation yields a porosity increase. However, it is striking and promising that permeability is also increasing.

4.5 Suitable sources of alkalinity

From equation (4.3) it is determined that availability of alkalinity might be a requirement to trap CO₂ as calcite in geothermal reservoirs, so that the reaction can be buffered and the solubility product of calcite is exceeded. Alkalinity can be provided either in situ through the weathering of feldspars or by surface water treatment with fly ashes.

In-situ alkalinity source

Numerical batch simulations were performed for the potential site at Stralsund with its confirmed geothermal resource (Kühn et al., 2002a). At first, the thermodynamic equilibrium of the chemical reactions was studied with regard to the technical process planned for this technology. The formation water was cooled, enriched with varying amounts of CO₂ and again brought into contact with the reservoir minerals (Table 4.2).

Table 4.2: Formation water composition and rock mineralogy of the Stralsund reservoir given for 58 °C reservoir temperature (Bartels and Iffland, 2000).

Water composition

pH	5.84
Calcium	353 (mmol L ⁻¹)
Magnesium	94 (mmol L ⁻¹)
Sodium	3970 (mmol L ⁻¹)
Potassium	17 (mmol L ⁻¹)
Chloride	4859 (mmol L ⁻¹)
Carbon dioxide	1.0 (mmol L ⁻¹)
Sulphate	3.85 (mmol L ⁻¹)
Mineral composition	
Quartz	81 (wt%)
K-feldspar	10 (wt%)
Plagioclase	5 (wt%)
Calcite	3.6 (wt%)
Anhydrite	0.4 (wt%)

Therefore the simulations were carried out at a temperature of 25 °C according to the assumption that the relevant reactions take place within the area of the geothermal reservoir where the injection temperature already governs the system. As expected, the pH decreases with an increasing amount of added CO₂ (Figure 4.4). Previous simulations and also the presented results demonstrate that weathering of plagioclase is a prerequisite for calcite precipitation. Without the buffering capacity of plagioclase no CO₂ can be bound. But plagioclase dissolution by itself is still insufficient. In order to increase the rate of disso-

lution and in turn increase the buffering capacity, kaolinite needs to be formed as a secondary silicate phase. Anhydrite is not a chemical driver of the reaction what can be deduced from the fact that its dissolution is constant and independent of the addition of CO₂. The amount of dissolved anhydrite solely depends on the difference between the formation temperature and the temperature of the injected water. This is due to the fact that the initial calcium concentration of the brine is high. Therefore, the additional and small increase in Ca ions resulting from dissolution of anhydrite does not affect the solubility product of calcite. However, the dissolution of anhydrite is still important with respect to the resulting changes in pore space. The threshold for porosity reduction is reached with an addition of $5.0 \cdot 10^{-4}$ mol CO₂ per kg water (Figure 4.4).

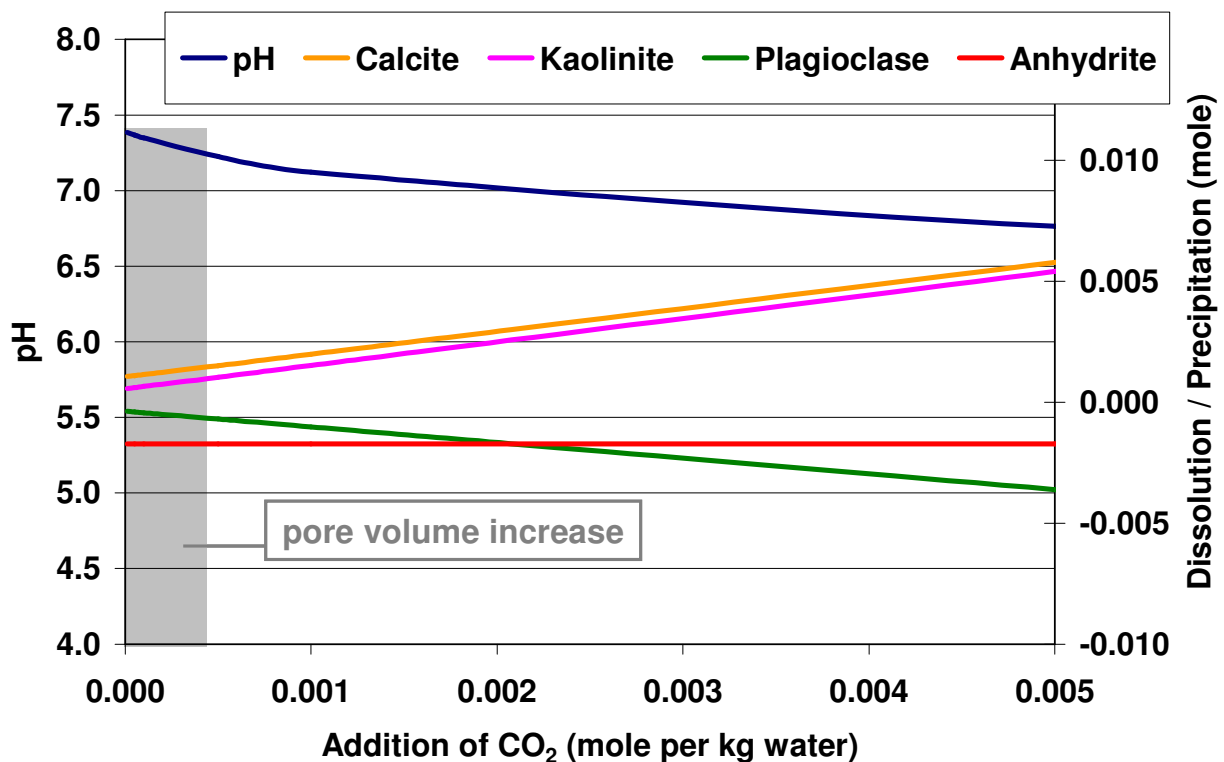


Figure 4.4: Thermodynamic batch reaction calculation at 25 °C for the Stralsund site. Initial chemical composition of the formation water and the reservoir rock are taken from Bartels and Iffland (2000). The pH decreases with increasing amount of added CO₂. Weathering of plagioclase (dissolution indicated by negative values) and precipitation of secondary kaolinite (indicated by positive values) are prerequisites for calcite precipitation. Anhydrite is not a chemical driver of the reaction.

Additional simulations were performed to take into account kinetic reactions and reaction rates were incorporated with respect to anhydrite and plagioclase dissolution and calcite precipitation. Reaction rates for anhydrite (equation 5) and calcite ($10^{-6.0}$ mol m⁻² s⁻¹; determined from Plummer et al., 1978) were used as determined in the laboratory experi-

ments. Plagioclase weathering ($10^{-9.5}$ mol m⁻² s⁻¹) is assumed to be 3 to 5 orders of magnitude slower than the calcite and anhydrite reaction rates, respectively (Palandri and Kharaka, 2004). Precipitation of kaolinite as secondary mineral was assumed to be in thermodynamic equilibrium with an infinite reaction rate. The saturation state (distance from equilibrium) was part of the rate equation. The mineral surface areas were neglected and taken as unity because no detailed information of the pore space structure of the Stralsund formation sandstone was available. Figure 4.5 displays changes of pH and the mineral composition versus time. It can be seen that the initial pH of 3.9 (due to saturation of the geothermal water with CO₂ for a pressure of 0.1 MPa) is increasing (diamonds) with the amount of dissolved plagioclase (dots). Kaolinite (squares) precipitates as secondary silicate. After 80 days, at a pH of 5.4, calcite precipitation kicks in. The reaction continues until the buffering capacity of plagioclase is exhausted.

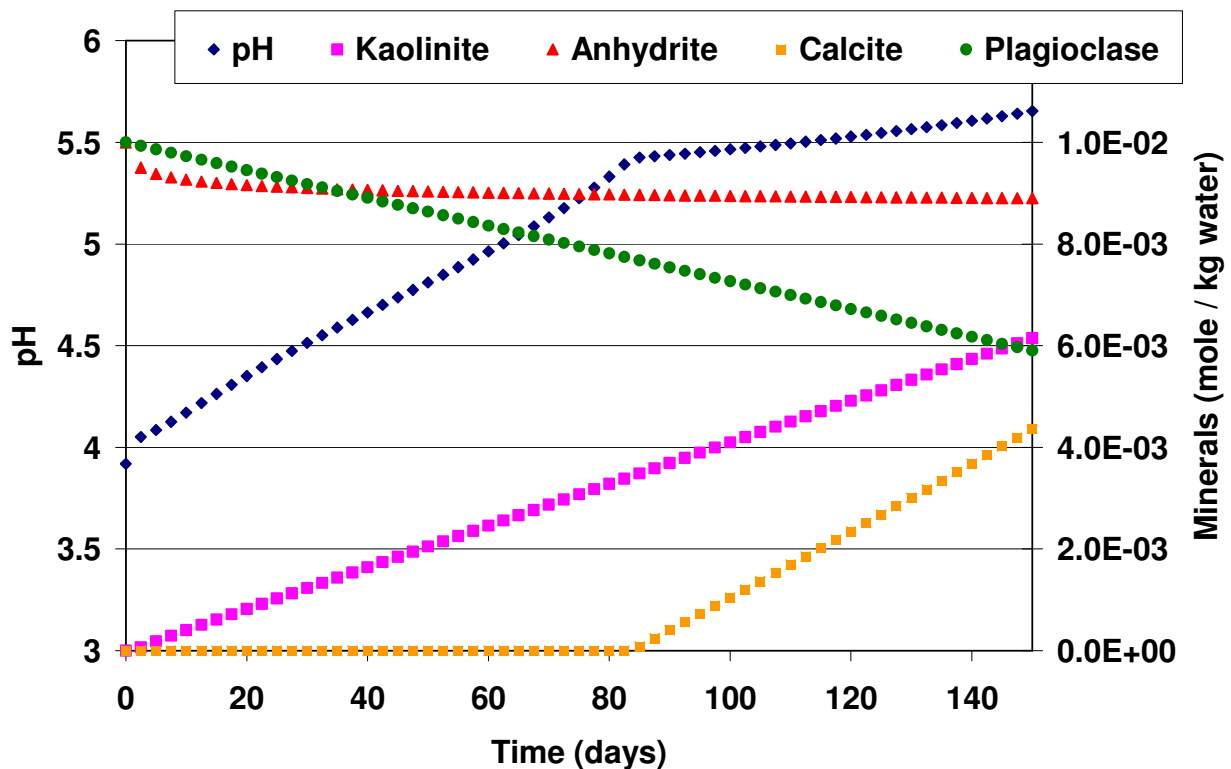


Figure 4.5: Kinetic batch reaction calculation for the Stralsund site. Initial chemical composition of the formation water and the reservoir rock are taken from Bartels and Iffland (2000). The reaction rate of anhydrite is given in equation (5) and the one for calcite is defined following Plummer et al. (1978). All others are taken from Palandri and Kharaka (2004). After 80 days, at a pH of 5.4 calcite precipitation kicks in.

For the purpose of comparing results, this period of 80 days can be translated into a saturation length: Assuming an average flow velocity between injection and production well (100 m per year for a distance of 1000 m between the wells) the saturation length is 22

meters. Hence, the region where calcite is precipitated is at least 22 meters away from the injection well. This is far enough not to endanger the well injectivity. Even though plagioclase weathering rates have been assumed to be very small they are fast enough to produce finally calcite between the wells.

Alkalinity provided from fly ash

As outlined above, surface treatment of the geothermal brine with fly ash, is a second alternative to supply alkalinity for the transformation of anhydrite into calcite. Our laboratory experiments showed (Back et al., 2008) that alkalinity is available from fly ash and that reaction rates are high. Recent batch reaction simulations show that calcite is precipitated from a mixture of geothermal formation water treated with fly ash with formation water enriched by the technological maximum amount of CO₂ (0.1 mol kg water, limit due to maximum pressure of 1 MPa in the aboveground equipment). In this case calcite is produced even without alkalinity supplied from rock forming minerals. As before, anhydrite dissolution is important to keep the pore space in the reservoir open. Comparison of different mixing ratios showed that calcite precipitation is maximized ($1.1 \cdot 10^{-3}$ mol kg⁻¹ water) by mixing the CO₂ enriched formation brine with only 0.1 wt% of the water treated with fly ash. At the same time $1.7 \cdot 10^{-3}$ mol kg⁻¹ water of anhydrite are dissolved resulting in an overall porosity increase of the system.

4.6 Summary and conclusions

Our study emphasizes that mineral trapping of carbon dioxide in geothermal reservoirs provides an alternative approach for the long-term and safe subsurface immobilisation of CO₂. Furthermore, sequestration of carbon dioxide combined with geothermal heat or power production offers an additional economical benefit. The feasibility of transforming anhydrite into calcite was proved by laboratory experiments as well as by numerical modelling of the associated chemical processes. Buffering capacity (alkalinity) derived from the reservoir rock or through surface water treatment with alkaline fly ash is essential for transforming anhydrite into calcite. Although it turns out that anhydrite is not the major player from the chemical point of view, its dissolution with concurrent pore space increase is important to balance the pore space reduction by precipitation of calcite and secondary silicates in the geothermal reservoir. Significant storage capacities are available in geological formations for millions of tonnes of carbon dioxide. Further studies, such as numerical simulations on multiple scales to be carried out in the future will yield extensive and accu-

rate process parameters to enable the development of innovative strategies for the realisation of a pilot field test on the technological scale.

Acknowledgement

The CO₂Trap project is part of the R&D-Programme GEOTECHNOLOGIEN funded by the German Ministry of Education and Research (BMBF) and German Research Foundation (DFG), Grant (03G0614A-C). This is publication no. GEOTECH – 247.

Epilogue

Conclusions Individual Chapters

The aim of this thesis was to propose a technical procedure that sufficiently fast removes CO₂ from flue gas by using alkaline residues. My study thereby focused on the reaction of lignite fly ashes, because they are available in huge amounts in Germany and are mostly deposited into landfills. The studied reaction of mineral carbonation sequesters CO₂ either directly as calcite or indirectly as an alkalinity-containing solution that is ready for injection into a proper aquifer for mineral trapping. The process offers a safe and long-term storage option for CO₂.

At the tested process conditions the determined conversion of 5.2 moles of CO₂ per kg fly ash ($\approx 0.23 \text{ kg kg}^{-1}$) accounts for a CO₂ sequestration capacity of nearly 3.5 million tons of CO₂ alone based on the available lignite fly ash in Germany.

Suspending lignite fly ash into the water, initially leads to the dissolution of free lime (CaO), anhydrite and Na-sulfate. The solution was quickly saturated with respect to calcium hydroxide and calcium sulfate at pH values of 12.5 to 12.8, which favored the dissolution kinetic of CO₂ and also caused the dissolution of more stable silicate phases of the lignite fly ash like glass particles or browmillerite (Ca₂(Fe, Al)₂O₅). Due to their lower solubility the dissolution of periclase (MgO) and brucite (Mg (OH)₂) occurred when the pool of CaO was nearly totally consumed and the pH dropped to below 10.8. Precipitation of calcite was observed already from the start of the experiments at high pH values and limited by the supply of dissolved CO₂. No precipitation of Mg carbonates was observed at the tested conditions and this period was to a significant extent controlled by the formation of dissolved carbon species. No significant release of heavy metals has been observed during the whole process at all tested process conditions.

In order to provide a rapid uptake at a time scale of minutes, high pH values are required to maximize CO₂-uptake rates. Establishing a balance between alkalinity providing and consuming reactions is therefore a prerequisite to achieve the adequate pH values, which can be best obtained at enhanced temperature and by maximizing the dissolution rate of CO₂.

In reaction with lignite fly ashes the CO₂ transfer can be mainly attributed to the presence of free lime (CaO) and periclase (MgO), which are typically contained in combustion residues and are thus regarded to suitable candidates for CO₂ sequestration. Ca and Mg

(hydr)oxides can be consequently used as proxies to estimate alkaline waste reaction with CO₂ valid for alkaline residues.

Consistent to the reaction sequence during the fly ash experiments, it was demonstrated in pure phase experiments that a feedback exists between the solubility of the two (hydr)oxides and the pH of the bulk solution. With CO₂ as the rate limiting step, the pH of the solution acts as master variable for the mineral dissolution and supply of dissolved CO₂ (**Chapter 2**).

In the CaO systems dissolution of gaseous CO₂ was the rate limiting step at concentrations larger than 0.05 mol L⁻¹, corresponding to pH values of ~ 12.7. Maximum CO₂ uptake rates coincided with the rate of calcite precipitation. In suspensions with MgO the pH was distinctly lower (between 10.3 and 9.3). The uptake rate of CO₂ was apparently limited by the detachment of Mg²⁺ and OH⁻ from the mineral lattice into the bulk solution. Beside the major controlling process of proton promoted dissolution i have shown that the presence of dissolved NaHCO₃ increases the dissolution rate of MgO until surface coverage with CO₃²⁻ is achieved. The conditions met in a CCS scenario, leading to low pH values and the presence of dissolved carbon species, are thus appraised to be favorable for the dissolution of alkaline oxides in general.

In MgO suspensions precipitation of hydromagnesite (Mg₅(CO₃)₄(OH)₂ · 4H₂O) was observed at temperatures greater than 50 °C already at low concentrations of dissolved Mg²⁺ and CO₃²⁻. Below 50 °C much higher concentrations of Mg and carbon species were necessary to initialize precipitation of a carbonate mineral which was in this case nesquehonite (MgCO₃ · 3H₂O). In terms of maximizing the degree of carbonate precipitation, operation conditions between 50 and 75 °C have been shown to be most appropriate for a technical realization.

Mg carbonate precipitation was slower than calcite precipitation and was depending strongly on the different boundary conditions. Hence, the fast and easily achieved precipitation of Ca carbonates emphasizes that Ca rich materials can be utilized preferentially at low energy demand.

In **Chapter 3** simulation in connection with additional laboratory experiments gave proof that the alkalinity based on MgO can be fully consumed for calcite precipitation if CaCl₂ is provided in the process solution. By adding CaSO₄ into the Mg-TDIC solution calcite precipitation was confirmed as well, however with lower reaction rates. Thereby a partial observed degassing of CO₂ from the suspension was observed, which is predominantly caused by the interaction between the stability of Mg-carbon and Mg-sulphate complexes.

The model was generally found as a very valuable tool since the exposure of all dissolved species and present mineral phases at each time-step was possible. The experimentally determined rate expressions of the dissolution of CaO/MgO and CO₂ have been successfully implemented in the model and were supplemented by available dissolution/precipitation rates of calcite and anhydrite taken from literature.

The general reaction sequence controlled by the consecutive reaction of Ca and Mg (hydr)oxides is confirmed by the simulation of lignite fly ash carbonation. Differences can be mainly assigned to the complex and partially unknown mineral compositions of the residues. Furthermore, kinetic and thermodynamic constants of particular mineral phases (e.g. brownmillerite, gehlenite) are missing in the available thermodynamic databases at present. Disparities were almost represented by divergent values of mineral dissolution and CO₂ uptake rates. The significant higher CO₂ neutralizing capacity, calculated by simulation, suggests that a large part of reactive CaO and MgO was still incorporated in the mineral matrix of the fly ashes and could not be dissolved at mild process conditions (25 °C).

In **Chapter 4** the knowledge from the reactivity of the lignite fly ashes could be finally used as input data for the numerical simulation of a mineral carbonation scenario of an operated geothermal reservoir containing anhydrite. It was proved that the injection a CO₂ enriched solution at reservoir conditions (depth: 1500 m, temperature: 58 °C) enables the precipitation of calcite, supplemented by anhydrite dissolution. The process offers a concurrent pore-space increase in the reservoir that is important to balance pore-space reduction by calcite precipitation or secondary silicates. The necessary buffering capacity for this process can be supplied from plagioclase in the reservoir rock and more effective by surface water treatment with lignite fly ashes. Already with an addition of 0.1 weight percent of fly ash per volume of the injection solution the amount of precipitated calcite was maximized.

Discussion and outlook

The previous chapters showed how the mineral carbonation of lignite fly ashes takes place and which process conditions are beneficial. From the laboratory and simulation derived results it can be concluded that the use of alkaline waste suspension for reaction with CO₂ might be a technically possible option also on larger scale by using unpurified CO₂ from flue gas at ambient T and p condition. The carbonation of alkaline waste is thereby independent from a specific power plant and can be hooked to any plant that generates CO₂. A main benefit is the fact that CO₂ treatment of fly ashes provides a sustainable end-product

for final deposition. In order to estimate its CCS potential and the economy of the process, however, a number of additional factors have to be considered:

The release of alkalinity from lignite fly ashes is fast and was limited by the supply of dissolved CO_2 in the used laboratory reactor system. Treatment pathways are required, in which the potential is utilized to a large extent within short periods of time. Caused by CO_2 limitation, the dissolution of CaO and MgO occurred one after another because the solution pH (> 10.8) was mainly controlled by the release of caustic alkalinity from CaO and therefore inhibited MgO dissolution. I have demonstrated that CO_2 dissolution can be most adequately increased by more intensive perturbation. By overcoming CO_2 limitation, the residence time in the reactor is appraised to be significantly decreased. The results suggest that the process should be most adequately adjusted at pH values between 8 and 10 in order to enable carbonate precipitation and the dissolution of Ca and Mg (hydr)oxides at the same time. The maximum neutralization capacity per kg lignite fly ash was achieved at the highest tested temperature of 75 °C. Since waste heat is generally available in the environment of a combustion plant, the aqueous carbonation process might be further examined at higher temperatures in order to enhance the kinetics and the net amount of alkalinity released.

Also with respect to Mg carbonate precipitation temperatures above 50 °C are suggested. As stated by several authors, the magnesium carbonate system exhibits a complex behaviour. I have evaluated the conditions necessary to allow the formation of hydromagnesite and nesquehonite by using pure MgO in the batch system. However, there is still a gap of knowledge concerning the exact surface chemistry and the complex reaction mechanisms leading to the precipitation of different Mg carbonate minerals. To allow the simulation of different CCS scenarios based on Mg carbonates, the evaluation of the kinetic rate constants of different Mg carbonates is thereby a major task within future work.

An important next step will be a pilot-scale study to provide more insight the technical constraints. Considering a technical realization, my findings from laboratory batch operations need to be up-scaled in a pilot plant and most appropriately assigned to continuous flow reactor systems. Technical approaches may be required for the proper disposal of both, the carbonated solid end-products and the process solution. This certainly will include the evaluation of different sorts of separation or filter techniques, respectively. Variable solutions for the enhanced distribution of CO_2 , like the use of commercial column internals, promise success and might be further improved on technical scale. The suitable technical selection will thereby depend significantly on the design of the chosen reaction system.

In the second part of this thesis we have explored different perspectives of related sequestration scenarios like the use of Ca containing solutions for enhanced calcite precipitation or the injection of CO₂ into geothermal reservoirs for mineral trapping. The latter was identified as a feasible option CO₂ sequestration, offering a huge theoretical storage capacity. However, higher economic and energy costs need to be generally adopted due to the required technical installations and guessed extensive monitoring programs of the reservoir conditions. Even though the pH of the brine is lowered by injection of CO₂ and leads to enhanced mineral dissolution, the release of Ca and Mg is mostly linked to silicate minerals, explaining why lower conversion rates are generally observed.

I have further shown that the addition of alkaline residues into waters containing dissolved Ca is appropriate for enhanced calcite precipitation. Thereby, the pH of the solution can be adjusted to values necessary for calcite precipitation. Huge amounts of Ca containing water are naturally present in limestone areas or high mineralized deep aquifers. In the course of oil production and coal mining they are often produced as wastewater (Song et al., 2006). Furthermore, the number of technical installations dealing with geothermal energy production using high mineralized brines is rising world-wide and could offer prospects for the surface treatment with CO₂.

Overall, kinetic and thermodynamic based geochemical modelling was found as valuable tool for the assessment of the CO₂ neutralizing capacity of such scenarios. The improved determination of the mineralogical composition of the residues as well as the extension of thermodynamic and kinetic constants of specific mineral phases was thereby pointed out as important task within future work. Due to the mostly observed presence of stoichiometric undefined glass compounds in combustion residues, inverse modelling is suggested as appropriate tool to identify lacking phases and estimate their thermodynamic/kinetic properties.

Related treatment options, like the semi-dry process route, as proposed by Bauer et al. (2011), are most promising to overcome technical constraints arising during the aqueous route, including the product handling, product drying and stability of e.g. toxic metals in the solid phase. These aspects have not been assessed in this work should and be considered in further studies.

With respect to the re-use of the carbonated residues, valuable options need to be taken into account. As part of an integrated recycling process, the overall energetic and economic costs can be most adequately reduced compared to other CCS scenarios (see Table 5.1, (IPCC, 2005)). Energetic and economical feasibility studies will thus have to indi-

vidually account for different treatment schemes, operational sites and the re-use of the carbonated end-products.

Table 5.1: Cost ranges for the components of a CCS system as applied to a given type of power plant or industrial source. The costs of the separate components cannot simply be summed to calculate the costs of the whole CCS system in US\$ CO₂⁻¹ avoided. All numbers are representative of the costs for large-scale, new installations, with natural gas prices assumed to be 2.8-4.4 US\$ GJ⁻¹ and coal prices 1-1.5 US\$ (IPCC, 2005)

CCS system components	Cost range (US\$ t ⁻¹ CO ₂ net captured)	remarks
Capture from a coal- or gas-fired power plant	15-75	Net costs of captured CO ₂ , compared to the same plant without capture
Capture from hydrogen and ammonia production or gas processing	5-55	Applies to high-purity sources requiring simple drying and compression
Capture from other industrial sources	25-115	Range reflects use of a number of different technologies and fuels.
Transportation	1-8	Per 250 km pipeline or shipping for mass flow rates of 5 (high end) to 40 (low end) MtCO ₂ yr ⁻¹ .
Geological storage	0.5-8	Excluding potential revenues from EOR ₁ or ECBM ₂ .
Geological storage: monitoring and verification	0.1-0.3	This covers pre-injection, injection, and post-injection monitoring, and depends on the regulatory requirements.
Ocean storage	5-30	Including offshore transportation of 100-500 km, excluding monitoring and verification.
Mineral carbonation	50-100	Range for the best case studied. Includes additional energy use for carbonation.

1: EOR: Enhanced Oil Recovery, 2: ECBM: Enhanced Coal Bed Methane recovery

Mineral trapping of CO₂ by using lignite fly ashes might be taken into further benefit, if the end-product is used as neutralizing agent for acid main drainage, which is mostly observed during lignite mining processes. A huge amount of carbonate minerals, needing mining and transportation, is commonly used as pH buffering material in open pits and might be partly replaced by carbonated fly ashes. Based on the evaluated neutralizing capacity of 3.5 million tons of CO₂ of the lignite fly ashes in Germany this corresponds to a potential saving of round 8 million tons of carbonate as feedstock material.

The use of alkaline residues is appraised as an attractive niche market to partly reclaim some of the CO₂ emitted during combustion processes. The carbonation process is thereby supposed to have numerous effects on the physical and chemical properties of the

end-products. In this respect further research is an important challenge to reassess potential uses for different carbonated residues in general.

Notations

notation	meaning	dimension
A	Initial surface area	m ²
ANC	Alcalinity neutralizing capacity	meq g ⁻¹
c	Molar amount	mol
CO ₂ uptake	Uptake amount of CO ₂	mmol g ⁻¹
CO ₂ uptake rate	Uptake rate of CO ₂	mmol s ⁻¹ L ⁻¹
EC	Electric conductivity	μS cm ⁻¹ , mS cm ⁻¹
k	Rate constant	-
k _{CO₂}	Forward dissolution rate of CO ₂	mmol L ⁻¹ s ⁻¹
K _H	Henry constant	mol L ⁻¹ atm ⁻¹
K _{SP}	Solubility product	-
l/s	Liquid to solid ratio	g L ⁻¹
M	mass	g
n	Reaction order	-
p	pressure	MPa
pCO ₂	Partial pressure of CO ₂	MPa
Q	Gas flux	m ³ s ⁻¹
R	Gas constant	atm L mol ⁻¹ K ⁻¹
R _f	Reaction rate	Mol m ² s ⁻¹
rpm	Rate per minute	rpm
S	Surface area per Liter	m ² L ⁻¹
SI	Saturation index	-
T	Temperature	°C, K
t	time	s
TDIC	Total dissolved inorganic carbon	mol L ⁻¹
TIC	Total inorganic carbon	mol L ⁻¹
V	volume	L, m ³
wt.-%	Weight percent	%
x	Dependence of reaction rate on surface area	-
Ω	Saturation with respect to mineral phase (IAP K ⁻¹)	-

References

- Adams, E.E. and Caldeira, K., (2008) Ocean Storage of CO₂. *Elements*, **4**(5): 319-324.
- Allison, J.D., Brown, D.S. and Novo-Gradac, K.J. (1990) MINTEQA2/PRODEFA2--A geochemical assessment model for environmental systems--version 3.0 users's manual: Environmental Research Laboratory, U.S. Environmental Protection Agency, Athens.
- Astrup, T., Dijkstra, J. J., Comans, R. N. J., Van der Sloot, H. A. and Christensen, T. H. (2006) Geochemical modeling of leaching from MSWI air-pollution-control residues. *Environmental Science & Technology*, **40**(11): 3551-3557.
- Aya, I., Kojima, R., Yamane, K., Brewer, P.G. and Peltzer, E.T., (2004) In situ experiments of cold CO₂ release in med-depth. *Energy*, **29**(9-10): 263-271.
- Bachu, S., Bonijolyb, D., Bradshawc, J., Burrussd, R., Hollowaye, S., Christensen, N.P. and Mathiassen, O.M. (2007) CO₂ storage capacity estimation: Methodology and gaps. *International Journal of Greenhouse Gas Control*, **1**(4): 430-443.
- Bachu, S. and Shaw, J.C., (2003) Evaluation of the CO₂ sequestration capacity in Alberta's oil and gas reservoirs at depletion and the effect of underlying aquifers. *Journal of Canadian Petroleum Technology*, **42**(9): 51-61.
- Baciacchi, R., Costa, G., Di Bartolomeo, E., Poletini, A., Pomi, R. (2009) The effects of accelerated carbonation on CO₂ uptake and metal release from incineration APC residues. *Waste Management*, **29**(12): 2994-3003.
- Baciacchi, R., Lategano, E., Marini, C., Poletini, A., Pomi, R., Postorino, P. and Rocca, S. (2010) Accelerated carbonation of different size fractions of bottom ash from RDF incineration. *Waste Management*, **30** (7): 1310-1317.
- Back, M., K. Vosbeck, M. Kühn, H. Stanjek, C. Clauser, and S. Peiffer, 2006, Pretreatment of CO₂ with fly ashes to generate alkalinity for subsurface sequestration, GHGT-8, 8th International Conference on Greenhouse Gas Control Technologies, 19.-22. June 2006, Trondheim, Norway.
- Back, M., Kuehn, M., Stanjek, H., Peiffer, S., (2008) Reactivity of alkaline lignite fly ashes towards CO₂ in water. *Environmental Science & Technology*, **42**(12): 4520-4526.
- Back, M., Bauer, M., Stanjek, H. and Peiffer, S. (2011) Sequestration of CO₂ after reaction with alkaline earth metal oxides CaO and MgO. *Applied Geochemistry*, **26**: 1097-1107.
- Baldwin, I.T. et al. (2005) Atmospheric CO₂ and ¹³CO₂; Exchange with the Terrestrial Biosphere and Oceans from 1978 to 2000: Observations and Carbon Cycle Implications,

- In: A History of Atmospheric CO₂ and Its Effects on Plants, Animals, and Ecosystems, **177**, 83-113, Springer Verlag.
- Bartels, J., J. Iffland (2000) Hydraulic, thermal, and mechanical behaviour of geothermal aquifers under exploitation: Analysis and assessment of petrographical / petrophysical and hydrochemical data and investigations as well as simulations: Project Final Report BMBF-0326995D, Landesamt für Umwelt, Naturschutz und Geologie Mecklenburg-Vorpommern 64 (in German).
- Béarat, H., McKelvy, M.J., Chizmeshya, A.V.G., Gormley, D. Nunez, R. and Squires, K. (2006) Carbon Sequestration via Aqueous Olivine Mineral Carbonation: Role of Passivating Layer Formation. *Environmental Science & Technology*, **40**: 4802-4808.
- Bennemann, J.R., (2003) Technology Roadmap for Biofixation of CO₂ and greenhouse gas abatement with microalgae, Second Annual Conference on Carbon Sequestration, U.S. Department of Energy, USA.
- Benson, S.M., Cole, D.R., (2008) CO₂ Sequestration in Deep Sedimentary Formations. *Elements*, **4**(5): 325-331.
- Bergmann, J. and Kleeberg, R. (1998) Rietveld analysis of disordered layer silicates, EPDIC 5 proceedings of the 5th European Conference on Powder Diffraction, Materials Science Forum: 300-305, Parma, Italy.
- Bergmann, P.D., Winter, E.M., Chen, Z.Y., (1997) Disposal of power plant CO₂ in depleted oil and gas reservoirs in Texas. *Energy Conversion and Management*, **38**(Suppl.): 211-216.
- Berner, R.A. (1975) The role of magnesium in the crystal growth of calcite and aragonite in sea water. *Geochimica et Cosmochimica Acta*, **39**: 489-504.
- Bertos, M. F.; Li, X.; Simons, S. J. R.; Hills, C. D.; Carey, P. J. (2004) Investigation of accelerated carbonation for the stabilisation of MSW incinerator ashes and the sequestration of CO₂. *Green Chemistry*, **6**: 428-436.
- Bonenfant, D. et al., (2008) CO₂ Sequestration by Aqueous Red Mud Carbonation at Ambient Pressure and Temperature. *Industrial & Engineering Chemistry Research*, **47**(20): 7617-7622.
- Brewer, P.G., Peltzer, E.T., Friederich, I., Aya, I., Yamane, K., (2000) Experiments on the ocean sequestration of fossil fuel CO₂: pH measurements and hydrate formation. *Marine Chemistry*, **72**(2-4): 83-93.

- Buhmann, D. and Dreybrodt, W., (1985) The Kinetics of Calcite Dissolution and Precipitation in Geologically Relevant Situations of Karst Areas. 1. Open System. *Chemical Geology*, **48**: 189-211.
- Casey W. H. (1991) On the relative dissolution rates of some oxide and orthosilicate minerals. *Colloid Interface Science*, **146**: 586–589.
- Casey, W.H. and Ludwig, C. (1996) The mechanism of dissolution of oxide minerals. *Nature*, **381**(6582): 506-509.
- Costa, G. et al. (2007) Current status and perspectives of accelerated carbonation processes on municipal waste combustion residues. *Environmental Monitoring and Assessment*, **135**(1-3): 55-75.
- Davies, P.J. and Bubela, B. (1973) Transformation of Nesquehonite into Hydromagnesite. *Chemical Geology*, **12**: 289-300.
- Davis, J.A. and Kent, D.B. (1990) Surface complexation modeling in aqueous geochemistry. In: Hochella, M.F., White, A.F. (Eds.), *Reviews in Mineralogy*. Mineralogical Society of America, Washington D.C, USA.
- DIW (2005) Innovative energy technologies and climate policy in Germany, In: Schumacher, K., Sands, R. D. (Eds.), *German Institute for Economic Research*, **509**, Berlin.
- Dreybrodt, W. and Buhmann, D., (1991) A Mass-Transfer Model for Dissolution and Precipitation of Calcite from Solutions in Turbulent Motion. *Chemical Geology*, **90**: 107-122.
- Dreybrodt, W., Lauckner, J., Liu, Z.H., Svensson, U. and Buhmann, D., (1996) The kinetics of the reaction $\text{CO}_2 + \text{H}_2\text{O} \rightarrow \text{H}^+ + \text{HCO}_3^-$ as one of the rate limiting steps for the dissolution of calcite in the system $\text{H}_2\text{O}-\text{CO}_2-\text{CaCO}_3$. *Geochimica Et Cosmochimica Acta*, **60**: 3375-3381.
- Duan, Z., and Sun, R. (2003) An improved model calculating CO_2 solubility in pure water and aqueous NaCl solutions from 273 to 533 K and from 0 to 2000 bar. *Chemical Geology*, **193**: 257-271.
- Duchesne, J. and Reardon, E.J. (1995) Measurement and Prediction of Portlandite Solubility in Alkali Solutions. *Cement and Concrete Research*, **25**: 1043-1053.
- EIA (2010) *International Energy Outlook 2010*. DOE/EIA-0484, U.S. Energy Information Administration, Washington, USA.

- Enders, M. (1995) Microanalytical characterization (AEM) of glassy spheres and anhydrite from a high-calcium lignite fly ash from Germany, *Cement and Concrete Research*, **25**(6): 1397-1377.
- EPA: Environmental Protection Agency (2002), Vol. 2000/532/EC2, Environmental Protection Agency, Ireland.
- Fernandez Bertos, M., Li, X., Simons, S.J.R., Hills, C.D., Carey, P.J., (2004) Investigations of accelerated carbonation for the stabilisation of MSW incinerator ashes and the sequestration of CO₂. *Green Chemistry*, **6**: 428-436.
- Fernandez Bertos, M.; Simons, S. J. R.; Hills, C. D.; Carey, P. J. (2004) A review of accelerated carbonation technology in the treatment of cement-based materials and sequestration of CO₂. *Journal of Hazardous Materials*, **112**, 193-205.
- Fernandez, A.I., Chimenos, J.M., Segarra, M., Fernandez, M.A. and Espiell, F. (1999) Kinetic study of carbonation of MgO slurries. *Hydrometallurgy*, **53**(2): 155-167.
- Furrer, G. and Stumm, W. (1986) The Coordination Chemistry of Weathering. 1. Dissolution Kinetics of Delta-Al₂O₃ and Beo. *Geochimica Et Cosmochimica Acta*, **50**: 1847-1860.
- Gerdemann, S.J., O'Connor, W.K., Dahlin, D.C., Penner, L.R. and Rush, H. (2007) Ex situ aqueous mineral carbonation. *Environmental Science & Technology*, **41**: 2587-2593.
- Giammar, D.E., Bruant, R.G. and Peters, C.A. (2005) Forsterite dissolution and magnesite precipitation at conditions relevant for deep saline aquifer storage and sequestration of carbon dioxide. *Chemical Geology*, **217**: 257-276.
- Hamyayun, R., Tomasko, D.L., (2000) High-Resolution Adsorption Isotherms of Supercritical Carbon Dioxide on Activated Carbon. *AIChE*, **10**(46): 2065-2075.
- Hänchen, M., Prigiobbe, V., Baciocchi, R. and Mazotti, M. (2008) Precipitation in the Mg-carbonate system-effects of temperature and CO₂ pressure. *Chemical Engineering Science*, **63**: 1012-1028.
- House, W.A. and Howard, J.R., 1984. Kinetics of carbon dioxide transfer across the air/water interface. *Faraday Discussion Chemical Society*, **77**: 33-46.
- Huijgen, W.J.J., Comans, R.N.J., (2003) Carbon dioxide sequestration by mineral carbonation - Literature Review 2003, Energy Research Center Netherlands, Petten, Netherlands.

- Huijgen, W.J.J., Comans, R.N.J., (2005) Carbon dioxide sequestration by mineral carbonation - Literature Review update 2005, Energy Research Center Netherlands, Petten, Netherlands.
- Huijgen, W. J. J.; Witkamp, G. J.; Comans, R. N. J. (2005) Mineral CO₂ sequestration by steel slag carbonation. *Environmental Science & Technology*, **39**: 9676-9682.
- Huijgen, W.J.J. and Comans, R.N.J. (2006a) Carbonation of steel slag for CO₂ sequestration: Leaching of products and reaction mechanisms. *Environmental Science & Technology*, **40**(8): 2790-2796.
- Huijgen, W. J. J.; Witkamp, G. J.; Comans, R. N. J. (2006b) Mechanisms of aqueous wollastonite carbonation as a possible CO₂ sequestration process. *Chemical Engineering Science*, **61**: 4242-4251.
- Huijgen, W. J. J.; Ruijg, G. J.; Comans, R. N. J.; Witkamp, G. J. (2006c) Energy consumption and net CO₂ sequestration of aqueous mineral carbonation. *Industrial & Engineering Chemistry Research*, **45**: 9184-9194.
- Huijgen, W.J.J., Comans, R.N.J., Witkamp, G.J., (2007b) Cost evaluation of CO₂ sequestration by aqueous mineral carbonation. *Energy Conversion and Management*, **48**(7): 1923-1935.
- Huntzinger, D.N., Gierke, J.S., Kawatra, S.K., Eisele, T.C. and Sutter, L.L. (2009) Carbon Dioxide Sequestration in Cement Kiln Dust through Mineral Carbonation. *Environmental Science & Technology*, **43**: 1986-1992.
- Iizuka, A., Fujii, M., Yamasaki, A. and Yanagisawa, Y. (2004) Development of a new CO₂ sequestration process utilizing the carbonation of waste cement. *Industrial & Engineering Chemistry Research*. **43**: 7880-7887.
- Iizuka, A., Katsuyama, Y., Fujii, M., Yamasaki, A., Yanagisawa, Y., (2004) Development of a new carbon dioxide sequestration scenario by the carbonation of waste cement. *Abstracts of Papers of the American Chemical Society*, **227**: U1095-U1095.
- IPCC, (2005) IPCC Special Report Carbon Dioxide Capture and Storage, In: Metz, B., Davidson, O., Conninck, H., Loos, M., Meyer, L. (Eds.), Cambridge University Press, Cambridge, United Kingdom.
- IPCC, (2007) *Climate Change 2007: The Physical Science Basis*. Contribution of Working Group I to the Fourth Assessment Report of the Intergovernmental Panel on Climate Change. Cambridge University Press, Cambridge, New York, USA.

- Jeschke, A.A., Vosbeck, K. and Dreybrodt, W. (2001) Surface controlled dissolution rates of gypsum in aqueous solutions exhibit nonlinear dissolution kinetics. *Geochimica Et Cosmochimica Acta*, **65**(1): 27-34.
- Kakizawa, M., Yamasaki, A., Yanagisawa, Y. (2001) A new CO₂ disposal process using artificial rock weathering of calcium silicate accelerated by acetic acid. *Energy*, **26**: 341-354.
- Kaszuba, J.P., Janecky, D.R. and Snow, M.G. (2003) Carbon dioxide reaction processes in a model brine aquifer at 200 degrees C and 200 bars: implications for geologic sequestration of carbon. *Applied Geochemistry*, **18**(7): 1065-1080.
- Kayser, M., and Kaltschmitt, M. (1996) Holistic energy and emission balance of hydrogeothermal heat production plants, In: Huenges, E., Erbas, K., and Schallenberg, K. (Eds.), *Hydrogeothermal plants: System analysis and emission balance: Scientific Technical Report STR96/08, Geothermie Report 96-1, GeoForschungsZentrum Potsdam, 19-72* (in German).
- Kempka, T., Waschbüsch, M., Fernández-Steeger, T. Azzam R., (2006) Sorptive storage of CO₂ on coal dust and flotation waste from coal processing in abandoned coal mines. In: Cotthem, A., Charlier, R., Thimus, J., Tshibangu, J. (Eds.), *EUROROCK 2006*. Taylor & Francis, Leiden, Netherlands.
- Kern, D.M., (1960) The hydration of carbon dioxide. *Journal of Chemical Education*, **37**: 14-23.
- Kloprogge, J.T., Martens, W.N., Nothdurft, L., Duong, L.V. and Webb, G.E. (2003) Low temperature synthesis and characterization of nesquehonite. *Journal of Materials Science Letters*, **22**: 825-829.
- Koinuma, H., (2007) Oxide materials research for global environment and energy with a focus on CO₂ fixation into polymers. *Reactive and Funtional Polymers*, **67**(11): 1129-1136.
- Kühn, M., Clauser, C., Vosbeck, K., Stanjek, H., Meyn, V., Back, M. and Peiffer, S. (2009) Mineral trapping of CO₂ in operated hydrogeothermal reservoirs. *Carbon dioxide sequestration in geological media*, 59. *AAPG Studies in Geology*: 545-552.
- Kühn, M., Bartels, J. and Iffland, J. (2002a) Predicting reservoir property trends under heat exploitation: Interaction between flow, heat transfer, transport, and chemical reactions in a deep aquifer at Stralsund, Germany. *Geothermics*, **31** (6): 725-749.

- Kühn, M., J. Bartels, H. Pape, W. Schneider, and C. Clauser C (2002b) Modeling chemical brine-rock interaction in geothermal reservoirs. In: Stober, I. and Bucher, K. (Eds.), Water-Rock Interaction, Kluwer Academic Publishers, Dordrecht, Netherlands.
- Kühn, M., S. Asmus, R. Azzam, M. Back, A. Busch, H. Class, C. Clauser, A. Dengel, T. Dose, J. Ewers, R. Helmig, K. Jaeger, T. Kempka, B.M. Krooß, R. Littke, S. Peiffer, R. Schlüter, H. Stanjek, J. Strobel, K. Vosbeck, and M. Waschbüsch (2005) CO₂Trap - Development and evaluation of innovative strategies for mineral and physical trapping of CO₂ in geological formations and of long-term cap rock integrity, In: Stroink, L. (Ed.), Investigation, utilisation and protection of the underground. GEOTECHNOLOGIEN Report, **6**: 42-59, Potsdam, Germany.
- Lackner, K.S., Wendt, C.H., Butt, D.P., Joyce, E.L., Sharp, D.H., (1995) Carbon-Dioxide Disposal in Carbonate Minerals. *Energy*, **20**(11): 1153-1170.
- Lekakh, S. N., Rawlins, C. H., Robertson, D. G. C., Richards, V. L. and Peaslee, K. D (2008) Kinetics of aqueous leaching and carbonization of steelmaking slag. *Metallurgical and Materials Transactions B-Process Metallurgy and Materials Processing Science*, **39**(1): 124-134.
- Liu, Z. H. and Dreybrodt, W. (1997) Dissolution kinetics of calcium carbonate minerals in H₂O-CO₂ solutions in turbulent flow: The role of the diffusion boundary layer and the slow reaction H₂O+CO₂ reversible arrow H⁺+HCO₃. *Geochim Cosmochim Acta*, **61**: 2879-2889.
- Marland, G., Boden, T.A., B., Andres, R.J. (2007) Global, Regional, and National Fossil-Fuel CO₂ Emissions. Carbon Dioxide Information Analysis Center, Oak Ridge National Laboratory, Tennessee, USA.
- Meima, J. A.; van der Weijden, R. D.; Eighmy, T. T.; Comans, R. N. J. (2002) Carbonation processes in municipal solid waste incinerator bottom ash and their effect on the leaching of copper and molybdenum. *Applied Geochemistry*, **17**: 1503-1513.
- Meima, J.A. and Comans, R.N.J. (1998) Application of surface complexation precipitation modeling to contaminant leaching from weathered municipal solid waste incinerator bottom ash. *Environmental Science & Technology*, **32**(5):688-693.
- Montes-Hernandez, G., Perez-Lopez, R., Ranard, F., Nieto, J.M. and Charlet, L. (2009) Mineral sequestration of CO₂ by aqueous carbonation of coal combustion fly-ash. *Journal of Hazardous Materials*, **161**(2-3): 1347-1354.

- Morse, J.W. and Berner, R.A. (1972b) Dissolution kinetics of calcium carbonate in sea water: II. A kinetic origin of the lysocline. *American Journal of Science*, **272**: 840-851.
- Nordstrom, D.K., Plummer, L. N., Langmuir, D., Busenberg, E., May, H. M., Jones, B. F. and Parkhurst, D. L. (1990) Revised Chemical-Equilibrium Data for Major Water-Mineral Reactions and Their Limitations. ACS Symposium Series. **416**: 398-413.
- O'Connor, W.K., Dahlin, D.C., Rush, G.E., Dahlin, C.L. and Collins, W.K. (2002) Carbon dioxide sequestration by direct mineral carbonation: process mineralogy of feed and products. *Minerals & Metallurgical Processing*, **19**: 95-101.
- Oelkers, E.H., Gislason, S.R. and Matter, J. (2008) Mineral Carbonation of CO₂. *Elements*, **4**(5): 333-337.
- Palandri, J.L., and Kharaka, Y.K. (2004) A compilation of rate parameters of water-mineral interaction kinetics for application to geochemical modelling: Open File Report 2004-1068. U.S. Geological Survey, Menlo Park, USA.
- Parkhurst, L. and Appelo, C.A.J., 1999. User guide to PHREEQC (Version 2)- A computer program for speciation, batch-reaction, one-dimensional transport, and inverse geochemical calculations, U.S. Department of Interior, U.S. Geological Survey, Denver, USA.
- Perez-Lopez, R., Montes-Hernandez, G., Nieto, J.M., Renard, F., Charlet, L. (2008) Carbonation of alkaline paper mill waste to reduce CO₂ greenhouse gas emissions into the atmosphere. *Applied Geochemistry*, **23**(8): 2292-2300.
- Pinsent, B.R.W., Pearson, L. and Roughton, F.J.W. (1956) The Kinetics of Combination of Carbon Dioxide with Hydroxide Ions. *Transactions of the Faraday Society*, **52**: 1512-1520.
- Pitzer, K.S. (1979) Theory-Ion Interaction approach. In: Pytkowicz, R.M. (Ed.): *Activity Coefficients in Electrolyte Solutions*, first edition, CRC Press, Boca Raton, USA.
- Plummer, L.N., Wigley, T.M.L. and Parkhurst, D.L. (1978) Kinetics of Calcite Dissolution in CO₂-Water Systems at 5-Degrees-C to 60-Degrees-C and 0.0 to 1.0 Atm CO₂. *American Journal of Science*, **278**(2): 179-216.
- Pokrovsky, O.S., Schott, J. and Thomas, F. (1999) Processes at the magnesium-bearing carbonates solution interface. I. A surface speciation model for magnesite. *Geochimica Et Cosmochimica Acta*, **63**: 863-880.

- Pokrovsky, O.S. and Schott, J. (2004) Experimental study of brucite dissolution and precipitation in aqueous solutions: Surface speciation and chemical affinity control. *Geochimica Et Cosmochimica Acta*, **68**: 31-45.
- Querol, X.; Umana, J. C.; Alastuey, A.; Ayora, C.; Lopez-Soler, A.; Plana, F. (2001) Extraction of soluble major and trace elements from fly ash in open and closed leaching systems. *Fuel*, **80**: 801-813.
- Raade, G. (1970) Dypingite, a new hydrous basic carbonate of magnesium from Norway. *American Mineralogist*, **55**: 1457-1465.
- Ramaswamy, V. et al. (2001) Radiative Forcing of Climate Change. In: *Climate Change 2001: The Scientific Basis*, Cambridge University Press, New York, USA.
- Ritchie, I.M., Xu, B.A. (1990) The kinetics of lime slaking. *Hydrometallurgy*, **23** (2-3): 377-396.
- Robie, R.A. and Hemingway, B.S. (1995) Thermodynamic properties of minerals and related substances at 298.15K and 1 bar (105 Pascals) pressure and at higher temperatures. U.S. Geological Survey Bulletin 2131, 461 S.
- Rubin, E.S. (2008) CO₂ Capture and Transport. *Elements*, 4(5): 311-317.
- RWE (1995) *Handbuch der Verwertung von Braunkohlenfilteraschen in Deutschland*; RWE-Aktiengesellschaft, Zentralbereich Forschung und Entwicklung, Essen, Germany.
- Sayles, F.L. and Fyfe, W.S. (1973) Crystallization of Magnesite from Aqueous-Solution. *Geochimica Et Cosmochimica Acta*, **37**: 87-99.
- Simons, B. (2001) CoStat CoHort Software, <http://www.cohort.com>, Monterey.
- Soong, Y. et al. (2006) CO₂ sequestration with brine solution and fly ashes. *Energy Conversion and Management*, **47**(13-14): 1676-1685.
- Soong, Y., Goodman, A.L., McCarthy-Jones, J.R., Baltrus, J.P. (2003) Experimental and simulation studies on mineral trapping of CO₂ with brine. *Energy Conversion and Management*, **45**: 1845-1859.
- Stolaroff, J.K., Lowry, G.V., Keith, D.W. (2005) Using CaO- and MgO-rich industrial waste streams for carbon sequestration. *Energy Conversion and Management*, **46**(5): 687-699.
- Stumm, W. and Morgan, J.J. (1996) *Aquatic chemistry*, third edition, John and Wiley Sons, Inc, New York, USA.

- Sverjensky, D.A. and Sahai, N. (1998) Theoretical prediction of single-site enthalpies of surface protonation for oxides and silicates in water. *Geochimica Et Cosmochimica Acta*, **62**: 3703-3716.
- Teir, S., (2006) Reduction of CO₂ emissions by producing calcium carbonates from calcium silicates and steelmaking slags. Licentiate of science in technology thesis, Helsinki Department of Technology, Helsinki, Sweden.
- Teir, S., Eloneva, S., Fogelholm, C.J. and Zevenhoven, R. (2007) Dissolution of steelmaking slags in acetic acid for precipitated calcium carbonate production. *Energy*, **32**: 528-539.
- Teir, S.; Eloneva, S.; Zevenhoven, R. (2005) Production of precipitated calcium carbonate from calcium silicates and carbon dioxide. *Energy Conversion and Management*, **46**: 2954-2979.
- Uibu, M. and Kuusik, R. (2009) Mineral Trapping of CO₂ Via Oil Shale Ash Aqueous Carbonation: Controlling Mechanism of Process Rate and Development of Continuous-Flow Reactor System. *Oil Shale*, **26**(1): 40-58.
- Uibu, M., Uus, M., Kuusik, R., (2009) CO₂ mineral sequestration in oil-shale wastes from Estonian power production. *Journal of Environmental Management*, **90**(2): 1253-1260.
- Uliasz-Bochenczyk, A. and Mokrzycki, E. (2006) Fly ashes from Polish power plants and combined heat and power plants and conditions of their application for carbon dioxide utilization. *Chemical Engineering Research & Design*, **84**(A9): 837-842.
- Uzdowski, E. (1982) Reactions and Equilibria in the Systems CO₂-H₂O and CaCO₃-CO₂-H₂O - a Review. *Neues Jahrbuch Für Mineralogie-Abhandlungen*, **144**(2): 148-171.
- Vasillev, S.V. and Vassileva, C.G. (2005) Methods for characterization of composition of fly ashes from coal-fired power stations: A critical overview, **19**(3): 1084-1098.
- Vermilye, D. A. (1969) Dissolution of MgO and Mg(OH)₂ in Aqueous Solutions. *Journal of the Electrochemical Society*, **116**: 1179-1183.
- Wilson, M., (1993) Magmatic differentiation. *Journal of the Geological Society*, **150**: 611-624.
- Wogelius, R.A., Refson, K., Fraser, D.G., Grime, G.W. and Goff, J.P. (1995) Periclase Surface Hydroxylation During Dissolution. *Geochimica Et Cosmochimica Acta*, **59**(9): 1875-1881.

References

- Wolff-Boenisch, D., Gislason, S.R. and Oelkers, E.H. (2006) The effect of crystallinity on dissolution rates and CO₂ consumption capacity of silicates. *Geochimica Et Cosmochimica Acta*, **70**: 858-870.
- Zevenhoven, R., Eloneva, S., Teir, S., (2006) Chemical fixation of CO₂ in carbonates: Routes to valuable products and long-term storage. *Catalysis Today*, **115**(1-4): 73-79.

Danksagung

Allen die mich während dieser Arbeit unterstützt haben möchte ich sehr herzlich danken. Mein besonderer Dank gilt dabei:

Stefan Peiffer für die herzliche Aufnahme am Lehrstuhl Hydrologie und die Möglichkeit meine Promotion durchzuführen. Danke für die lebhaften Diskussionen, für die zahlreichen Korrekturen und die geduldige Unterstützung während meiner Zeit in Bayreuth und darüber hinaus.

Markus Bauer für Deinen großen Arbeitseinsatz als Ideengeber, Kritiker und Motivator in vielen wichtigen Momenten. Ohne Dich wäre die Arbeit nicht in jetziger Form entstanden. Besonderer Dank für Deinen Rückhalt als Freund und die schönen Stunden in und außerhalb des Büros.

Danke den Mitarbeiter der Forschungsgruppe CO₂-Trap der RWTH Aachen für die schöne gemeinsame Zeit während zahlreicher Arbeitstreffen, Konferenzen und Exkursionen: Michael Kühn und Katrin Vosbeck für die Unterstützung, den lebhaften Austausch unter anderem während unserer Workshops in Aachen und Bayreuth. Helge Stanjek und Dennis Künkel für die tatkräftige Unterstützung bei der mineralogischen Charakterisierung der Flugaschen.

Ich danke allen TAs, Diplomanden Hiwis und wissenschaftlichen Angestellten für die Unterstützung und die schöne gemeinsamen Zeit am Lehrstuhl. Martina Rohr, Jutta Eckert, Karin Söllner, Heidi Zier, Sonja Weber, Bettina Kuppinger, Klaus-Holger Knorr, Michael Radke, Lina Fürst, Sandra Werb, Martina Hunner, Stefan Metzger und viele Weitere. Martina Heider, vielen Dank für Dein großes Engagement, Dein Ideenreichtum und Deine Ausdauer.

Thomas Heidelberg und Tiziana Boffa Ballaran für die Hilfe am XRD und EMS (BGI Bayreuth). Ingrid Otto (FAN; Bayreuth) für die Durchführung der BET-Messungen. Gunter Ilgen für die Unterstützung am ICP-OES. Jörg Gerchau (FAN, Bayreuth) für seinen großen

Einsatz bei Aufbau und Entwicklung von Steuer- und Messtechnik sowie als Helfer in jeder Not.

Jan Fleckenstein, Tobias Goldhammer, Tobias Heitmann, Julia Beer, Sabine Thüns, Beate Fulda, Christian Blodau, und Oliver Will. Schön dass Ihr alle da wart! Katrin Hellige für die schönen gemeinsamen Stunden und die vielen ermutigenden Gespräche in Bayreuth und NRW. Charlotte Ockert für das Korrekturlesen und Sara Hassel für die tatkräftige Unterstützung bei der Layout-Gestaltung.

Besonderer Dank gilt allen Freunden, meinen Eltern und meinen Geschwistern, für die Unterstützung und das Vertrauen über all die Jahre an mich.

Ich danke dem Bundesministerium für Bildung und Forschung, das die Finanzierung für die Durchführung dieser Arbeit ermöglichte.

Erklärung

Hiermit erkläre ich, dass ich diese Arbeit selbständig verfasst und keine anderen als die angegebenen Quellen und Hilfsmittel verwendet habe. Ich erkläre ferner, dass ich an keiner anderen Hochschule als der Universität Bayreuth ein Promotionsverfahren begonnen und diese oder eine gleichartige Doktorprüfung endgültig nicht bestanden habe.

Köln, Oktober 2011